ÇUKUROVA UNIVERSITY
INSTITUTE OF NATURAL AND APPLIED SCIENCES

MSc THESIS

Bülent BÜYÜKGÜZEL

MICROCONTROLLER BASED MAXIMUM POWER POINT TRACKER FOR SOLAR PANELS

DEPARTMENT OF ELECTRICAL AND ELECTRONICS ENGINEERING

ADANA, 2011

ÇUKUROVA UNIVERSITY
INSTITUTE OF NATURAL AND APPLIED SCIENCES

MICROCONTROLLER BASED MAXIMUM POWER POINT TRACKER FOR SOLAR PANELS

Bülent BÜYÜKGÜZEL

MSc THESIS

DEPARTMENT OF ELECTRICAL AND ELECTRONICS ENGINEERING

We certify that the thesis titled above was reviewed and approved for the award of degree of the Master of Science by the board of jury on 17 / 02 / 2011.

………………...................	…………………….............	....
Asst.Prof.Dr. Murat AKSOY	Assoc.Prof.Dr. Ulus ÇEVİK	Asst.Prof.Dr. Mutlu AVCI
SUPERVISOR	MEMBER	MEMBER

This MSc Thesis is written at the Department of Institute of Natural And Applied Sciences of Çukurova University.
Registration Number:

Prof. Dr. İlhami YEĞİNGİL
Director
Institute of Natural and Applied Sciences

Not: The usage of the presented specific declerations, tables, figures, and photographs either in this thesis or in any other reference without citiation is subject to "The law of Arts and Intellectual Products" number of 5846 of Turkish Republic

ABSTRACT

MSc THESIS

MICROCONTROLLER BASED MAXIMUM POWER POINT TRACKER FOR SOLAR PANELS

Bülent BÜYÜKGÜZEL

CUKUROVA UNIVERSITY
INSTITUTE OF NATURAL AND APPLIED SCIENCES
DEPARTMENT OF ELECTRICAL AND ELECTRONICS ENGINEERING

Supervisor : Asst.Prof.Dr. Murat AKSOY
Year : 2011, Pages: 131
Jury : Asst.Prof.Dr. Murat AKSOY
: Assoc.Prof.Dr. Ulus ÇEVİK
: Asst.Prof.Dr. Mutlu AVCI

Solar energy is one of the most important renewable energy sources. Unfortunately, photovoltaic (PV) power systems have two major problems: the conversion efficiency and the amount of electric power generated by solar panels changes continuously with weather conditions.

Maximum power point tracking (MPPT) techniques should be used in photovoltaic systems to maximize the PV panel output power by tracking continuously the maximum power point (MPP) which depends on panel's temperature and on irradiance conditions. Especially for low-cost implementations, the perturb and observe (P&O) maximum power point tracking algorithm is the most commonly used method due to its ease of implementation.

Key Words: Solar energy Maximum power point tracking, MPP, MPPT, P&O, Photovoltaic

ÖZ

YÜKSEK LİSANS TEZİ

SOLAR PANELLER İÇİN MİKRODENETLEYİCİ TABANLI MAKSİMUM GÜÇ NOKTASI İZLEYİCİ

Bülent BÜYÜKGÜZEL

ÇUKUROVA ÜNİVERSİTESİ
FEN BİLİMLERİ ENSTİTÜSÜ
ELEKTRİK-ELEKTRONİK MÜHENDİSLİĞİ ANABİLİM DALI

Danışman : Yrd. Doç. Dr. Murat AKSOY
Yıl: 2011, Sayfa: 131
Jüri : Yrd. Doç. Dr. Murat AKSOY
: Doç.Dr. Ulus ÇEVİK
: Yrd. Doç. Dr. Mutlu AVCI

Güneş enerjisi en önemli yenilenebilir enerji kaynaklarından birisidir. Ne yazık ki fotovoltaik güç sistemleri iki büyük probleme sahiptir: ışınım-elektrik enerjisi dönüştürme verimliliği ve solar paneller tarafından üretilen enerji miktarının hava şartları ile sürekli olarak değişmesi.

PV sistemlerde, PV panel sıcaklığına ve ışınıma bağlı olan maksimum güç noktasının (MGN) sürekli olarak takip edilerek PV panel çıkış gücünün en yüksek seviyeye çıkartılması için Maksimum Güç Noktası İzleme (MGNİ) teknikleri kullanılmalıdır. Özellikle düşük maliyeli uygulamalar için Karıştır ve Gözle maksimum güç noktası izleme algoritması kolay uygulanabilir olması nedeniyle en yaygın kullanılan yöntemdir.

Anahtar Kelimeler: Güneş enerjisi, Maksimum güç noktası izleyici, MGN, MGNİ, Karıştır ve Gözle, Fotovoltaik

ACKNOWLEDGEMENTS

I would like to thank my supervisor Assist.Prof.Dr.Murat AKSOY for his helps, advices and supports throughout my work.

I would like to thank my beloved wife and son for their patience and encouragement.

This thesis is dedicated to my mother and my father.

CONTENTS **PAGE**

LIST OF TABLES **PAGE**

LIST OF FIGURES **PAGE**

LIST OF SYMBOLS AND ABBREVIATIONS

Symbols	Description	Unit
h	Planck's Constant	Js
k	Boltzmann' constant	J/K
σ	Stefan-Boltzmann's constant	$W/(m^2K^4)$
λ	Wave length of photon	nm
c	Speed of light	m/s
f	Frequency	Hz
Eg	Energy band gap	eV
q	Charge of an electron	C
I	Current	A
I_{PH}	Photon generated current	A
I_D	Diode current	A
I_0	Diode saturation current	A
I_{SC}	Short circuit current	A
I_{MPP}	Maximum power point current	A
V	Voltage	V
V_T	Thermal voltage	V
V_{OC}	Open circuit voltage	V
V_D	Diode voltage	V
V_{MPP}	Maximum power point voltage	V
R_S	Serial resistance	Ω
R_{SH}	Shunt resistance	Ω
n,n_1,n_2	Diode quality factor	-
A	Combined diode quality factor	-
n_s	number of series connected cell	-
D	Duty cycle	-
α_{ISC}	I_{SC} Temperature coefficient	%/K
α_{VOC}	V_{OC} Temperature coefficient	mV/K

Abbreviations	Description
PV	Photovoltaic
MPP	Maximum Power Point
MPPT	Maximum Power Point Tracking
AM	Air Mass
P&O	Perturb and Observe
IC	Incremental Conductance
STC	Standard Test Condition
NOCT	Nominal Operating Cell Temperature
PWM	Pulse With Modulation
SEPIC	Single Ended Primary Inductance
PI	Proportional and Integral

1. INTRODUCTION

1.1. Why Solar Energy?

For the last few hundred years humans have been using up fossil fuels that took around 400 million years to form and store underground. It has become clear that, even if those reserves were unlimited, we could not continue to burn them with impunity. The resulting carbon dioxide emissions and increased global warming would almost certainly lead to a major environmental crisis. So the danger is now seen as a double - edged sword: on the one side, fossil fuel depletion; on the other, the increasing inability of the natural world to absorb emissions caused by burning what fuel remains.

Solar power, a clean renewable resource with zero emission, has got tremendous potential of energy which can be harnessed using a variety of devices. With recent developments, solar energy systems are easily available for industrial and domestic use with the added advantage of minimum maintenance. Most of the developed countries are switching over to solar energy as one of the prime renewable energy source. The current architectural designs make provision for photovoltaic cells and necessary circuitry while making building plans.

1.2. Solar Energy

The Sun sends an almost unimaginable amount of energy towards Planet Earth around 10^{17} W. In electrical supply terms this is equivalent to the output of about one hundred million modern fossil fuel or nuclear power stations. To state it another way, the Sun provides in about an hour the present energy requirements of the entire human population for a whole year. It seems that all we need do to convert society from carbon to solar is to tap into a tiny proportion of this vast potential.

The Sun's power density (the power per unit area) just above the Earth's atmosphere is known as the solar constant and equals 1366 W/m^2. This is reduced by around 30% as it passes through the atmosphere, giving an insolation at the Earth's surface of about 1000 W/m^2 at sea level on a clear day. This value is the accepted standard for 'strong sunshine' and is widely used for testing and calibrating terrestrial PV cells and systems. Another important quantity is the average power density received over the whole year, known as the annual mean insolation. A neat way of estimating it is to realize that, seen from the Sun, the Earth appears as a disk of radius R and area πR^2. But since the Earth is actually spherical with a total surface area $4 \pi R^2$, the annual mean insolation just above the atmosphere must be 1366/4 = 342 W/m^2. However it is shared very unequally, being about 430 W/m^2 over the equator, but far less towards the Polar Regions which are angled well away from the Sun (Lynn, 2010).

If we know the average insolation at a particular location, it is simple to estimate the total energy received over the course of a year (1 year = 8760 hours). For example Adana, mean insolation of about 180 W/m^2, have annual energy totals of about 180 × 8760/1000 = 1600 kWh/m^2. Distribution of the yearly sum of the global irradiation is illustrated in Figure 1.1 for Turkey (http://ec.europa.eu/dgs/jrc).

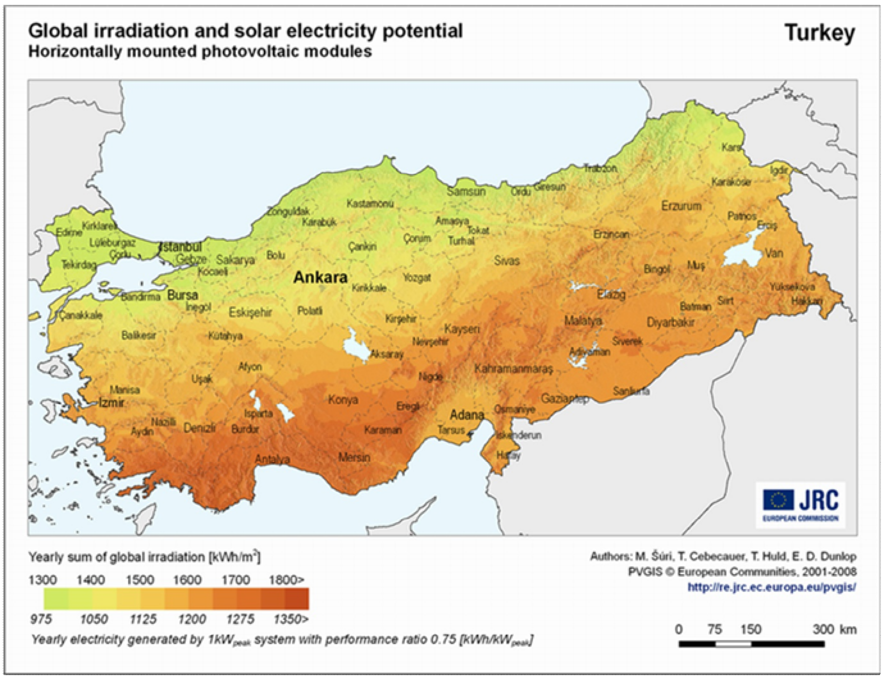

Figure 1.1. Distribution of the yearly sum of the global irradiation of Turkey

1.3. The Photovoltaic Effect and PV cell

Photovoltaic (abbreviated PV) is the most direct way to convert solar radiation into electricity and is based on the photovoltaic effect, which was first observed by Henri Becquerel in 1839. It is quite generally defined as the emergence of an electric voltage between two electrodes attached to a solid or liquid system upon shining light onto this system. Practically all photovoltaic devices incorporate a p-n junction in a semiconductor across which the photo voltage is developed as shown in Figure 1.2.

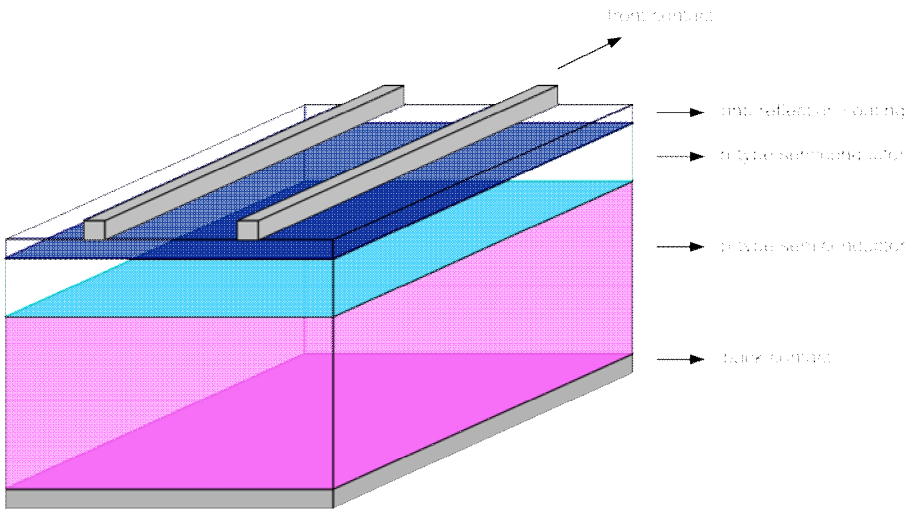

Figure 1.2. Typical PV cell structure formed by p and n type semiconductors

The PV process works by the photovoltaic effect in semiconductor materials. When light strikes the cell, a portion of it is absorbed within the semiconductor material and knocks electrons loose, enabling an electrical charge to flow freely within the material. PV cells have an in-built electric field that acts to force electrons, freed by light absorption, to flow in a certain direction. The field is created by doping (controlled introduction of impurities) in silicon with elements such as phosphorus or boron to create n-type or p-type zones. By placing metal contacts on the top and bottom of the PV cell, the current can be put to work by passing through an external circuit. The current is generated silently with no moving parts, no emissions and the cells need no maintenance, apart from keeping the top surface of the module clean for the passage of light (Goetzberger & Hoffmann, 2005).

Equivalent circuit of the PV cell is shown in Figure 1.3. It consists of a diode representing the action of the p-n junction together with a current generator representing the light generated current I_L.

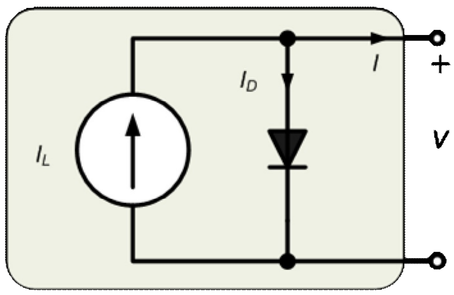

Figure 1.3. Equivalent circuit of the PV cell

Current which is transferred outside of the PV cell is obtained using this equivalent circuit as below.

$$I = I_L - I_0\left[\exp\left(\frac{qV}{kT}\right) - 1\right] \tag{1.1}$$

Typical I-V characteristic of PV cell is shown in Figure 1.4. Output power of the PV cell equals the product of its voltage and current. No power is produced on open circuit (maximum voltage, zero current) or short circuit (maximum current, zero voltage). The full rated power is obtained by operating the cell slightly below maximum voltage and current at its maximum power point (MPP).

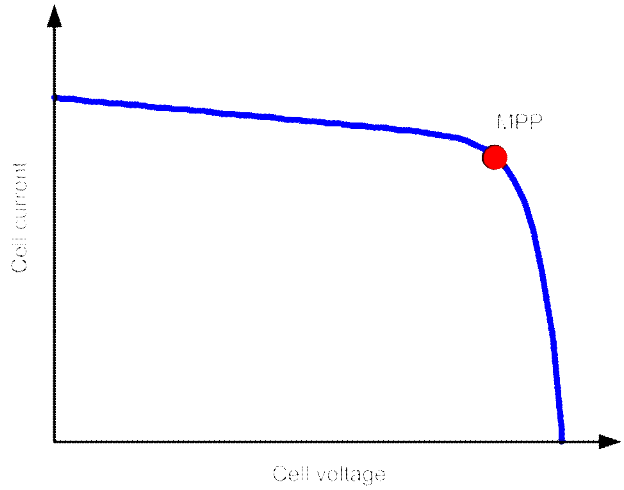

Figure 1.4. I-V curve of the PV cell

As it will be explained later, an increase in solar radiation causes the output current to increase and the horizontal part of the curve moves upward. An increase in cell temperature causes the voltage to move leftward, while decreasing temperature produces the opposite effect. So, photovoltaic cell characteristic varies with solar radiation and cell temperature.

1.4. Maximum Power Point Tracking

Solar power is an alternative technology that will hopefully lead us away from our petroleum dependent energy sources. The major problem with solar panel technology is that the efficiencies for solar power systems are still poor and the costs per kilo-watt-hour (kWh) are not competitive, in most cases, to compete with petroleum energy sources. Solar panels themselves are quite inefficient (approximately 30%) in their ability to convert sunlight to energy.

Moreover, the solar cell I-V characteristic is nonlinear and varies with irradiation and temperature. There is a unique point on the V-I or V-P curve of the PV, called the Maximum Power Point (MPP), at which the entire PV system operates with maximum efficiency and produces its maximum output power. The location of the MPP is not known, but can be located, either through calculation models or by search algorithms. Therefore Maximum Power Point Tracking (MPPT) techniques are needed to maintain the PV array's operating point at its MPP.

1.5. Operation Principle of the MPPT

If the array is operating at any point at voltage V and current I on the I-V curve, the power generation is $P = VI$ watts. If the operation moves away from the preceding point such that the current is now $I + \Delta I$, and the voltage is $V + \Delta V$, then the new power is as follows:

$$P + \Delta P = (V + \Delta V)(I + \Delta I) \tag{1.2}$$

which, after ignoring a small term, simplifies to the following:

$$\Delta P = \Delta V \cdot I + \Delta I \cdot V \tag{1.3}$$

ΔP would be zero if the array were operating at the peak power point, which necessarily lies on a locally flat neighborhood. Therefore, at the peak power point, the preceding expression in the limit becomes:

$$\frac{dV}{dI} = -\frac{V}{I} \tag{1.4}$$

We note here that dV/dI is the dynamic impedance of the source (Z_D), and V/I the static impedance (Z_S). Thus, at the peak power point, the following relation holds:

$$Z_D = -Z_S \tag{1.5}$$

To obtain this condition , in the other words , to work PV at MPP operating point of the PV is adjusted by MPPT using DC-DC converter as shown in Figure 1.5.

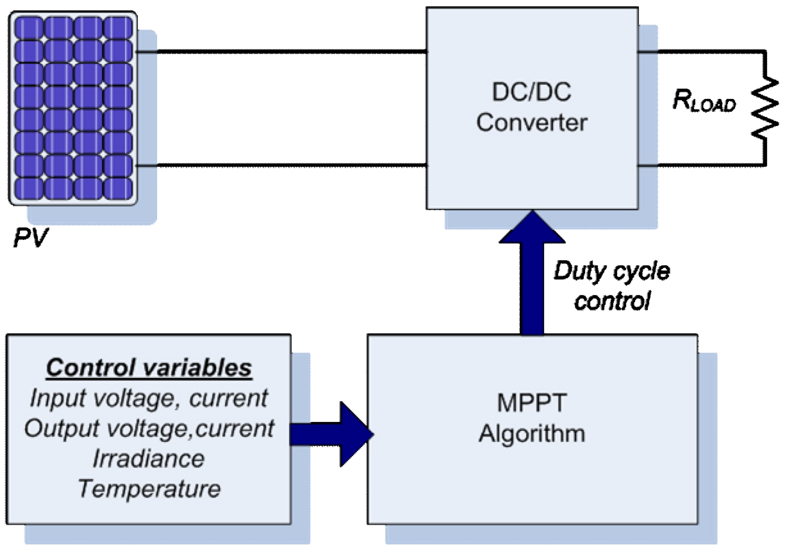

Figure 1.5. MPPT system

Many MPPT techniques have been proposed in the literature. Examples are the Perturb and Observe (P&O) method, the Incremental Conductance (IC) method (Hohm & Ropp, 2002), the Artificial Neural Network method (Sun, Wu, Li, & Zhao, 2002) , the Fuzzy Logic method (Kottas, Boutalis, & Karlis, 2006).The P&O and IC techniques, as well as variants thereof, are the most widely used.

The P&O algorithms operate by periodically perturbing (i.e. incrementing or decrementing) the array terminal voltage and comparing the PV output power with that of the previous perturbation cycle. If the PV array operating voltage changes and power increases ($dP/dV|_{PV}>0$), the control system moves the PV array operating point in that direction; otherwise the operating point is moved in the opposite direction. In the next perturbation cycle the algorithm continues in the same way (Dolara, Faranda, & Leva, 2009).

There are many different P&O methods available in the literature. Most common used P&O methods are the classic, the optimized and the three-point P&O algorithms. In the classic P&O technique, the perturbations of the PV operating point have a fixed magnitude. In the optimized P&O technique, an average of several samples of the array power is used to dynamically adjust the magnitude of the perturbation of the PV operating point. In the three-point weight comparison method, the perturbation direction is decided by comparing the PV output power on three points of the P-V curve.

In this thesis, the classic P&O technique is implemented as MPPT algorithm with SEPIC topology DC-DC converter.

2. THE SOLAR RESOURCE

The source of insolation (*insolation: in*cident *sol*ar Radi*ation*) is, of course, the sun that gigantic, 1.4 million kilometer diameter, thermonuclear furnace fusing hydrogen atoms into helium. The resulting loss of mass is converted into about 3.8×10^{20} MW of electromagnetic energy that radiates outward from the surface into space. To design and analyze solar systems, we need to know how much sunlight is available.

2.1. The Solar Spectrum

Every object emits radiant energy in an amount that is a function of its temperature. The usual way to describe how much radiation an object emits is to compare it to a theoretical abstraction called a *blackbody*. A blackbody is defined to be a perfect emitter as well as a perfect absorber. As a perfect emitter, it radiates more energy per unit of surface area than any real object at the same temperature. As a perfect absorber, it absorbs all radiation that impinges upon it; that is, none is reflected and none is transmitted through it. The wavelengths emitted by a blackbody depend on its temperature as described by *Planck's law*:

$$E_\lambda = \frac{3.47 \times 10^8}{\lambda^5 \left[\exp\left(\frac{14.400}{\lambda T} \right) - 1 \right]} \tag{2.1}$$

where E_λ is the emissive power per unit area of a blackbody (W/m^2 μm), T is the absolute temperature of the body (K), and λ is the wavelength (μm) (Gilbert, 1998).

The sun can be modeled using Equation (2.1). Modeling the sun itself as a 5800 K (5526 °C) blackbody results in the emission spectrum plotted in Figure 2.1. The area under Planck's curve between any two wavelengths is the power emitted between those wavelengths, so the total area under the curve is the total radiant power emitted.

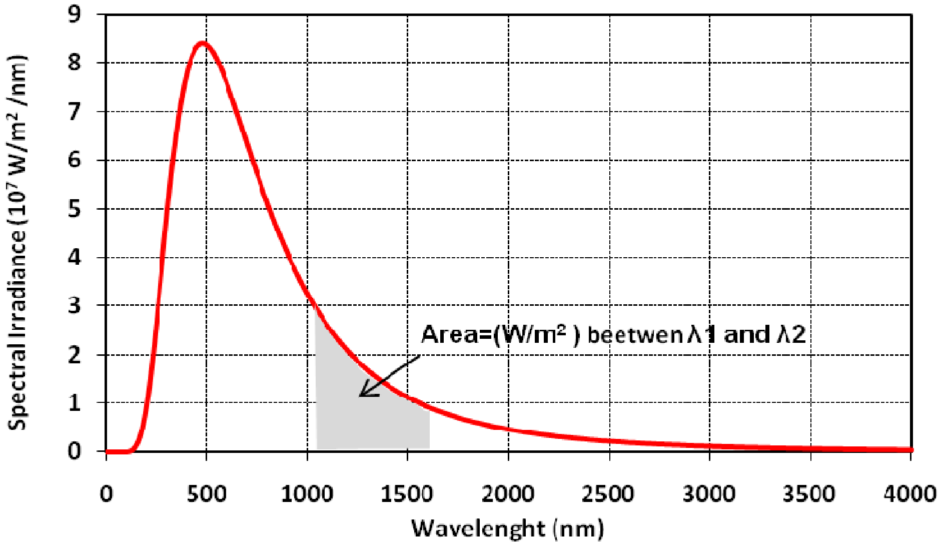

Figure 2.1. Spectral emissive power of the 5800 K blackbody

That total is conveniently expressed by the *Stefan–Boltzmann law of radiation*:

$$E = A\sigma T^4 \tag{2.2}$$

where E is the total blackbody emission rate (W), σ is the Stefan–Boltzmann constant (5.67×10^{-8} W/m^{2}K^4), T is the absolute temperature of the blackbody (K), and A is the surface area of the blackbody (m^2).(Gilbert, 1998)

2.2. Solar Constant, Irradiance, Air Mass Number

Energy delivered by the sun, or any radiant power source, can be described by its irradiance. Irradiance is defined to be the radiant power incident per unit area on a surface, usually measured in Watts per square meter. The irradiance of the sun in space just outside of the atmosphere is about 1353 kW/m^2. Because this number is so commonly used, it is also called the solar constant.

Radiation from the sun's surface is reasonably constant (Muneer, 2004). Although this, by the time it reaches the earth's surface it is highly variable owing to absorption and scattering in the earth's atmosphere. The length of the path h_2 taken by the sun's rays as they pass through the atmosphere, divided by the minimum possible path length h_1, which occurs when the sun is directly overhead, is called the air mass ratio, AM

$$\mathrm{AM} = \frac{h_2}{h_1} = 1/\cos\varpi \tag{2.3}$$

where h_1 is path length through the atmosphere with the sun directly overhead , h_2 is path length through the atmosphere to reach a spot on the surface, and ω is angle between h_1 an h_2 as shown in Figure 2.2.

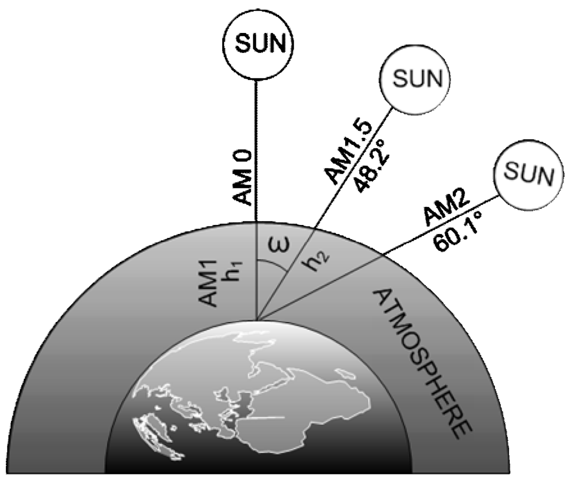

Figure 2.2. Relation between paths of the sun's rays and air mass ratio

Thus, an air mass ratio of AM1 means that the sun is directly overhead. By convention, AM0 means no atmosphere, that is, it is the extraterrestrial solar spectrum. Often, an air mass ratio of 1.5 is assumed for an average solar spectrum at the earth's surface.

2.3. The Effect of Atmosphere on Sunlight

As sunlight enters the Earth's atmosphere some is absorbed, some is scattered and some passes through unaffected by the molecules in the atmosphere and is either absorbed or reflected by objects at ground level. Different molecules do different things. Water vapor, carbon dioxide and ozone, for example, have several significant absorption wavelengths. Ozone plays an important role by absorbing a significant amount of radiation in the ultraviolet region of the spectrum, while water vapor and carbon dioxide absorb primarily in the visible and infrared parts of the spectrum (Messenger & Ventre, 2004).

The impact of the atmosphere on incoming solar radiation for air mass ratio 1.5 is shown in Figure. 2.3. As sunlight passes through more atmospheres, less energy arrives at the earth's surface and the spectrum shifts some toward longer wavelengths.

As a result if the angle is increased, the path for sunlight increases, the air mass number increases, and the intensity of the solar spectrum decreases.

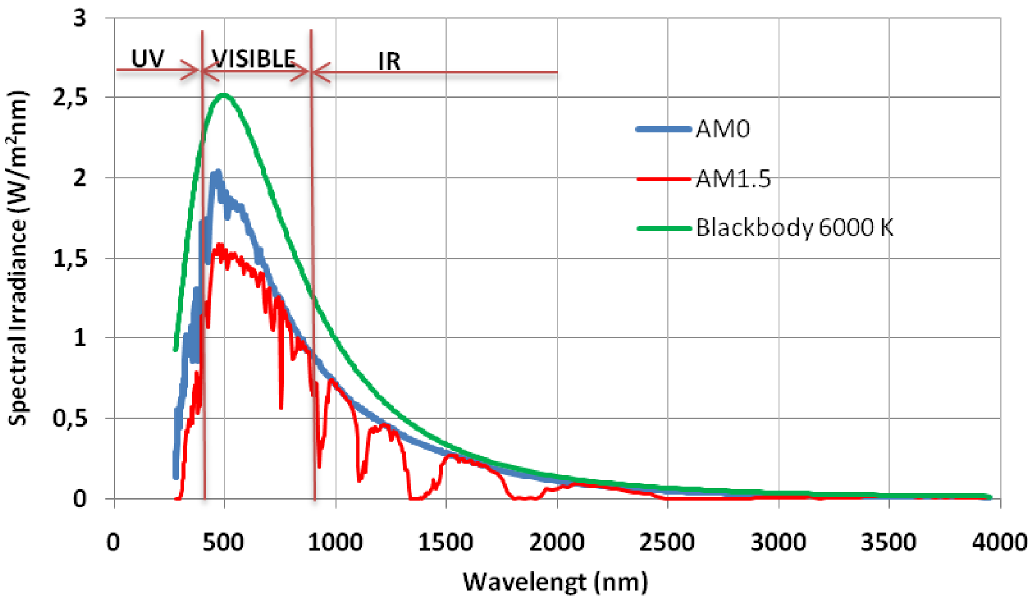

Figure 2.3. Solar spectrum for extraterrestrial (AM0) and AM1.5

3. PHYSICS OF THE PV CELLS

3.1. Semiconductor Material Types

Silicon and other semiconductor materials used for solar cells can be crystalline, polycrystalline, microcrystalline or amorphous. Microcrystalline material has grains smaller than 1 µm, polycrystalline smaller than 1 mm and multicrystalline smaller than 10 cm. The structure of the different material types is illustrated in Figure 3.1.

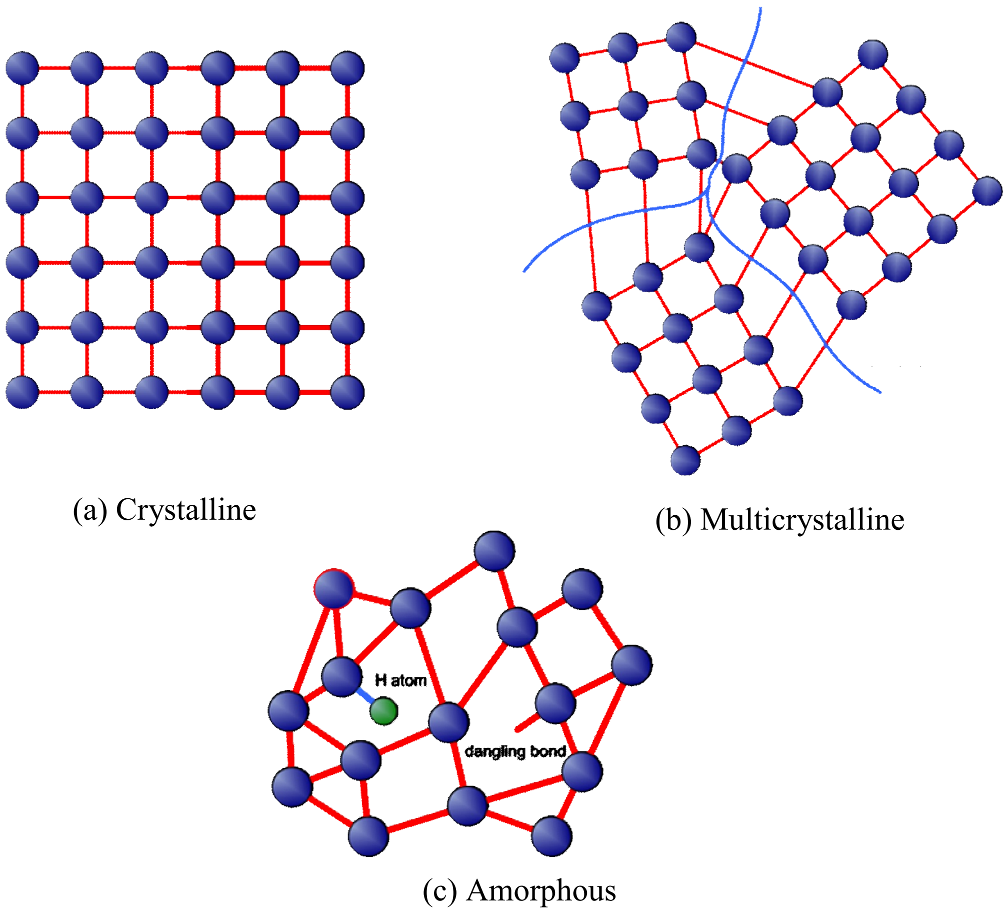

Figure 3.1. Semiconductor materials (Wenham & Green, 2007)

3.1.1. Crystalline Silicon

Crystalline silicon has an ordered crystal structure as shown in Figure 3.1(a), with each atom ideally lying in a pre-ordained position. It therefore allows ready application of the theories and techniques developed for crystalline material, and exhibits predictable and uniform behavior. It is, however, the most expensive type of silicon, because of the careful and slow manufacturing processes required. The cheaper multicrystalline or polycrystalline silicon (poly-silicon), and amorphous silicon are therefore increasingly being used for PV cells, despite their less ideal qualities.

3.1.2. Multicrystalline Silicon

Multicrystalline silicon is shown in Figure 3.1(b) . The techniques for production of multicystalline or polycrystalline silicon are less critical, and hence cheaper, than those required for single crystal material. The grain boundaries reduce the cell performance by blocking carrier flows, allowing extra energy levels in the forbidden gap, thereby providing effective recombination sites, and providing shunting paths for current flow across the p-n junction. To avoid significant recombination losses at grain boundaries, grain sizes in the order of a few millimeters are required. This also allows single grains to extend from the front to the back of a cell, providing less resistance to carrier flow and generally decreasing the length of grain boundaries per unit of cell. Such multicrystalline material is widely used for commercial PV cell production.

3.1.3. Amorphous Silicon

Amorphous silicon can be produced, in principle, even more cheaply than polysilicon. With amorphous silicon, there is no long-range order in the structural arrangement of the atoms, resulting in areas within the material containing unsatisfied or dangling bonds as shown in Figure 3.1(c). These in turn result in extra energy levels within the forbidden gap, making it impossible to dope the semiconductor when pure, or to obtain reasonable current flows in a solar cell configuration. It has been found that the incorporation of atomic hydrogen in amorphous silicon, to a level of 5–10%, saturates the dangling bonds and improves the quality of the material. It also increases the band gap (Eg) from 1.1 eV in crystalline silicon to 1.7 eV, making the material much more strongly absorbing for photons of energy above the latter threshold (Wenham & Green, 2007).

3.2. Intrinsic Semiconductors

As shown in Figure 3.2 , an atom is imposed of a nucleus, which contains positively charged protons and neutral neutrons, and negatively charged electrons that, in the classical sense, orbit the nucleus. The electrons are distributed in various “shells” at different distances from nucleus, and electron energy increases as shell radius increases. Electrons in the outermost shell are called valence electrons, and the chemical activity of a material is determined primarily by the number of such electrons.

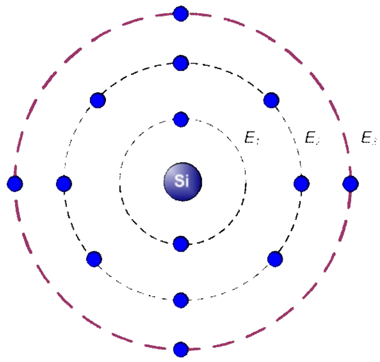

Figure 3.2. Atomic structure of Silicon atom

Element in the periodic table can be grouped according to the number of valence electrons. Table 3.1 shows a portion of the periodic table in which the more common semiconductors are found. Silicon (Si) and germanium (Ge) are in group IV elemental semiconductors. In contrast, gallium arsenide is a group III-V compound semiconductor.

Table 3.1. Group III-IV-V elements

III	IV	V
B	C	
Al	Si	P
Ga	Ge	As

Figure 3.3(a) shows five no interacting silicon atoms, with four valence electrons of each atom shown as dashed lines emanating from the atom. As a silicon atoms come into close proximity to each other, the valence electrons interact to form a crystal. The final crystal structure is a tetrahedral configuration in which each silicon atom has four nearest neighbors, as shown in Figure 3.3(b). The valence electrons are shared between atoms, forming what are called covalent bonds. Germanium, gallium arsenide, and many other semiconductor materials have the same tetrahedral configuration.

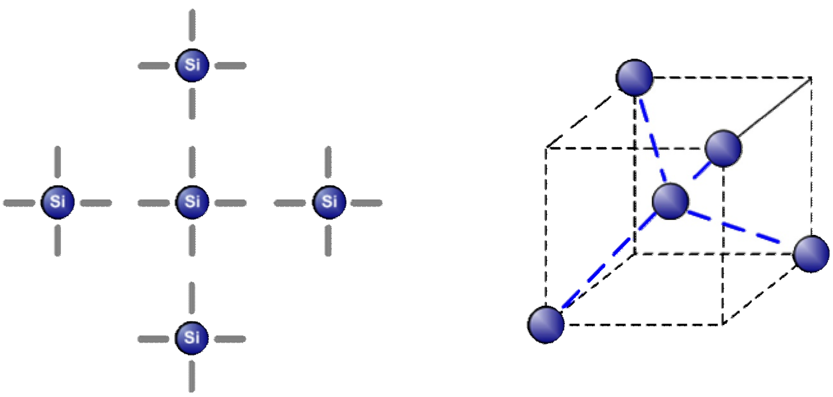

(a) (b)

Figure 3.3. Silicon atoms in crystal matrix (Neamen, 1996)

Figure 3.4(a) is a two dimensional representation of lattice formed by the five silicon atoms in Figure 3.3(a). An important property of such a lattice is that valence electrons are always available on the outer edge of the silicon crystal so that additional atoms can be added to form very large single crystal structures.

A two dimensional representation of a silicon single crystal is shown in Figure 3.4(b) for T=0 °K where T is temperature. Each line between atoms represents a valence electron. At T=0 °K, each electron is in its lowest possible energy state, so each covalent bonding position is filled. If a small electric field is applied to this material, the electrons will not move, because they will still be bound to their individual atoms. There for at T=0 °K, silicon is insulator; that is no charge flows through it.

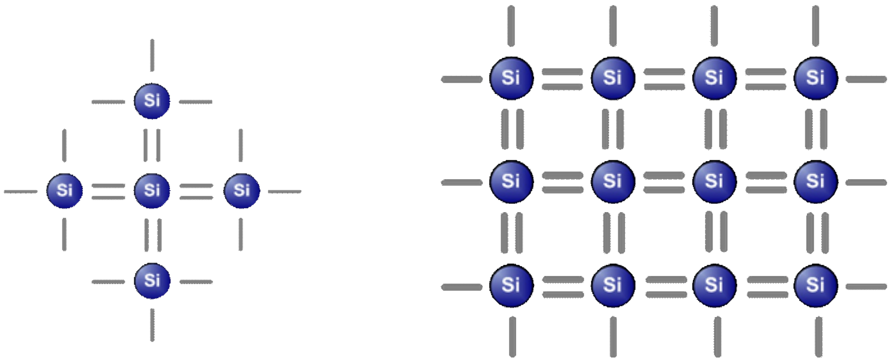

(a) (b)

Figure 3.4. Covalent bonding and silicon crystal (Neamen, 1996)

If the temperature increases, the valence electron will gain the thermal energy. Any such electron may gain enough thermal energy to break the covalent bond and move away from its original position (Figure 3.5). The electron will then be free to move within the crystal.

Since the net charge of the material is neutral, if a negatively charged electron breaks its covalent bond and moves away from its original position, a positively charged empty state is created at that position (Figure 3.5). As the temperature increases more covalent bonds are broken and more free electrons and positive empty states are created.

In order to break the covalent bond, a valence electron must gain a minimum energy, E_g, called to band gap energy. Materials that have large band gap energies, in the range of 3 to 6 electron- volts (eV), are insulators because, at room temperature, essentially no free electrons exist in these materials. In contrast, materials that contain very large numbers of free electrons at room temperature are conductors.

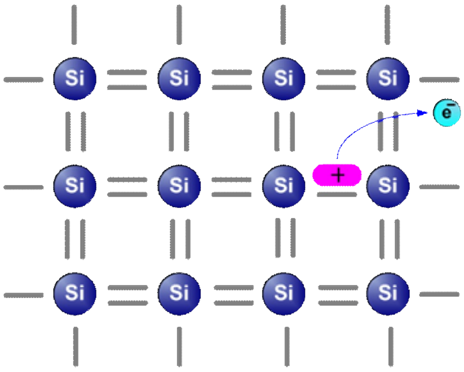

Figure 3.5. Breaking of a covalent bond

In a semiconductor, the band gap energy is on the order of 1 eV. The net flow of free electrons in a semiconductor causes a current. In addition, a valence electron that has a certain thermal energy and is adjacent to an empty state may move into that position, as shown in Figure 3.6 making it appear as if a positive charge is moving through the semiconductor. This positively charged particle is called a hole.

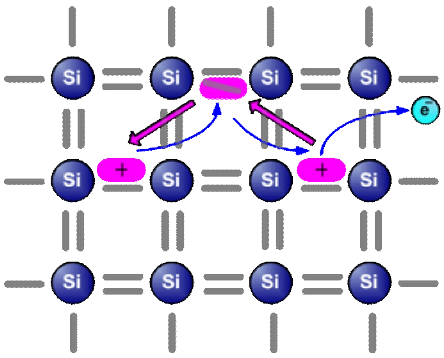

Figure 3.6. Movement of the positively charged hole in the silicon crystal

In semiconductors, then, two types of charged particles contribute to the current: the negatively charged free electron, and the positively charged hole. This description of a hole is greatly oversimplified, and is meant only to convey the concept of the moving positive charge.

The concentration of electrons and holes are important parameters in the characteristics of a semiconductor material, because they directly influence the magnitude of the current. An *intrinsic semiconductor* is a single crystal semiconductor material with no other types of atoms within the crystal. In an intrinsic semiconductor, the density of electrons and holes are equal, since the thermally generated electrons and holes are the only sources of such particles (Neamen, 1996).

On the other hand, the band model describes behavior of the electrons in terms of the energy levels between valence and conduction bands. Briefly, the electrons in covalent bonds have energies corresponding to those in the valence band. In the conduction band the electrons are free. The forbidden gap corresponds to the minimum energy (band gap energy) needed to release an electron from a covalent bond to the conducting band where it can conduct a current as shown in Figure 3.7. The holes remaining conduct in the opposite direction in the valence band, as described for the bond model (Wenham & Green, 2007).

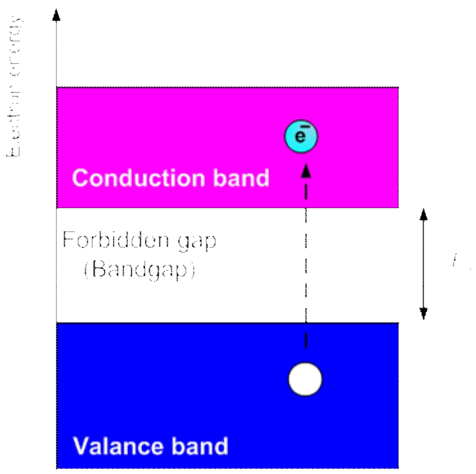

Figure 3.7. Representation of the energy bands for electron in solid

3.3. Extrinsic Semiconductors

Because the electron and hole concentrations in an intrinsic semiconductor are relatively small, only very small currents are possible. However, these concentrations can be greatly increased by adding controlled amounts of certain impurities. A desirable impurity is one that enters the crystal lattice and replaces one of the semiconductor atoms, even though the impurity atom does not have the same valance electron structure. For silicon, the desirable substitutional impurities are from the group III and V elements.

The most common group V elements used for this purpose are phosphorus and arsenic. For example, when a phosphorus atom substitutes for a silicon atom, as shown in Figure 3.8 (a), four of its valance electrons are used to satisfy the covalent bond requirements. The fifth valance electron is more loosely bound to the phosphorus atom. At room temperature, this electron has enough thermal energy to break the bond, thus being free to move through the crystal and contribute to the electron current in the semiconductor.

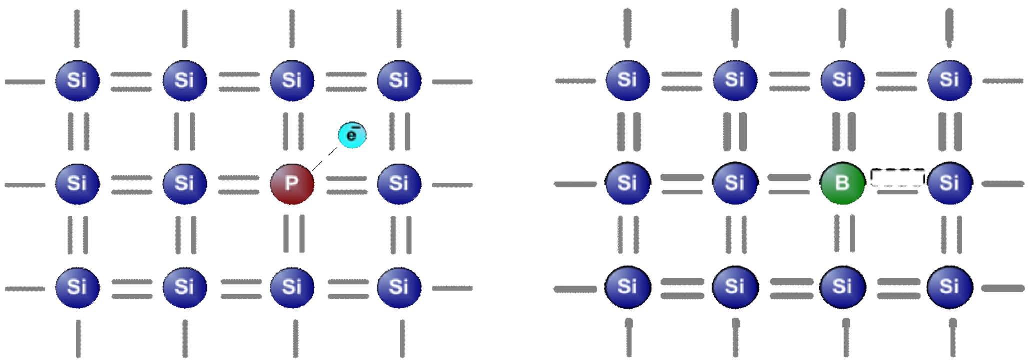

(a) (b)

Figure 3.8. Silicon lattice doped with phosphorous and boron atoms

The phosphorus atom is called a donor impurity, since it donates an electron that is free to move. Although the remaining phosphorus atom has a net positive charge, the atom is immobile in the crystal and cannot contribute to the current. Therefore, when a donor impurity is added to a semiconductor, free electrons are created without generating holes. This process is called doping and it allows us to control the concentration of free electrons in a semiconductor.

A semiconductor that contains donor impurity atoms called an ***n-type*** semiconductor (for the negatively charged electrons).

The most common group III element used for silicon doping is boron. When a boron atom replaces a silicon atom, its three valence electron s are used to satisfy the covalent bond requirements for three of the four nearest silicon atoms as shown in Figure 3.8(b). This leaves one position open. At room temperature, adjacent silicon valence electrons have sufficient thermal energy to move into this position, thereby creating a hole. The boron atom then has a net negative charge, but cannot move, and a hole is created that can contribute to a hole current.

Because the boron atom has accepted a valence electron, the boron is therefore called an acceptor impurity. Acceptor atoms lead to the creation of holes without electrons being generated. This process, also called doping, can be used control the concentration of holes in a semiconductor.

A semiconductor that contains acceptor impurity atoms is called a ***p-type*** semiconductor (for the positively charged hole created).

The materials containing impurity atoms are called ***extrinsic semiconductors*** or ***doped semiconductors***. The doping process, which allows us to control the concentrations of free electrons and holes, determines the conductivity and currents in the material.

In an n-type semiconductor, electrons are called the ***majority carrier*** because they far outnumber the holes, which are termed the ***minority carrier***. In contrast, in a p-type semiconductor, the holes are majority carrier and electrons are minority carrier (Neamen, 1996).

3.4. The p-n Junction

Where an n-type semiconductor comes into contact with a p-type semiconductor, a p-n junction is formed as shown in Figure 3.9 . Since there is a concentration difference of holes and electrons between two types of semiconductors, holes diffuse from the p type region into the n-type region and, similarly, electrons from the n-type material diffuse into the p-type region. As the carriers diffuse, the charged impurities (ionized acceptors in the p-type material and ionized donors in the n-type material) are uncovered. As these impurity charges are uncovered, an electric field (or electrostatic potential difference) is produced, which limits the diffusion of the holes and electrons. The transition region between the n-type and the p-type semiconductors is called the *space-charge region*. It is also often called the *depletion region*, since it is effectively depleted of both holes and electrons.

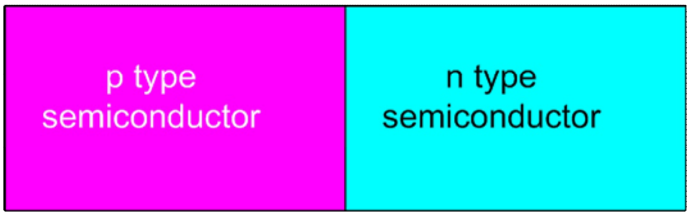

Figure 3.9. The p-n junction

Assuming that the p-type and the n-type regions are sufficiently thick, the regions on either side of the depletion region are essentially charge-neutral (often termed quasi-neutral). The electrostatic potential difference resulting from the junction formation is called the built-in voltage, V_{bi}. It arises from the electric field created by the exposure of the positive and the negative space charge in the depletion region as shown in Figure 3.10 (Luque & Hegedus, 2003).

3.5. The p-n Junction Diode

Anyone familiar with semiconductors will immediately recognize that what has been described thus far is just a common, conventional p–n junction diode, the characteristics of which are presented in Figure 3.11. If we were to apply a voltage V_d across the diode terminals, forward current would flow easily through the diode from the p-side to the n-side; but if we try to send current in the reverse direction, only a very small ($\approx 10^{-12}$ A/cm^2) reverse saturation current I_0 will flow. This reverse saturation current is the result of thermally generated carriers with the holes being swept into the p-side and the electrons into the n-side. In the forward direction, the voltage drop across the diode is only a few tenths of a volt.

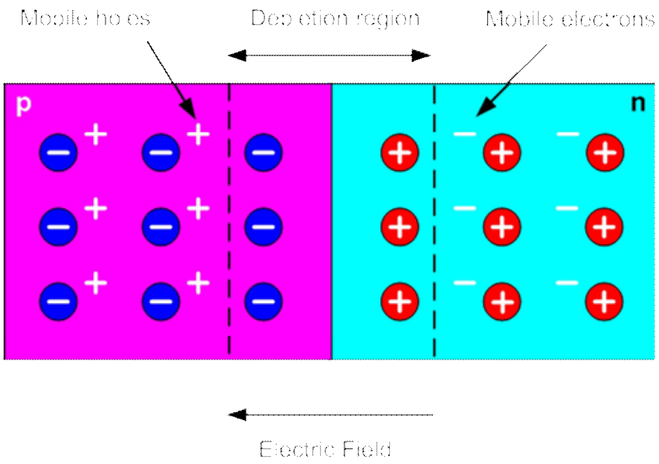

Figure 3.10. p-n junction diode and build-in electric field

The voltage–current characteristic curve for the p–n junction diode is described by the following diode Equation:

$$I_D = I_0\left[\exp\left(\frac{qV_D}{kT}\right) - 1\right] \quad (3.1)$$

where

- I_O is the reverse saturation current of diode (A),
- I_D is the diode current (A)
- q is the electron charge (1.602×10^{-19} C),
- V_D is the voltage across the diode, from p-side to n-side (V),
- k is the Boltzmann's constant (1.381×10^{-23} J/K),
- T is the junction temperature in Kelvin (K).(Gilbert, 1998)

Note that, the reverse saturation current is due to the diffusive flow of minority electrons from the p-side to the n-side and the minority holes from the n-side to the p-side. Hence I_O, reverse saturation current depends on the diffusion coefficient of electrons and holes. The minority carriers are thermally generated so the reverse saturation current is almost unaffected by the reverse bias but is highly sensitive to temperature changes. I_0 , reverse saturation current of diode increases as T increases and decreases as material quality increases. Temperature dependence of the I_0 is very import for PV cells. Called as *thermal voltage kT/q* term (V_T) is 25.85 mV at 300 K.

While the diode Equation (3.2) is appropriate for our purposes, it should be noted that in some circumstances it is modified with an "ideality factor" n, a number between 1 and 2, which accounts for different mechanisms responsible for moving carriers across the junction. The resulting equation is then

$$I_d = I_0\left[\exp\left(\frac{qV_D}{nkT}\right) - 1\right] \tag{3.2}$$

where the ideality factor n is 1 if the transport process is purely diffusion, and $n \approx 2$ if it is primarily recombination in the depletion region.

3.6. Optical Absorption in a Semiconductor

The unit energy of light, called a photon, is hv, where v is the light frequency and h is Planck's constant. The wavelength of light λ is related to the frequency by

$$\lambda = \frac{c}{v} = \frac{hc}{E_{ph}} \tag{3.3}$$

where E_{ph} is the photon energy hv in electron volts and c is the speed of light. When a semiconductor is illuminated, photons may or may not be absorbed, depending on the photon energy and the band-gap energy E_g. Photons with energy smaller than E_g

are not readily absorbed by the semiconductor because there is no energy state available in the forbidden gap to accommodate an electron as shown in Figure 3.11(a). Thus light is transmitted through and the material appears transparent. If E_{ph}=E_g, photons are absorbed to create electron-hole pairs, as shown in Figure 3.11(b). When the photon energy is greater than E_g, an electron-hole pair is generated and, in addition, the excess energy E_{ph}-E_g is dissipated as heat as shown as Figure 3.11(c) (Yang, 1978).

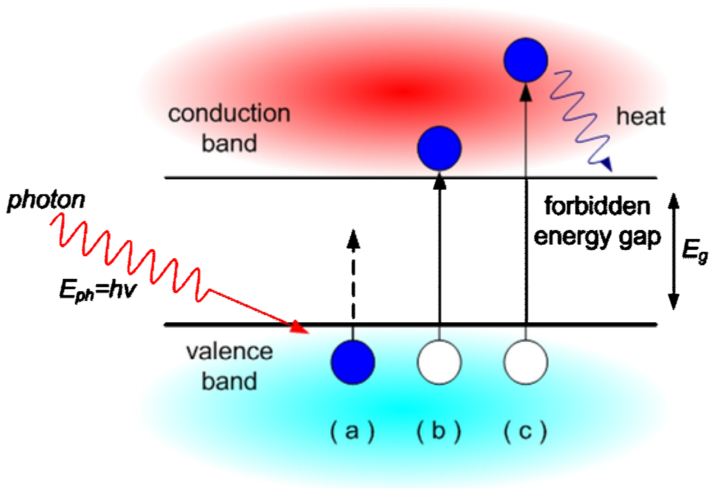

Figure 3.11. Creation of the electron-hole pairs by photons

3.7. Recombination

When the illumination is stopped, the system must return to a state of equilibrium and the electron-hole pairs generated by the light must disappear. With no external source of energy, the electrons and holes wander around until they meet up and recombine. Any defects or impurities within or at the surface of the semiconductor promote recombination.

The carrier lifetime of a material is defined as the average time for recombination to occur after electron-hole generation. For silicon, this is typically 1 µs. Similarly, the carrier diffusion length is the average distance a carrier can move from point of generation until it recombines. For silicon, this is typically 100–300 µm. These two parameters give an indication of material quality and suitability for solar cell use. However, no power can be produced from a semiconductor without a means of giving directionality to the moving electrons. Therefore, functional solar cells are typically produced from semiconductor material by the addition of a rectifying p-n junction (Wenham & Green, 2007).

3.8. Why p-n Junction? To Create Electric Field

As long as a solar cell is exposed to photons with energies above the band gap energy, hole–electron pairs will be created. The problem is, of course, that those electrons can fall right back into a hole, causing both charge carriers to disappear. To avoid that recombination, electrons in the conduction band must continuously be swept away from holes. In photovoltaic cells this is accomplished by creating a built-in electric field within the semiconductor itself that pushes electrons in one direction and holes in the other. To create the electric field, two regions are established within the crystal. On one side of the dividing line separating the regions, pure (intrinsic) silicon is purposely contaminated with very small amounts of a trivalent element from column III of the periodic chart; on the other side, pentavalent atoms from column V are added (Gilbert, 1998).

3.9. From p-n Junction to Solar Cell

When the p-n junction is exposed to light, because of photons are absorbed, electron– hole pairs are generated in silicon atoms in both sides of the junction, i.e., electrons are excited from the valence band to the conduction band, leaving holes behind. These electrons, however, will soon fall back into holes causing charge carriers to disappear. If these mobile charge carriers reach the vicinity of the junction, the electric field in the depletion region will push the holes into the p-side and push the electrons into the n-side, as shown in Figure 3.12. The p-side accumulates holes and the n-side accumulates electrons, which creates a voltage that can be used to deliver current to a load.

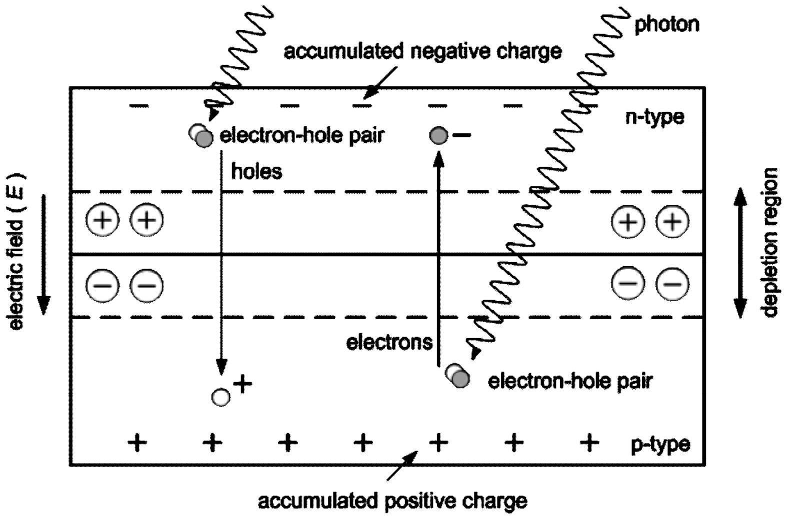

Figure 3.12. Electric field and electron-hole pairs in the p-n junction solar cell

If electrical contacts are attached to the top and bottom of the cell, electrons will flow out of the n-side into the connecting wire, through the load and back to the p-side as shown in Fig. 3.13.

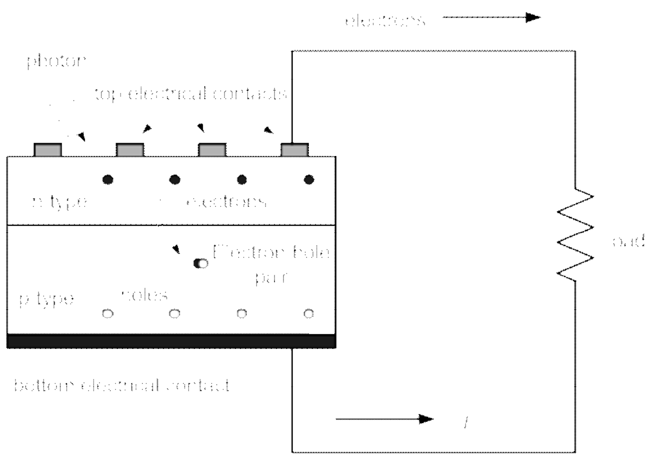

Figure 3.13. Creation electric current and electrons flow in the solar cell

Since wire cannot conduct holes, it is only the electrons that actually move around the circuit. When they reach the p-side, they recombine with holes completing the circuit. By convention, positive current flows in the direction opposite to electron flow, so the current arrow in the figure shows current going from the p-side to the load and back into the n-side (Gilbert, 1998).

In other words, when a PV cell is illuminated, a photocurrent and photo voltage are generated. Absorption of photons of energy greater than the band-gap energy of the semiconductor creates excess minority carriers throughout the illuminated region of the cell (the light intensity in the cell interior falls off exponentially with distance into the cell, but often it penetrates into the base layer). The photo generated minority carriers in the illuminated cell behave like the much smaller population of thermally generated minority carriers in the dark cell. That is, they diffuse from the quasi-neutral regions towards the junction, where they are swept across it by the strong junction field. These fluxes of photo generated minority carriers give rise to the photo generation currents I_{e-ph} and I_{h-ph} , consisting respectively of photo generated electrons drifting from the p to the n side of the junction and photo generated holes drifting the other way. The sum of the two is the overall photocurrent I_{ph}.

The photocurrent is directly proportional to the absorbed photon flux but independent of bias (provided that the junction field is always high enough to sweep carriers across the junction) (Archer & Hill, 2001).

4. THE MODEL OF THE PV CELL

The behavior of photovoltaic (PV) cells can be modeled with an equivalent circuit included current source, diodes and resistors.

4.1. The Simplest Model of the PV Cell

The simplest model of a PV cell is shown as an equivalent circuit in Fig.4.1 that consists of an ideal current source in parallel with an ideal diode. The current source represents the current generated by photons (often denoted as I_{PH} or I_L), and its output is constant under constant temperature and constant incident radiation of light.

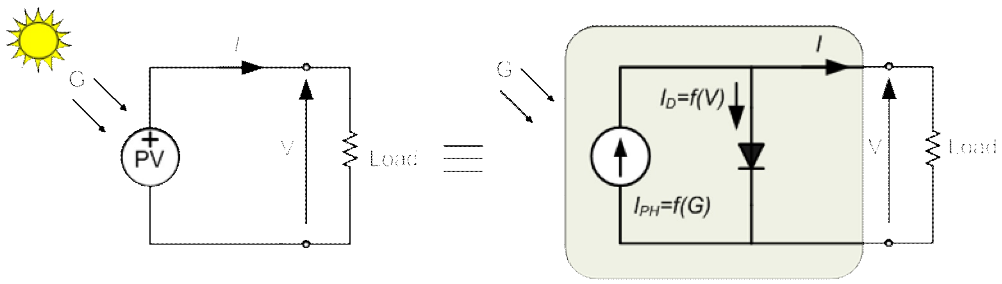

Figure 4.1. Simplest equivalent circuits of the PV

There are two key parameters frequently used to characterize a PV cell.

- Short Circuit Current (I_{SC}) :
  Shorting together the terminals of the cell, as shown in Figure 4.2 (a), no current flows in the (real) diode since $V_d = 0$, so all of the current from the ideal source flows through the shorted leads. Thus photon generated current (I_{PH} or I_L) will equal to short circuit current (I_{SC}).
- Open Circuit Voltage (V_{OC}) :

As shown in Figure 4.2. (b), when there is no connection to the PV cell (open-circuit), the photon generated current is shunted internally by the intrinsic p-n junction diode. This gives the open circuit voltage (V_{OC}).

The PV module or cell manufacturers usually provide the values of these parameters in their datasheets.

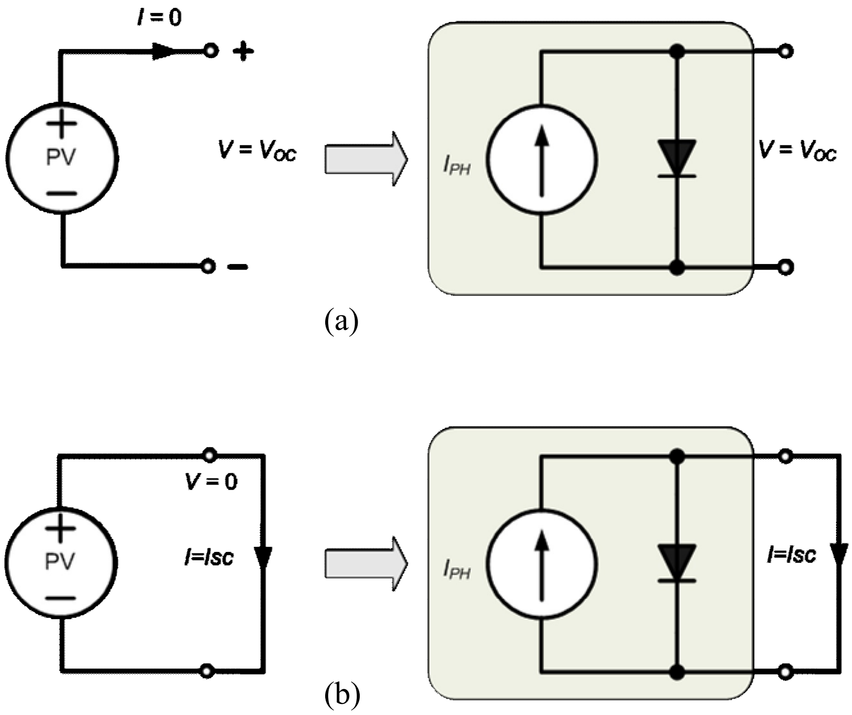

Figure 4.2. Short circuit and open circuit conditions of the PV

The output current I from the PV cell is found by applying the Kirchoff's current law (KCL) on the equivalent circuit shown in Figure 4.1.

$$I = I_{SC} - I_D \tag{4.1}$$

Where, I_{SC} is the short circuit current that is equal to the photo generated current (I_{PH} or I_L), and I_D is the current shunted through the intrinsic diode.

The diode current I_D is given by the diode equation:

$$I_D = I_0 \left[\exp\left(\frac{qV_D}{kT} \right) - 1 \right] \tag{4.2}$$

From Equation (4.1), we find

$$I_D = I_{SC} - I \tag{4.3}$$

and then substituting Equation (4.3) into Equation (4.2) gives current-voltage relationship of the PV cell.

$$I = I_{SC} - I_0 \left[\exp\left(\frac{qV_D}{kT} \right) - 1 \right] \tag{4.4}$$

It can be easily understood that the second term in Equation (4.4) is just the diode equation with a negative sign. That means that a plot of Equation (4.4) is just I_{SC} added to the diode curve turned upside-down as shown in Figure 4.3.

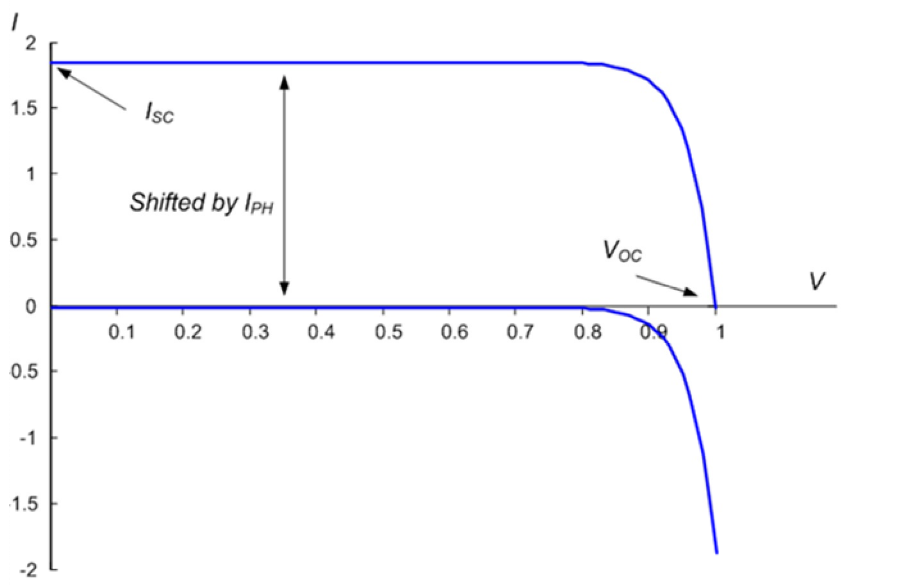

Figure 4.3. PV cell I-V curve and Effect of the photo generated current

The reverse saturation current of diode I_0 is constant under the constant temperature and found by setting the open-circuit condition as shown in Figure 4.2. (b). Using the Equation (4.4), let $I = 0$ (no output current) and we can solve for I_0.

$$I = I_{SC} - I_0\left[\exp\left(\frac{qV_{OC}}{kT}\right) - 1\right] \tag{4.5}$$

$$0 = I_{SC} - I_0\left[\exp\left(\frac{qV_{OC}}{kT}\right) - 1\right] \tag{4.6}$$

$$I_{SC} = I_0\left[\exp\left(\frac{qV_{OC}}{kT}\right) - 1\right] \tag{4.7}$$

$$I_0 = \frac{I_{SC}}{\exp\left(\frac{qV_{OC}}{kT}\right) - 1} \tag{4.8}$$

And we can also find open circuit voltage (V_{OC}) of the PV cell from Equation (4.8);

$$V_{OC} = \frac{kT}{q}\ln\left(\frac{I_{SC}}{I_0} + 1\right) \tag{4.9}$$

As before explained, photo generated current I_{PH} and also short-circuit current, I_{SC}, is directly proportional to solar insolation, which means that we can calculate photo generated current at any irradiance level if the value of I_{SC}, is known from data sheet under standard test condition (STC- G_0=1000W/m^2 at the air mass AM=1.5).

So,

$$I_{SC}\big|_G = \left(\frac{G}{G_0}\right) I_{SC}\big|_{G_0} \tag{4.10}$$

For example when considering PV cell that has below specification at STC (Insolation / irradiance is 1000W/m2 – full sun);

- V_{OC} = 0.55V (=20V/36)
- I_{SC} = 2A

We can calculate ISC value at 500W/m2 (half sun) using Equation (4.10).

$$I_{SC}\Big|_{G=500\,\mathrm{W/m^2}} = \left(\frac{500}{1000}\right)2 = 1\mathrm{A}$$

Figure 4.5 shows that current and voltage relationship (often called as an I-V curve) of this PV cell simulated by MATLAB using the simplest equivalent circuit model.

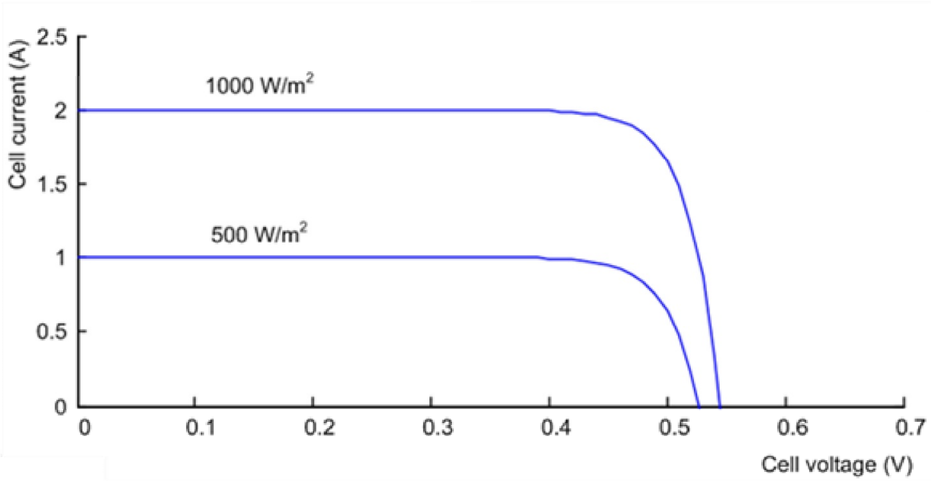

Figure 4.4. I-V curve of the PV cell at different irradiance level

4.2. The I-V curve of the PV and Its Key Parameters

Consider, for the moment, a single PV module that you want to connect to a load. The load might be a dc motor driving a pump or it might be a battery, for example. Before the load is connected, the module sitting in the sun will produce an open-circuit voltage V_{OC}, but no current will flow as shown in Figure 4.2(a). If the terminals of the module are shorted together the short circuit current I_{SC} will flow, but the output voltage will be zero. This condition is shown in Figure 4.2(b). In both cases, since power is the product of current and voltage, no power is delivered by the module and no power is received by the load. When the load is actually connected, some combination of current and voltage will result and power will be delivered. To figure out how much power, we have to consider the I –V characteristic curve of the module as well as the I –V characteristic curve of the load.

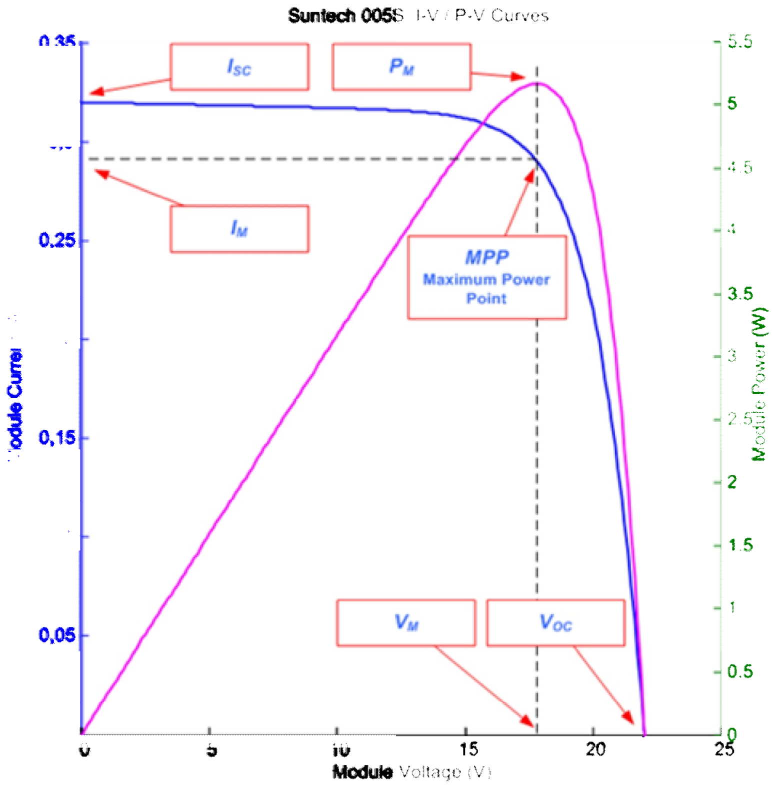

Figure 4.5. I-V and P-V curve of a PV module

Figure 4.5 shows a generic I –V and P−V curve for a PV module obtained using MATLAB, identifying several key parameters including the open-circuit voltage V_{OC} and the short circuit current I_{SC}. Also shown is the product of voltage and current, that is, power delivered by the module. At the two ends of the I –V curve, the output power is zero since either current or voltage is zero at those points.

The maximum power point (MPP) is that spot near the knee of the I –V curve at which the product of current and voltage reaches its maximum. The voltage and current at the MPP are sometimes designated as V_M and I_M for the general case and designated V_R and I_R (for rated voltage and rated current) under the special circumstances that correspond to idealized test conditions.

Another way to visualize the location of the maximum power point is by imagining trying to find the biggest possible rectangle that will fit beneath the I –V curve. As shown in Figure 4.6, the sides of the rectangle correspond to current and voltage, so its area is power.

Another quantity that is often used to characterize module performance is the fill factor (FF). The fill factor is the ratio of the power at the maximum power point to the product of V_{OC} and I_{SC}, so FF can be visualized as the ratio of two rectangular areas, as is suggested in Figure 4.6.

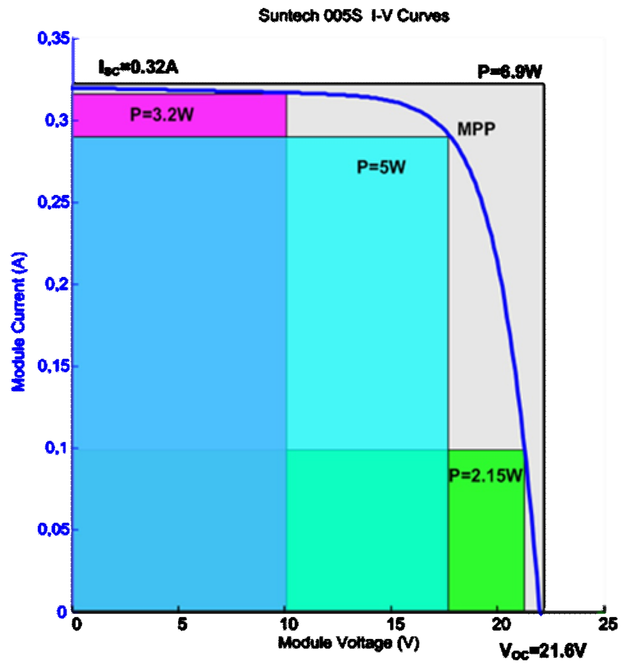

Figure 4.6. Rectangles for Fill Factor

$$\text{Fill Factor (FF)}=\frac{\text{Power at the maximum power point}}{V_{OC}I_{SC}}=\frac{V_M I_M}{V_{OC}I_{SC}} \tag{4.11}$$

4.3. Factors That Affect Characteristics of the PV Cell

The model of the solar cell described in section 4.1 takes into account an ideal behavior of a solar cell based on an ideal diode and ideal current source. Sometime this level-one model is insufficient to accurately represent characteristics of the solar cell. There are several effects which have not been taken into account and that may affect the solar cell response.

4.3.1. Series Resistance

One of the main limitations of the model comes from the series resistive losses which are present in practical solar cells. In fact, the current generated in the solar cell volume travels to the contacts through resistive semiconductor material, both, in p-type region, not heavily doped in general, and in n-type region, which although heavily doped, is narrow. Besides these two components, the resistance of the metal grid, contacts and current collecting bus also contribute to the total series resistive losses. It is common practice to assume that these series losses can be represented by a lumped resistor, R_S, called the series resistance of the solar cell.

4.3.2. Shunt Resistance

Solar cell technology in industry is the result of mass production of devices generally made out of large area wafers, or of large area thin film material. A number of shunt resistive losses are identified, such as localized shorts at the emitter layer or perimeter shunts along cell borders are among the most common. This is represented generally by a lumped resistor, R_{SH}, in parallel with the intrinsic device (Castaner & Silvestre, 2002).

4.3.3. Recombination

It occurs when light - generated electrons and holes, instead of being swept across the p – n junction and collected, meet up and are annihilated. The wastage of charge carriers adversely affects both the voltage and current output from the cell, reducing its efficiency. Some recombination takes place as electrons and holes wander around in the body of the cell (bulk recombination), but most occurs at impurities or defects in the crystal structure near the cell's surfaces, edges, and metal contacts (Lynn, 2010).

4.3.4. Non ideality of the Diffusion Diode

In practice few devices exhibit a totally ideal I−V characteristic with ideality coefficient equal to unity. For this reason it is common practice to also add a parameter 'n' (a number between 1 and 2 which typically increase as the current decreases) to account for these non idealities and diode model can be modified to take into account this effect (Castaner & Silvestre, 2002).

4.4. Shunt and Series Resistances (parasitic resistances) Added PV Model

This circuit includes a series resistance and a diode in parallel with a shunt resistance as shown in Figure 4.7.

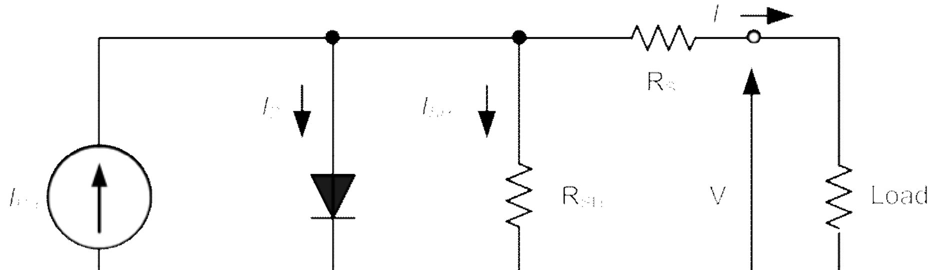

Figure 4.7. Model of the PV cell with parasitic resistances

Application of Kirchhoff's Current Law on the equivalent circuit results in the current flowing to the load;

$$I = I_{PH} - I_D - I_{SH} \tag{4.12}$$

If the diode current and the current through the shunt resistance (I_D and I_{SH} respectively) are expanded, Equation (2.3) is obtained.

$$I = I_{PH} - I_0\left[\exp\left(\frac{q(V + IR_S)}{kT}\right) - 1\right] - \frac{V + IR_S}{R_{SH}} \tag{4.13}$$

To account diode non ideality briefly mentioned before we can add parameter *n* to the diode term in Equation 4.13.

$$I = I_{PH} - I_0\left[\exp\left(\frac{q(V + IR_S)}{nkT}\right) - 1\right] - \frac{V + IR_S}{R_{SH}} \tag{4.14}$$

The effect of these parasitic resistances on the I –V characteristic is shown in Figures 4.7 and 4.8.

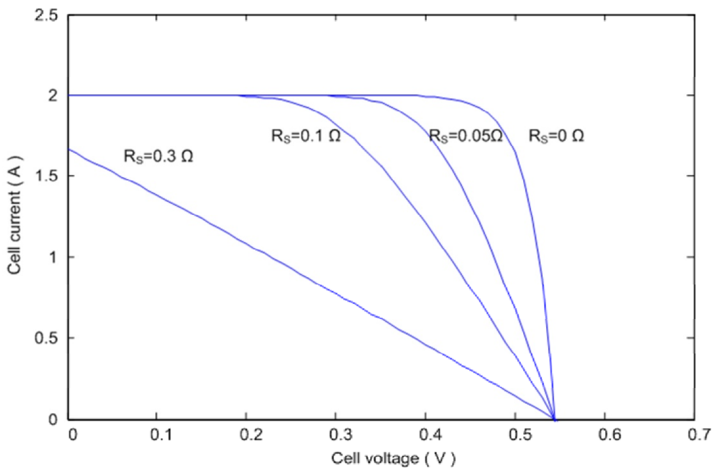

Figure 4.8. Effect of the serial resistance on the PV cell characteristics

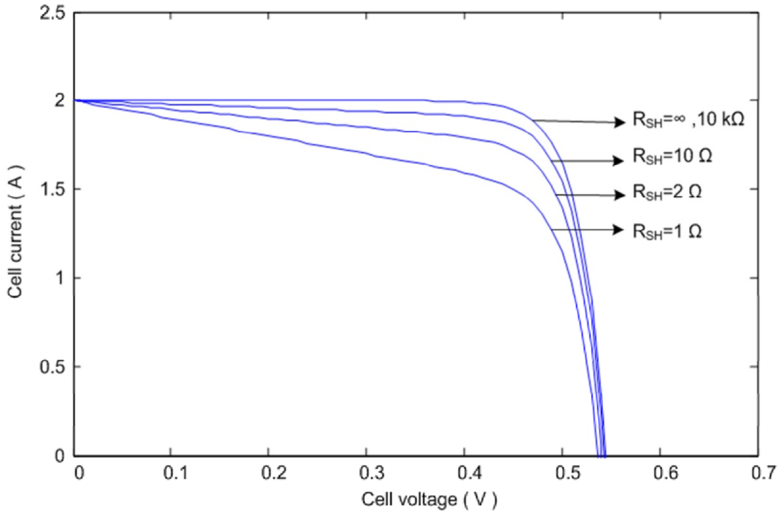

Figure 4.9. Effect of the shunt resistance on the PV cell characteristics

As can also be seen in Equation (4.13), the shunt resistance, R_{SH}, has no effect on the short circuit current, but reduces the open-circuit voltage. Conversely, the series resistance, R_S, has no effect on the open-circuit voltage, but reduces the short-circuit current.

4.5. Recombination Diode, Shunt and Series resistances Added PV Model

It has so far been assumed that there is no recombination loss in the depletion region (space charge region) in the equivalent circuit of the PV cell. However, in real solar cells, depletion-region recombination represents a substantial loss mechanism. So, recombination at the depletion region of solar cells is most important recombination. This is relevant at low voltage bias and can be represented in an equivalent circuit by a second diode term with a saturation density current J_{02}, which is different from the saturation density current of the ideal solar cell diode, and a given ideality diode factor different to 1, it is most often assumed to equal 2.

Assuming that the recombination rate is constant across the space charge region, the resulting recombination rate can be expressed as a recombination current I_{DR} in the depletion region

$$I_{DR} = I_0 \left[\exp\left(\frac{qV_D}{2kT} \right) - 1 \right] \tag{4.15}$$

Adding this depletion layer recombination current to Equation (4.13) gives the two diode model expression in Equation 4.16 and equivalent circuit as shown Figure 4.10 (Archer & Hill, 2001).

$$I = I_{PH} - I_{01} \left[\exp\left(\frac{q(V + I \cdot R_S)}{kT} \right) - 1 \right] - I_{02} \left[\exp\left(\frac{q(V + IR_S)}{2kT} \right) - 1 \right] - \frac{V + IR_S}{R_{SH}} \tag{4.16}$$

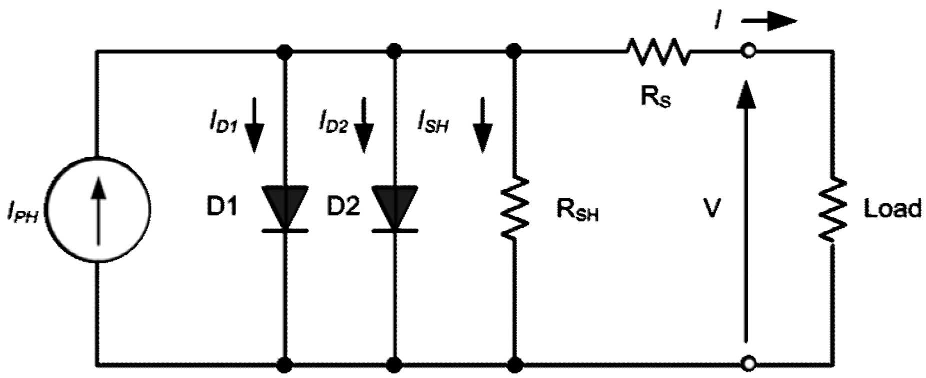

Figure 4.10. Two diode model of the PV cell

In practice, most measured I−V curves of solar cells can be approximated by several exponential regions in the dark forward I−V characteristic revealing the presence of several dark current components. We can take this behavior into account by empirically introducing the ideality factors n_1 and n_2 as explained before in the section 4.2.4 so that Equation (4.15) can be expressed as

$$I = I_{PH} - I_{01}[\exp\left(\frac{q(V + I \cdot R_S)}{n_1 kT}\right) - 1] - I_{02}[\exp\left(\frac{q(V + I \cdot R_S)}{n_2 kT}\right) - 1] - \frac{V + I \cdot R_S}{R_{SH}} \quad (4.17)$$

It is often more convenient to rewrite Equation (4.16) as

$$I = I_{PH} - I_0[\exp\left(\frac{q(V + I \cdot R_S)}{A_0 kT}\right) - 1] - \frac{V + I \cdot R_S}{R_{SH}} \quad (4.18)$$

4.6. From Cell to Module

Since an individual cell produces only about 0.5 V, they are rarely used individually in PV applications. Instead, the basic building block for PV applications is a module consisting of a number of pre-wired cells with similar characteristics in series, all encased in tough, weather resistant packages.

4.6.1. Building of the Module

A typical module has 36 cells in series and is often designated as a 12V. These 12V PV modules are suitable for 12V battery charging systems. Large 72 cell modules are now quite common, some of which have all of the cells wired in series, in which case they are referred to as 24V modules and these modules are generally used in the 24V battery charging systems (Gilbert, 1998).

Under peak sunlight (100 mW/cm^2), the maximum current delivered by a cell is approximately 30 mA/cm^2. Cells are therefore paralleled to obtain the desired current.

Multiple modules can be wired in series to increase voltage and in parallel to increase current, the product of which is power. An important element in PV system design is deciding how many modules should be connected in series and how many in parallel to deliver whatever energy is needed. Such combinations of modules are referred to as an array. Figure 8.28 shows this distinction between cells, modules, and arrays.

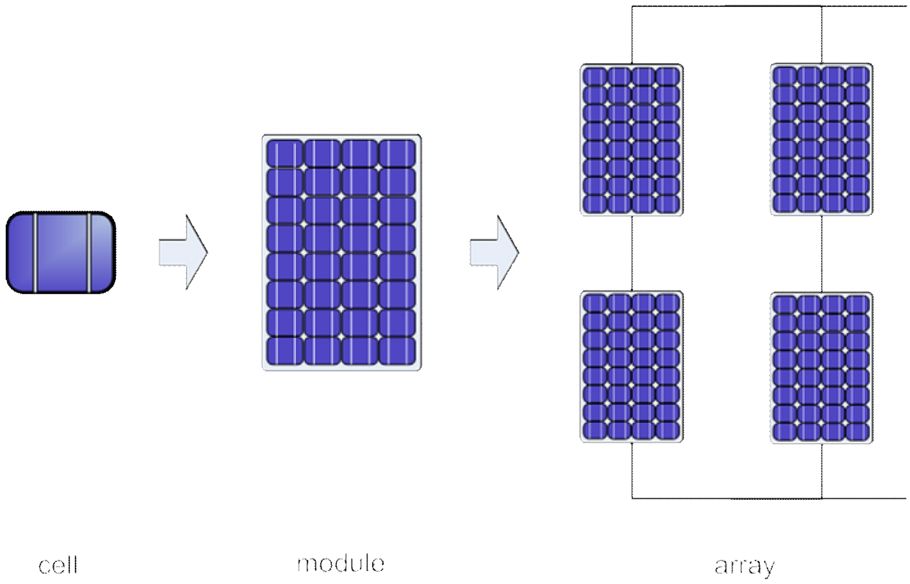

Figure 4.11. PV cell, module and array

4.6.2. The Model of the Series Connected Cells

When the cell model is defined, then the model of other structure (module and array) can be developed. If whole cells are fabricated with common qualities and subjected to a similar state of irradiance and thermal conditions, then the module and array model may be extracted easily, by using Thevenin or Norton equivalent circuits. If the module contains ns series cells, then I_{PH} and I_0 values will be the same in all cells. It is also evident that the string's series resistance is equal to $n{\cdot}R_S$. To calculate the shunt resistance, I_{PH} and I_0 shall be considered as a current source at first, and then this source shall be converted to its Thevenin equivalent circuit, and it becomes clear that the string shunt resistance is equal to $n{\cdot}R_{SH}$. According to this we have figure which shows the string equivalent circuit.

Since all the series diodes in each branch are similar, it is possible to simplify the circuit by assuming just an equivalent diode for each branch. The voltage across new parallel diodes in series shall be divide into *n* before using in it string model calculations. So the extracted string model is similar to the cell model entirely except that the values of its series and shunt resistances are *n* times higher (Shekoofa & Taherbaneh, 2007).

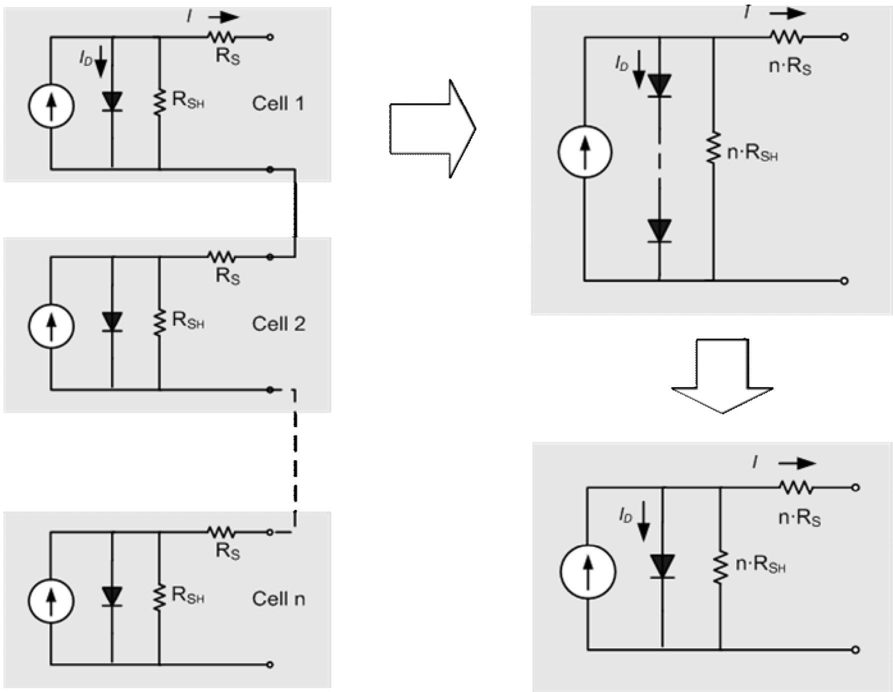

Figure 4.12. Equivalent circuit of the PV module

5. MODELLING OF THE PV USING MATLAB

MATLAB (for **mat**rix **lab**oratory) is a numerical computing environment and fourth-generation programming language. Developed by MathWorks, MATLAB allows matrix manipulations, plotting of functions and data, implementation of algorithms, creation of user interfaces, and interfacing with programs written in other languages, including C, C++, and Fortran.

Although MATLAB is intended primarily for numerical computing, an optional toolbox uses the MuPAD symbolic engine, allowing access to symbolic computing capabilities. An additional package, Simulink, adds graphical multidomain simulation and Model-Based Design for dynamic and embedded systems. MATLAB is widely used in academic and research institutions as well as industrial enterprises (http://www.mathworks.com/).

The use of the equivalent electric circuits makes it possible to model characteristics of a PV cell. The method used here is implemented in MATLAB programs for simulation. The method used here is proposed by Sera et al (2007).There is no difference between modeling of the PV cell and PV module. When the PV cells are wired together in series, the current output is the same as the single cell, but the voltage output is the sum of each cell voltage. So voltage parameter, especially diode voltage, must be divided by the number of cell.

The general current-voltage characteristic of a PV panel based on the single exponential model is:

$$I = I_{PH} - I_0 \left[\exp\left(\frac{V + I \cdot R_S}{n_s V_T} \right) - 1 \right] - \frac{V + I \cdot R_S}{R_{SH}} \tag{5.1}$$

In the above equation, V_T is the junction thermal voltage;

$$V_T = \frac{AkT_{STC}}{q} \tag{5.2}$$

where

- I_{PH} , the photo generated current in STC (Standard Test Conditions)
- I_0 , dark saturation current in STC
- R_S, module series resistance
- R_{SH}, module shunt resistance
- A ,diode quality factor

are the five parameters of the model, while k is Boltzmann's constant, q is the charge of electron, n_s is the number of cells in the PV module connected in series, and T_{STC} (° K) is the temperature at STC. It is a common practice to neglect the term ' −1 ' in Equation (5.1), as in silicon devices, the dark saturation current is very small compared to the exponential term.

5.1. Determination of the PV Module Parameters from Datasheet Values

In order to construct a model of the PV module, which exhibits the specifications described in the datasheet, using the above-mentioned single-diode model, there are five parameters to be determined: I_{PH}, I_0, A, R_S, and R_{SH}. The goal is to find all these parameters without any measurement, using only the data from the product datasheet.

In this thesis, the Suntech STP005S-12/Db PV module was chosen for modeling. The module has 36 series connected monocrystalline cells and provides 5W peak power at standard test condition. The key specifications of STP005 PV panel are shown in Table 5.1.

I_{PH}, I_0, A, R_S, and R_{SH} are not given in datasheet as can be seen in Table 5.1. These parameters can be found using open circuit voltage (V_{OC}), short circuit current (I_{SC}), Optimum operating voltage, (V_{MPP}) Optimum operating current (I_{MPP}) given in Table 5.1.

Table 5.1. The key specifications of PV module taken from the datasheet

Parameter	Value
Cell Type	Mono crystalline silicon
Cell area	62.5mm x 15.62mm
Number of cell	36
Open circuit voltage (V_{OC})	21.6V
Short circuit current (I_{SC})	0.32A
Optimum operating voltage (V_{MPP})	17.4V
Optimum operating current(I_{MPP})	0.29A
Peak power at STC	5W
Short circuit current temperature coefficient	0.555 ± 0.01 %/ K
Open circuit voltage temperature coefficient	-78 ± 10 mV/ K
Peak power temperature coefficient	-0.48 ± 0.005 %/ K
NOCT	45 ± 2℃

5.1.1. Starting Equations

Equation (5.1) can be written for the three key operating points of the I-V characteristic of the PV module:

- the short-circuit point,
- the maximum power point,
- the open-circuit point.

$$I_{SC} = I_{PH} - I_0 \exp\left(\frac{I_{SC} R_S}{n_s V_T}\right) - \frac{I_{SC} R_S}{R_{SH}} \tag{5.3}$$

$$I_{MPP} = I_{PH} - I_0 \exp\left(\frac{V_{MPP} + I_{MPP} R_S}{n_s V_T}\right) - \frac{V_{MPP} + I_{MPP} R_S}{R_{SH}} \tag{5.4}$$

$$I_{OC} = 0 = I_{PH} - I_0 \exp\left(\frac{V_{OC}}{n_s VT}\right) - \frac{V_{OC}}{R_{SH}} \tag{5.5}$$

An additional equation can be derived using the fact that on the P-V characteristic of the panel, at the MPP, the derivative of power with voltage is zero.

$$\left.\frac{dP}{dV}\right|_{\substack{V=V_{MPP}\\ I=I_{MPP}}} = 0 \tag{5.6}$$

So far there are four equations available, but there are five parameters to find, therefore a fifth equation has to be found. For this purpose can be used the derivative of the current with the voltage at short-circuit conditions, which is mainly determined by the shunt resistance R_{SH}.

$$\left.\frac{dI}{dV}\right|_{I=I_{SC}} = -\frac{1}{R_{SH}} \tag{5.7}$$

5.1.2. Parameter Extraction

From the expression of the current at short-circuit and open circuit conditions, the photo-generated current I_{ph} and the dark saturation current I_o can be expressed:

$$I_{PH} = I_0 \exp\left(\frac{V_{OC}}{n_s VT}\right) + \frac{V_{OC}}{R_{SH}} \tag{5.8}$$

By inserting Equation (5.8) into Equation (4.13), it takes the form:

$$I_{SC} = I_0\left[\exp\left(\frac{V_{OC}}{n_s V_T}\right) - \exp\left(\frac{I_{SC} R_S}{n_s V_T}\right)\right] + \frac{V_{OC} - I_{SC} R_S}{R_{SH}} \tag{5.9}$$

The second term in the parenthesis from the above equation can be omitted, as it has insignificant size compared to the first term. Than Equation (5.19) becomes:

$$I_{SC} = I_0 \exp\left(\frac{V_{OC}}{n_s V_T}\right) + \frac{V_{OC} - I_{SC} R_S}{R_{SH}} \tag{5.10}$$

Solving the above equation for I_0 result in:

$$I_0 = \left(I_{SC} - \frac{V_{OC} - I_{SC} R_S}{R_{SH}}\right) \exp\left(-\frac{V_{OC}}{n_s V_T}\right) \tag{5.11}$$

Equations (5.8) and (5.11) can be inserted into Equation (5.4), which will take the form:

$$\begin{aligned} I_{MPP} = I_{SC} - \frac{V_{MPP} + I_{MPP} R_S - I_{SC} R_S}{R_{SH}} - \\ \left(I_{SC} - \frac{V_{OC} - I_{SC} R_S}{R_{SH}}\right) \exp\left(\frac{V_{MPP} + I_{MPP} R_S}{n_s V_T}\right) \end{aligned} \tag{5.12}$$

The above expression still contains three unknown parameters: R_S, R_{SH} and A. The derivative of the power with voltage at MPP can be written as:

$$\left.\frac{dP}{dV}\right|_{\substack{V = V_{MPP} \\ I = I_{SC}}} = \frac{d(IV)}{dV} = I + \frac{dI}{dV} V \tag{5.13}$$

Thereby, to obtain the derivative of the power at MPP, the derivative of Equation (5.12) with voltage should be found. However, Equation (5.12) is a transcendent equation, and it needs numerical methods to express I_{MPP}. Equation (5.12) can be written in the following form:

$$I = f(I, V) \tag{5.14}$$

where f *(I, V)* is the right side of Equation (5.12). By differentiating Equation (5.14):

$$dI = dI\,\frac{\partial f\left(I,V\right)}{\partial I} + dV\,\frac{\partial f\left(I,V\right)}{\partial V} \tag{5.15}$$

The derivative of the current with voltage results in:

$$\frac{dI}{dV} = \frac{\frac{\partial}{\partial V} f\left(I,V\right)}{1 - \frac{\partial}{\partial I} f\left(I,V\right)} \tag{5.16}$$

From Equations (5.16) and (5.13) results:

$$\left.\frac{dP}{dV}\right|_{\substack{V=V_{MPP}\\ I=I_{MPP}}} = I_{MPP} + \frac{V_{MPP}\,\frac{\partial}{\partial V} f\left(I,V\right)}{1 - \frac{\partial}{\partial I} f\left(I,V\right)} \tag{5.17}$$

From the above:

$$\left.\frac{dP}{dV}\right|_{\substack{V=V_{MPP}\\ I=I_{MPP}}} = I_{MPP} + V_{MPP}\,\frac{-\frac{\left(I_{SC}R_{SH} - V_{OC} + I_{SC}R_S\right)\exp\left(\frac{V_{MPP} + I_{MPP}R_S - V_{OC}}{n_s V_T}\right)}{n_s V_T R_{SH}} - \frac{1}{R_{SH}}}{1 + \frac{\left(I_{SC}R_{SH} - V_{OC} + I_{SC}R_S\right)\exp\left(\frac{V_{MPP} + I_{MPP}R_S - V_{OC}}{n_s V_T}\right)}{n_s V_T R_{SH}} + \frac{R_S}{R_{SH}}} \tag{5.18}$$

There are two equations, Equations (5.12) and (5.18) with three unknowns. Equation (5.7) can be used as the third equation. Equations (5.7), (5.17) and (5.18) lead to:

$$-\frac{1}{R_{SH}}\bigg|_{I=I_{SC}} = \frac{-\dfrac{\left(I_{SC}R_{SH} - V_{OC} + I_{SC}R_S\right)\exp\left(\dfrac{I_{SC}R_S - V_{OC}}{n_s V_T}\right)}{n_s V_T R_{SH}} - \dfrac{1}{R_{SH}}}{1 + \dfrac{\left(I_{SC}R_{SH} - V_{OC} + I_{SC}R_S\right)\exp\left(\dfrac{I_{SC}R_S - V_{OC}}{n_s V_T}\right)}{n_s V_T R_{SH}} + \dfrac{R_S}{R_{SH}}} \tag{5.19}$$

It is possible now to determine all the three unknown parameters, the R_S, A, and R_{SH} using Equations (5.12), (5.18) and (5.19). As these equations do not allow separating the unknowns and solving them analytically, they are solved using numerical methods. The flowchart for determining these variables is shown in Figure 5.1.

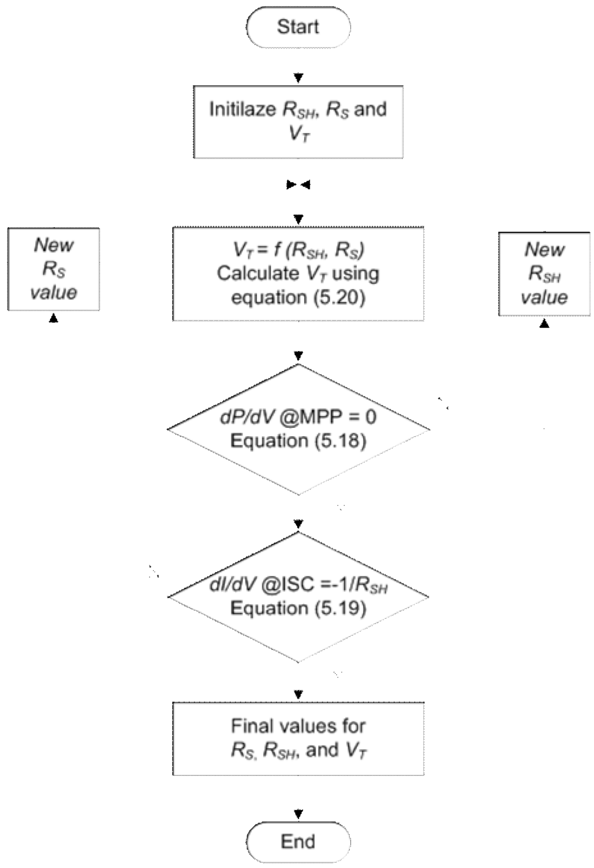

Figure 5.1. Flowchart for determining R_S, R_{SH}, and V_T

$V_T = f(R_S, R_{SH})$, in the flowchart, can be obtained from Equation (5.12):

$$V_T = \frac{V_{MPP} + I_{MPP} R_S - V_{OC}}{n_s \ln \left[\dfrac{(I_{MPP} - I_{SC})(R_{SH} + R_S) + V_{MPP}}{-\left[I_{SC} (R_S + R_{SH}) - V_{OC} \right]} \right]} \tag{5.20}$$

5.2. Construction of Full Characteristic Model of the PV Module

5.2.1. Expression of the Photo Current and Dark Saturation Current

The first equations when constructing the model of the PV module are the expression of Equation (5.11) and Equation (5.15), in STC.

The expression of the dark saturation current I_0 in Equation (5.11), repeated here,

$$I_0 = \left(I_{SC} - \frac{V_{OC} - I_{SC} R_S}{R_{SH}} \right) \exp\left(-\frac{V_{OC}}{n_s V_T} \right)$$

Using Equation (4.23) we find photo current I_{PH} as ;

$$I_{PH} = I_0 \exp\left(\frac{V_{OC}}{n_s V_T} \right) + \frac{V_{OC}}{R_{SH}} \tag{5.21}$$

The above expressions are considered in STC. To include the effects of the environment, e.g. temperature and irradiance, these equations has to be completed with corresponding terms.

5.2.2. Irradiance Dependence of I_{SC} and I_0

Both of them are considered to be directly proportional to the irradiation. So:

$$I_{sc}(G) = GI_{sc} \ , I_{ph}(G) = GI_{ph} \tag{5.22}$$

In other words, if the value I_{sc} is known from datasheet, under the standard test condition , G_{STC} then the short circuit current and photo current at any other irradiance , G is given by:

$$I_{sc}\big|_G = \left(\frac{G}{G_{STC}}\right) I_{sc}\big|_{STC} \ , \ I_{ph}\big|_G = \left(\frac{G}{G_{STC}}\right) I_{ph}\big|_{STC} \tag{5.23}$$

5.2.3. Open Circuit Voltage Temperature and Irradiance Dependence

In order to include the irradiance dependence in the equation of V_{oc}, the open-circuit voltage can be expressed from Equation (5.5):

$$V_{OC}\big|_G = \ln\left(\frac{I_{PH}\big|_G R_{SH} - V_{OC}\big|_G}{I_0 R_{SH}}\right) n_s V_T \tag{5.24}$$

The above equation needs to be solved numerically. Using the Newton-Raphson algorithm, the result can be found after a few iterations, using the open-circuit voltage at STC. The Newton's method is described as:

$$x_{n+1} = x_n - \frac{f(x_n)}{f'(x_n)} \tag{5.25}$$

where $f'(x)$ is the derivative of the function, $f(x) = 0$, x_n is a present value, and x_{n+1} is a next value.

Rewriting the Equation (4.25) gives the following function:

$$f\left[V_{OC}\big|_G\right] = -V_{OC}\big|_G + \ln\left(\frac{I_{PH}\big|_G R_{SH} - V_{OC}\big|_G}{I_0 R_{SH}}\right) n_s V_T = 0 \tag{5.26}$$

$$f'\left[V_{OC}\big|_G\right] = -\frac{n_s V_T}{I_{PH}\big|_G R_{SH} - V_{OC}\big|_G} - 1 \qquad (5.27)$$

Then, substituting Equations (5.26) and (5.27) into Equation (5.25) we obtain;

$$\left(V_{OC}\big|_G\right)_{n+1} = \left(V_{OC}\big|_G\right)_n - \frac{\ln\left(\dfrac{I_{PH}\big|_G R_{SH} - \left(V_{OC}\big|_G\right)_n}{I_0 R_{SH}}\right) n_s V_T - \left(V_{OC}\big|_G\right)_n}{\left(-\dfrac{n_s V_T}{I_{PH}\big|_G R_{SH} - \left(V_{OC}\big|_G\right)_n} - 1\right)} \qquad (5.28)$$

The open-circuit voltage shows a linear dependence with the temperature:

$$V_{OC}\big|_T = V_{OC} + \alpha_{VOC}\left(T - T_{STC}\right) \qquad (5.29)$$

where $\propto_{VOC}$ is open circuit voltage temperature coefficient, T_{STC} is temperature at the standard test condition.

5.2.4. Temperature Dependence of the Short Circuit Current

The short-circuit current of the PV panel depends linearly on the temperature:

$$I_{SC}\big|_T = I_{SC}\left(1 + \frac{\alpha_{ISC}}{100}\left(T - T_{STC}\right)\right) \qquad (5.30)$$

where $\propto_{ISC}$ is short circuit current temperature coefficient.

5.2.5. Temperature Dependence of the Dark Saturation Current

The dark saturation current does not depend on the irradiance conditions, but it shows a strong dependence with temperature (Castaner & Silvestre, 2002).

Castaner and Silvestre give a formula which shows a non-linear dependence with temperature:

$$J_0 = BT^{XTI} \exp\left(\frac{-Eg}{kT}\right) \tag{5.31}$$

where J_0 is the dark saturation current density, B and XTI are constants , and E_g is the semiconductors band gap energy. B and XTI are independent on temperature. It can also be used, a cubic dependence of I_o on temperature (Gow & Manning, 1999)(Walker, 2001):

$$I_0\big|_T = I_0\big|_{T_1}\left(\frac{T}{T_1}\right)^{\frac{3}{A}} \exp\left[\frac{-qEg}{Ak}\left(\frac{1}{T_1}-\frac{1}{T_2}\right)\right] \tag{5.32}$$

where $I_0\big|_{T1}$ is the dark saturation current calculated at a given reference (standard) temperature. E_g is the band gap energy of the semiconductor.

A different way is used, proposed by Sera and Teodorescu (Sera, Teodorescu, & Rodriguez, 2007), to calculate temperature dependence of dark saturation current in this thesis.

By updating the parameters of Equation (5.21) with their corresponding temperature coefficients:

$$I_0\big|_T = \left[I_{SC}\big|_T - \frac{V_{OC}\big|_T - I_{SC}\big|_T R_S}{R_{SH}}\right] \exp\left(-\frac{V_{OC}\big|_T}{n_s V_T}\right) \tag{5.33}$$

As the expression of I_0 in Equation (5.21) is valid in STC (based on the Shockley equations), it is a natural step to consider it valid also at other temperatures than the STC, as the Shockley equation includes the temperature effects. The temperature dependence of all the parameters in Equation (5.21) is given in the data sheet.

5.2.6. Temperature Dependence of the Photo Current

The photo-current temperature dependence can be expressed by including in Equation (5.22) the temperature effect:

$$I_{PH}\big|_T = I_0\big|_T \exp\left(\frac{V_{OC}\big|_T}{n_s V_T}\right) + \frac{V_{OC}\big|_T}{R_{SH}} \tag{5.34}$$

5.3. Full Characteristic Model

The parameters in Equations (5.23), (5.25), (5.30), (5.31), (5.34) and (4.35) can be inserted in Equation (5.1) to obtain the I-V relationship of the PV module, which takes into account the irradiance and temperature conditions.

$$I\big|_{T,G} = I_{PH}\big|_{T,G} - I_0\big|_T \left[\exp\left(\frac{V + I\big|_{T,G} R_S}{n_s V_T\big|_T}\right) - 1\right] - \frac{V + I\big|_{T,G} R_S}{R_{SH}} \tag{5.35}$$

Equation (5.35) is a complex equation because the solution of current is recursive by inclusion of a series resistance in the model. Although it may be possible to find the answer by simple iterations, the Newton's method is chosen for rapid convergence of the answer as described in section 5.3.3. Assuming that rewriting Equation (5.35) gives the following function;

$$f(I) = -I + I_{PH} - I_0\left[\exp\left(\frac{V + IR_S}{n_s V_T}\right) - 1\right] - \frac{V + IR_S}{R_{SH}} = 0 \tag{5.36}$$

$$I_{n+1} = I_n - \frac{f(I_n)}{f'(I_n)} \tag{5.37}$$

Plugging Equation (5.36) into the Equation (5.37) gives a following recursive equation, and the output current (I) is computed iteratively using MATLAB.

$$I_{n+1} = I_n - \frac{I_{PH} - I_n - I_0\left[\exp\left(\frac{V + I_n R_S}{n_s V_T}\right) - 1\right] - \frac{V + I_n R_S}{R_{SH}}}{-1 - \frac{R_S}{n_s V_T} I_0\left[\exp\left(\frac{V + I_n R_S}{n_s V_T}\right) - 1\right] - \frac{R_S}{R_{SH}}} \quad (5.38)$$

Computation steps of current of the PV module I_{MODULE} is summarized as flowchart shown in Figure 5.2 (Sera, Teodorescu, & Rodriguez, 2007).

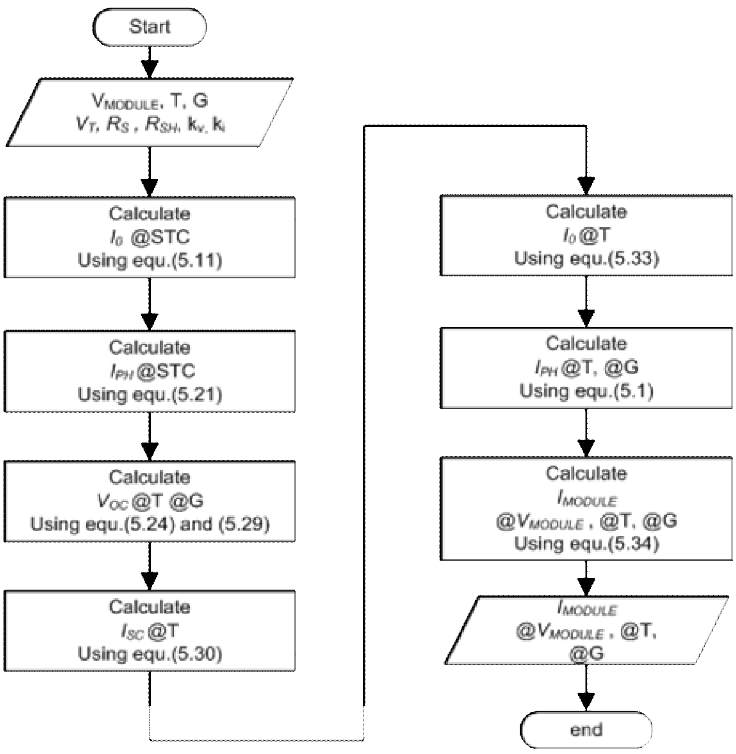

Figure 5.2. Computation process of the current of the PV module

5.4. Verification of the Model

To verify accuracy of the model, real data and simulation data must be compared. For this, datasheet of ShellSQ75 module is used because of that this datasheet provides I−V curves of the module. ShellSQ75 module parameters taken from datasheet and calculated by MATLAB are given in Table 5.2. Comparison results are shown in Figure 5.3.

Table 5.2. Key parameters of the Shell SQ75 PV module

From Datasheet	From MATLAB
• I_{SC}=4.8 A	• R_S=0.2966 Ω
• I_{MPP}=4.4 A	• R_{SH}=506 Ω
• V_{OC}=21.7 V	• V_T= 0.0368 V
• V_{MPP}=17 V	• A=1.4320 (quality factor)
• n_s=36 serial cells	
• α_{ISC}=0.014±0.01 %/ K	
• α_{VOC}=−81±10 mV/ K	

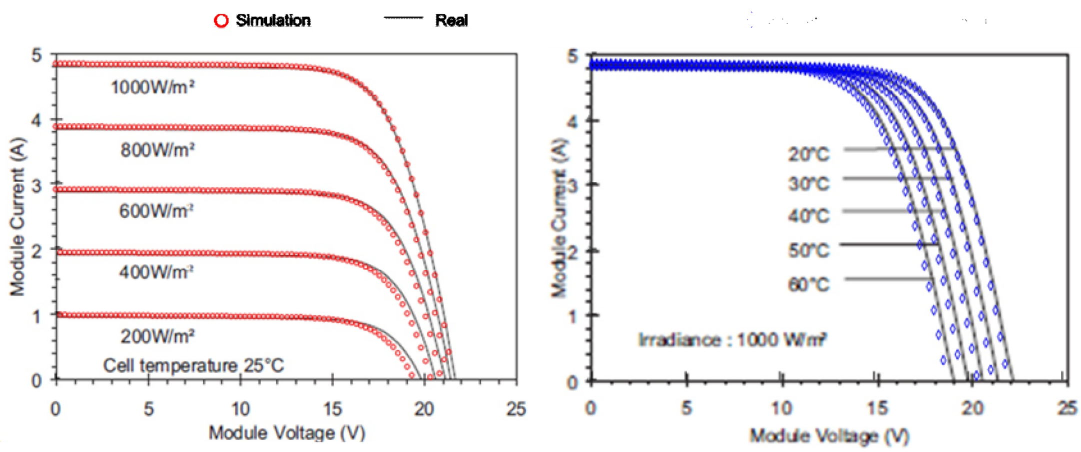

Figure 5.3. Comparison results of the PV model

Differences between datasheet and model are given in table

Table 5.3. Comparison of the datasheet and model

T (°C)	*G* (kW/m^2)	DATASHEET		MODEL		DIFFERENCE (%)	
		V_{OC} (V)	I_{SC} (A)	V_{OC} (V)	I_{SC} (A)	V_{OC} (V)	I_{SC} (A)
25	0.2	19,81	0,95	19,44	0,96	1,86	-1,05
25	0.4	20,60	1,91	20,45	1,92	0,72	-0,52
25	0.6	21,15	2,87	20,95	2,88	0,94	-0,34
25	0.8	21,62	3,85	21,21	3,84	1,89	0,25
25	1	21,70	4,80	21,4	4,80	1,38	0,00
20	1	22,02	4,81	21,98	4,79	0,18	0,41
30	1	21,36	4,83	21,23	4,80	0,61	0,62
40	1	20,65	4,86	20,47	4,81	0,87	1,02
50	1	19,78	4,87	19,59	4,81	0,96	1,23
60	1	19,05	4,89	18,84	4,82	1,10	1,43

Results are show that real data obtained from datasheet and simulation data obtained using model explained this chapter and given above parameters is very consistent.

5.5. Simulation Results of the PV Model

Key parameters of the Suntech STP005S PV module are given in Table 5.3. R_S, R_{SH}, V_T and A values computed by MATLAB using processing steps summarized as flowchart shown in Figure 5.1.

Table 5.4. Key parameters of the STP005S PV module

From Datasheet	From MATLAB
• I_{SC}=0.32 A	• $R_S=1.40\ \Omega$
• I_{MPP}=0.29 A	• $R_{SH}=3659\ \Omega$
• V_{OC}=21.6 V	• $V_T= 0.0418\ V$
• V_{MPP}=17.4 V	• *A=1.6254 (quality factor)*
• n_s=36 serial cells	
• α_{ISC}=0.555±0.01 %/ K	
• α_{VOC}=−78±10 mV/ K	

The model of the Suntech STP005S formed with parameters computed by MATLAB and taken from PV module datasheet is simulated using MATLAB and results are shown in Figure 5.4 and Figure 5.5.

While Figure 5.4 shows I-V curve at different temperature levels and constant irradiance (1 kW/m^2) level, Figure 5.5 shows I-V curve at different irradiance levels and constant temperature (25 °C).

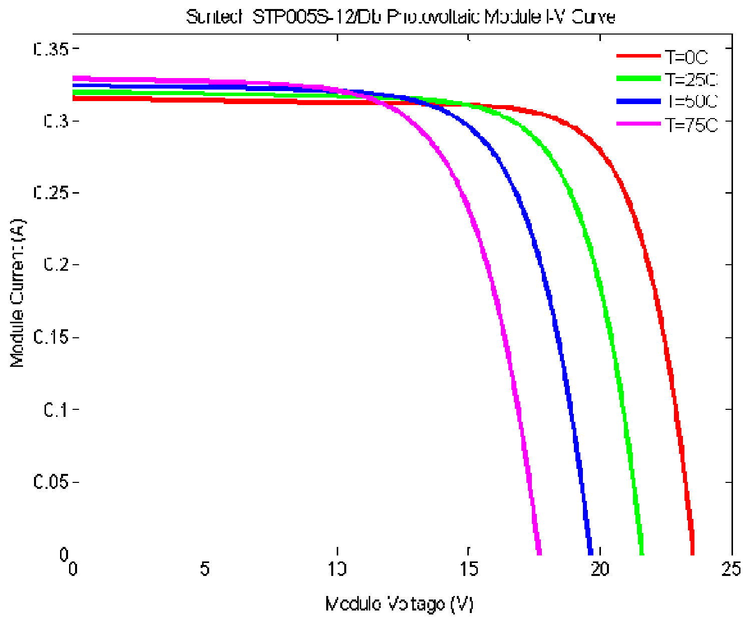

Figure 5.4. STP005S I-V curves at different temperatures and G=1kW/m^2

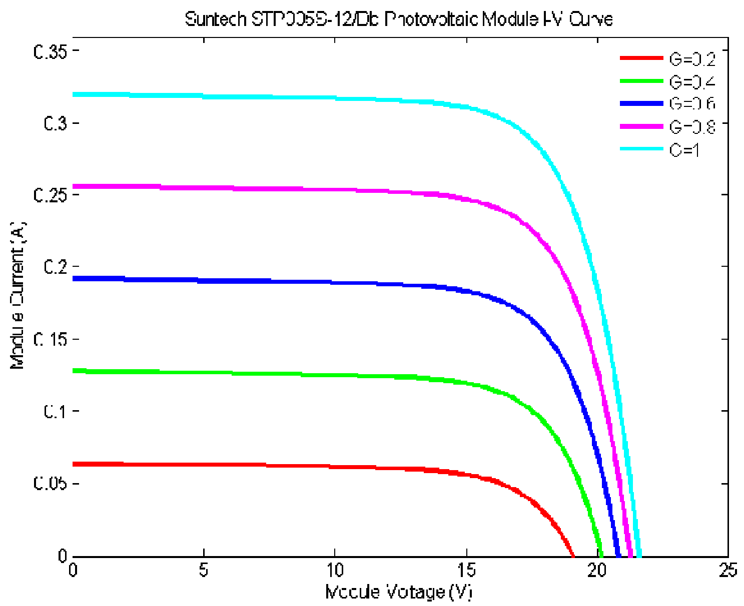

Figure 5.5. STP005S I-V curves at different irradiances and T=25 °C

6. MPPT

At a given temperature and insolation level, PV cells supply maximum power at one particular operation point called the maximum power point (MPP). Unlike conventional energy sources, it is desirable to operate PV systems at its MPP.

6.1. Operating Point

While the I–V curve for a photovoltaic cell, module, or array defines the combinations of voltage and current that are permissible under the existing ambient conditions, it does not by itself tell us anything about just where on that curve the system will actually be operating. This determination is a function of the load into which the PVs deliver their power. Just as PVs have an I–V curve, so do loads. As shown in Figure 6.1, the same voltage is across both the PVs and load, and the same current runs through the PVs and load. Therefore, when the I–V curve for the load is plotted onto the same graph that has the I–V curve for the PVs, the intersection point is the one spot at which both the PVs and load are satisfied. This is called the *operating point* (Gilbert, 1998).

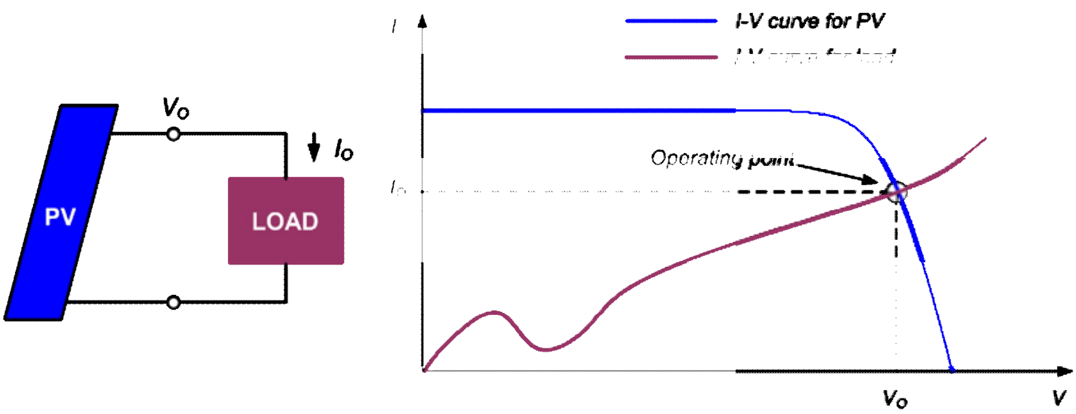

Figure 6.1. PV I-V curve and operating point

6.2. Maximum Power Point

To illustrate the importance and need for load curves, consider a simple resistive load as shown in Figure 6.2. For the load,

$$V = IR \qquad \text{or} \qquad I = \left(\frac{1}{R}\right)V \tag{6.1}$$

which, when plotted on current versus voltage axes, is a straight line with slope 1/R. As R increases, the operating point where the PV and resistance I–V curves intersect moves along the PV I–V curve from left to right.

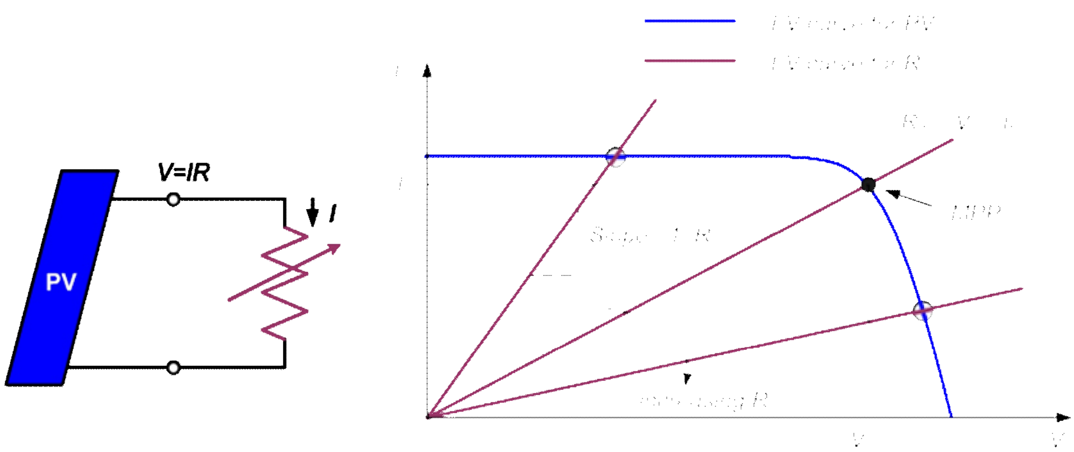

Figure 6.2. PV I-V curve with resistive load line

Since power delivered to any load is the product of current and voltage, there will be one particular value of resistance that will result in maximum power:

$$R_m = \frac{V_m}{I_m} \tag{6.2}$$

where V_m and I_m are the voltage and current at the maximum power point (MPP) (Gilbert, 1998).

Under the special conditions at which modules are tested, the MPP corresponds to the rated voltage V_R (V_M) and current I_R (I_M) of the module. That means the best value of resistance, for maximum power transfer, should be V_R/I_R under STC. As Figure 6.3 shows, however, with a fixed resistance the operating point slips off the MPP as conditions change and the module becomes less and less efficient.

At a given temperature and insolation level, PV cells supply maximum power at one particular operation point called the maximum power point (MPP) as mentioned before. However, the MPP locus varies over a wide range, depending on PV array temperature and insolation intensity as shown in Figure 6.3. Instantaneous shading conditions and ageing of PV cells also affect the MPP locus. In addition, the load electrical characteristics may also vary.

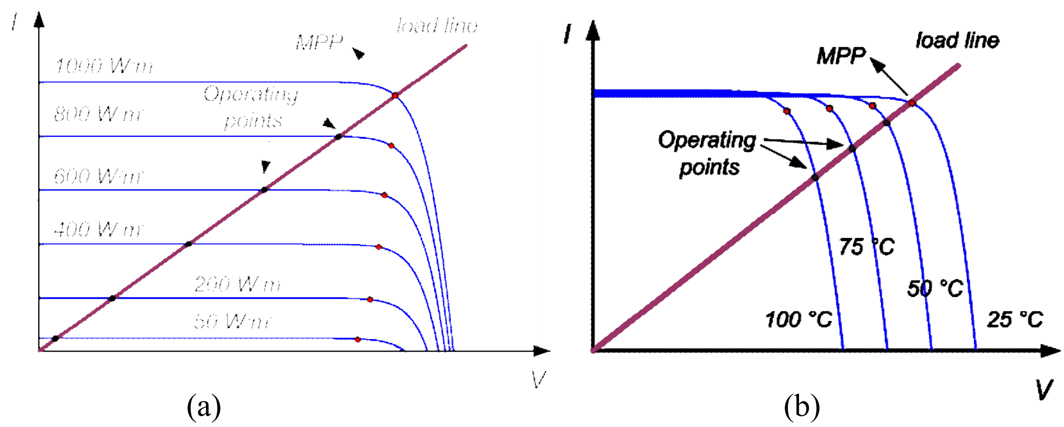

Figure 6.3. PV I-V curve at different irradiance and temperature with load line

Thus, to achieve operation at the MPP, a time varying matching network called the *maximum power point tracking* network (MPPT) is required that interfaces the varying source and possibly the varying load (Gilbert, 1998).

6.3. Role of the MPPT

Operation at the MPP cannot be achieved unless a tunable matching network is used that interfaces the load to the PV array as can be seen in Figure 6.4. The role of this matching network is to ensure operation of the PV array at its MPP, regardless of atmospheric conditions and load variations. MPPT circuits should ensure extraction of maximum available power from the PV array, by its loading at the MPP.

The main components of the MPPT circuit are its power stage and the controller. As the power stage is realized by means of a switched mode DC–DC converter, most commonly with PWM control, the control input is denoted by the duty cycle D.

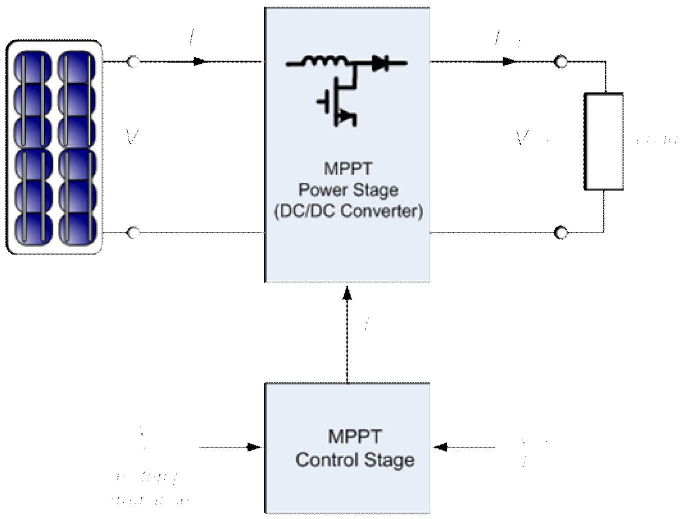

Figure 6.4. MPTT as an interface between PV and load

6.4. DC-DC Converter

In a DC–DC converter, the dc input voltage is converted to a dc output voltage having a larger or smaller magnitude, possibly with opposite polarity or with isolation of the input and output ground references.

The output voltage in DC-DC converters is generally controlled using a switching concept. A basic dc-dc converter circuit known as the buck converter is illustrated in Figure 6.5 (a).

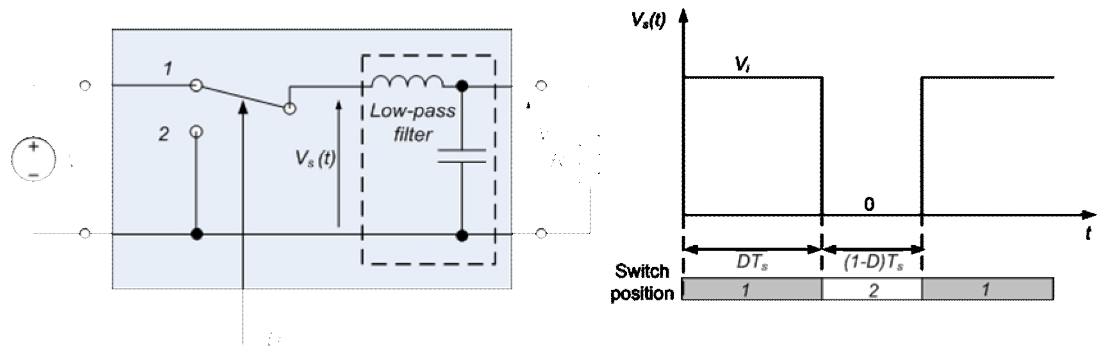

(a) (b)

Figure 6.5. Buck DC-DC converter and waveform

A single-pole double-throw (SPDT) switch is connected to the dc input voltage V_i as shown. $V_S(t)$ is equal to V_i when the switch is in position 1, and is equal to zero when the switch is in position 2 as shown in Figure 6.5(b). The switch position is varies periodically, such that $V_S(t)$ is a rectangular waveform having period T_s and duty cycle D. The duty cycle is equal to the fraction of time that the switch is connected in position 1, and hence $0 \leq D \leq 1$. The switching frequency f_s is equal to $1/T_s$. In practice, the SPDT switch is realized using semiconductor devices such as diodes, power MOSFETs, IGBTs, BJTs. Typical switching frequencies lie in the range 1 kHz to 1 MHz, depending on the speed of the semiconductor devices.

The switch network changes the dc component of the voltage. It can be shown using Fourier analysis that the dc component of a waveform is given by its average value. The average value of $V_S(t)$ is given by

$$\langle V_S(t) \rangle = \frac{1}{T_S} \int_0^{T_S} V_S(t)dt = DV_i \tag{6.3}$$

(Note that $\langle \ \rangle$ sign denotes average value.)

The integral is equal to the area under the waveform, or the height V_i multiplied by the time DT_s. It can be seen that the switch network reduces the dc component of the voltage by a factor equal to the duty cycle D. Since $0 \leq D \leq 1$, the dc component of $V_S(t)$ is less than or equal to V_i .

The power dissipated by the switch network is ideally equal to zero. When the switch contacts are closed, then the voltage across the contacts is equal to zero and hence the power dissipation is zero. When the switch contacts are open, then there is zero current and the power dissipation is again equal to zero. Therefore, the ideal switch network is able to change the dc component of voltage without dissipation of power.

In addition to the desired dc voltage component V_S, the switch waveform $V_S(t)$ also contains undesired harmonics of the switching frequency. In most applications, these harmonics must be removed, such that the converter output voltage $V_o(t)$ is essentially equal to the dc component $V_o = V_s$. A low-pass filter is employed for this purpose. The converter of Fig. 1 contains a single-section L-C low-pass filter. The filter has corner frequency f_0 given by

$$f_0 = \frac{1}{2\pi LC} \tag{6.4}$$

The corner frequency f_0 is chosen to be sufficiently less than the switching frequency f_s, so that the filter essentially passes only the dc component of $V_S(t)$. To the extent that the inductor and capacitor are ideal, the filter removes the switching harmonics without dissipation of power. Thus, the converter produces a dc output voltage whose magnitude is controllable via the duty cycle D, using circuit elements that (ideally) do not dissipate power.(Erickson & Maksimovic, 2004)

The conversion ratio M(D) is defined as the ratio of the dc output voltage V to the dc input voltage V_i under steady-state conditions:

$$M(D) = \frac{V_o}{V_i} \tag{6.5}$$

6.5. Transformer Model of the DC-DC Converter

As illustrated in Figure 6.6, any switching converter contains three ports: a power input, a power output, and a control input. The input power is processed as specified by the control input, and then is output to the load. Ideally, these functions are performed with 100% efficiency, and hence

$$P_{in} = P_{out} \tag{6.6}$$

or,

$$V_{in} I_{in} = V_{out} I_{out} \tag{6.7}$$

These relationships are valid only under equilibrium (dc) conditions: during transients, the net stored energy in the converter inductors and capacitors may change, causing Equations (6.6) and (6.7) to be violated.

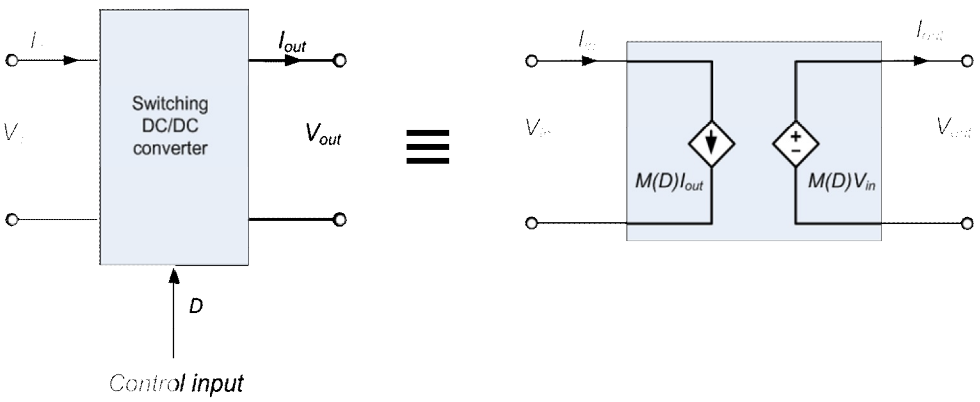

Figure 6.6. Equivalent circuit of the DC-DC converter

It can be expressed that the converter output voltage in an equation of the from

$$V_{out} = M(D)V_{in} \tag{6.8}$$

where *M(D)* is the equilibrium conversion ratio of the converter as mentioned before. For example, *M(D) = D* for the buck converter, and *M(D) = 1/(1 – D)* for the boost converter. In general, for ideal PWM converters operating in the continuous conduction mode and containing an equal number of independent inductors and capacitors, it can be shown that the equilibrium conversion ratio *M* is a function of the duty cycle D and is independent of load.

Substitution of Equation (6.8) into Equation (6.7) yields

$$I_{in} = M(D)I_{out} \tag{6.9}$$

Hence, the converter terminal currents are related by the same conversion ratio. Equations (4.78) and (4.79) suggest that the converter could be modeled using dependent sources, as in Figure 6.6. An equivalent but more physically meaningful model can be obtained through the realization that Equations (6.6) to (6.9) coincide with the equations of an ideal transformer. In an ideal transformer, the input and output powers are equal, as stated in Equations (6.6) and (6.7). Also, the output voltage is equal to the turns ratio times the input voltage. This is consistent with Equation (6.8), with the turns ratio taken to be the equilibrium conversion ratio *M(D)*. Finally, the input and output currents should be related by the same turns ratio, as in Equation (6.9).

Thus, it can be modeled the ideal dc-dc converter using the ideal dc transformer model as shown in Figure 6.7.(Erickson & Maksimovic, 2004)

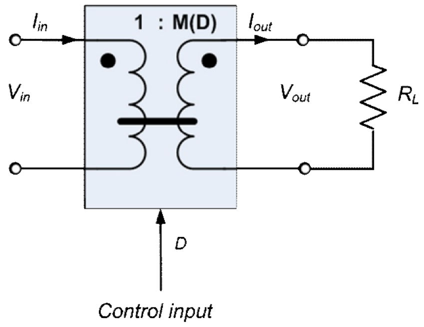

Figure 6.7. Ideal transformer model of the ideal DC-DC converter

6.6. Load Matching Mechanism

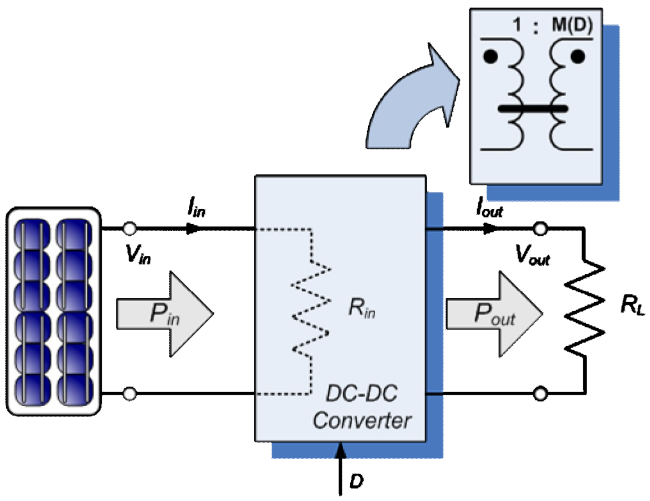

Figure 6.8. DC-DC converter as a load of the PV

As described before, when PV is directly coupled with a load, the operating point of PV is dictated by the load (or impedance to be specific). The resistance of load is described as below.

$$R_L = V_{out} / I_{out} \tag{6.10}$$

where V_o is the output voltage, and I_o is the output current.

The optimal load for PV is described as:

$$R_{op} = V_{mpp} / I_{mpp} \tag{6.11}$$

where V_{MPP} and I_{MPP} are the voltage and current at the MPP respectively. When the value of R_L matches with that of R_{opt}, the maximum power transfer from PV to the load will occur. These two are, however, independent and rarely matches in practice. The goal of the MPPT is to match the resistance of load to the optimal resistance of PV.

From the Equation (6.6),

$$\frac{I_{in}}{I_{out}} = \frac{V_{out}}{V_{in}} \tag{6.12}$$

Note that Equation (6.12) is well known classic transformer equation. Substituting equations $I_{in} = V_{in} / R_{in}$ and $I_{out} = V_{out} / R_L$ to Equation (6.12),

$$\frac{V_{in} / R_{in}}{V_{out} / R_L} = \frac{V_{out}}{V_{in}} \tag{6.13}$$

Rearranging Equation (6.13)

$$R_{in} = \left(\frac{V_{in}}{V_{out}} \right)^2 R_L \tag{6.14}$$

From the Equation (4.78):

$$\frac{V_{in}}{V_{out}} = \frac{1}{M(D)} \tag{6.15}$$

Substituting Equation (6.12) to Equation (6.15) we obtain

$$R_{in} = \frac{R_L}{\left(M(D)\right)^2} \tag{6.16}$$

Equation (6.16) indicate that, R_{in} is function of the R_L and *M(D)*. At the same time it is clear that for a certain R_L value, R_{in} can be adjusted by adjusting *M(D)* .

6.7. Simulation of the Load Matching Mechanism Using SPICE

DC-DC converter load matching mechanism can be easily simulated using LTSPICE. LTSPICE is a free of charge high performance Spice III simulator, schematic capture and waveform viewer with enhancements and models for easing the simulation of switching regulators. LTSPICE is provided by Linear Technology.

Figure 6.9 shows simulation circuit arranged for this purpose. Simulation circuit consists PV module modeled using electrical parameters of the Suntech STP005S solar module, PWM section and boost converter ($M(D)$=1/(1-D)) with 100Ω load resistance.

Some important electrical parameters of the STP005P solar module are given as below:

- V_{OC}=21.6 V
- I_{SC}=0.32 A
- V_{MPP}=17.4 V
- I_{MPP}=0.29 A
- P_{MPP}=5 W

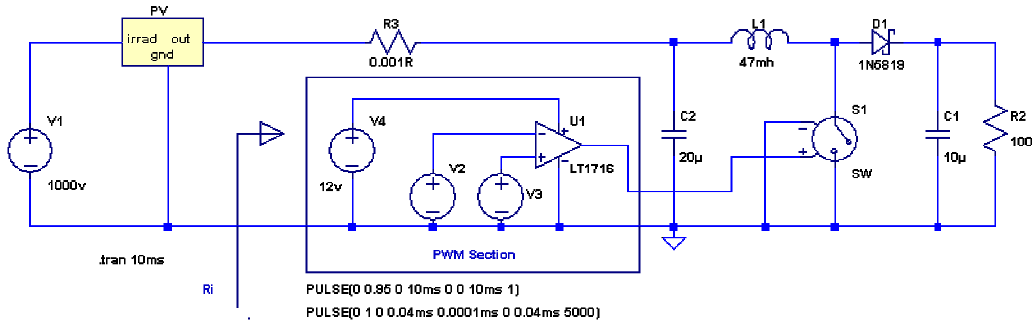

Figure 6.9. Simulation circuit of the load matching

I-V and P-V curve of the PV module obtained by LTSPICE simulation are shown in Figure 6.10. I-V and P-V curves show that optimum load resistance of the PV module s 55 Ω at 1000 W/m^2 insolation level. So, PV module can only provide maximum power to a load in condition that load resistance is 55 Ω.

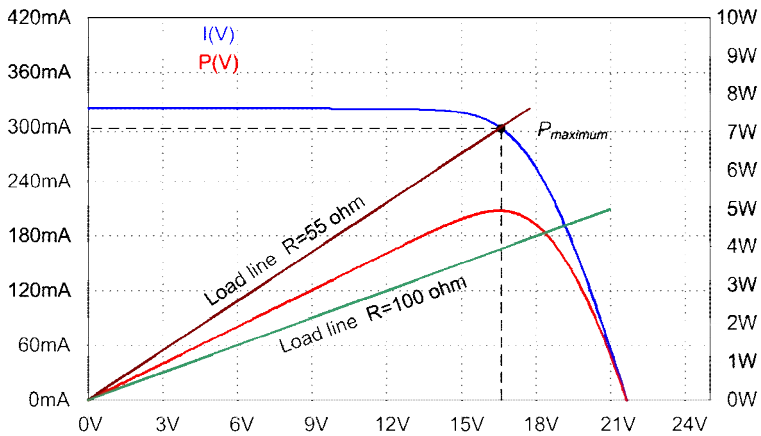

Figure 6.10. I-V and P-V curvers of the STP005P

It can be seen from simulation results given in Figure 6.11 that input resistance of the DC/DC converter R_i is varied from 0 up to R_L (100 Ω) by duty ratio of the DC/DC converter. According to simulation results R_i is 56 Ω if D=0.28.

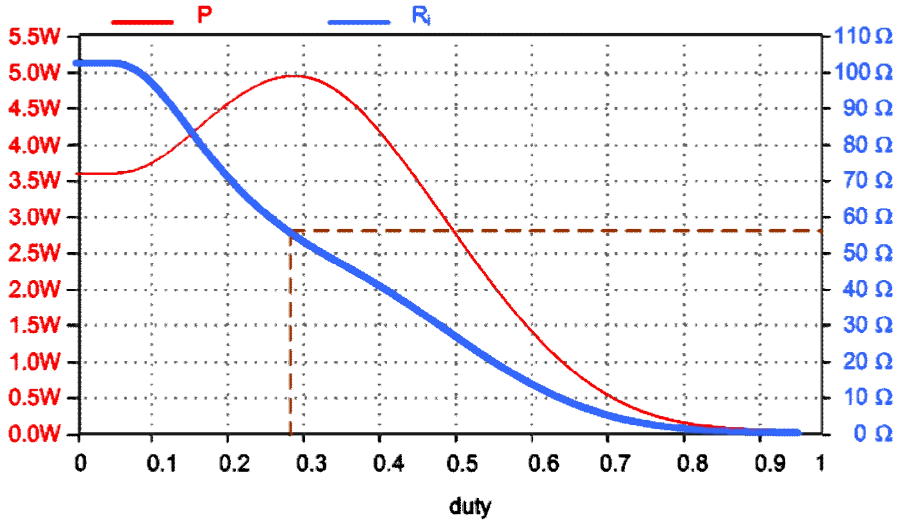

Figure 6.11. Relation between R_i, P and duty cycle

Using Equation (6.17) and boost converter conversion ratio, we can find;

$$R_i = \frac{100}{(1/1-0.28)^2} = 51.84\ \Omega \tag{6.18}$$

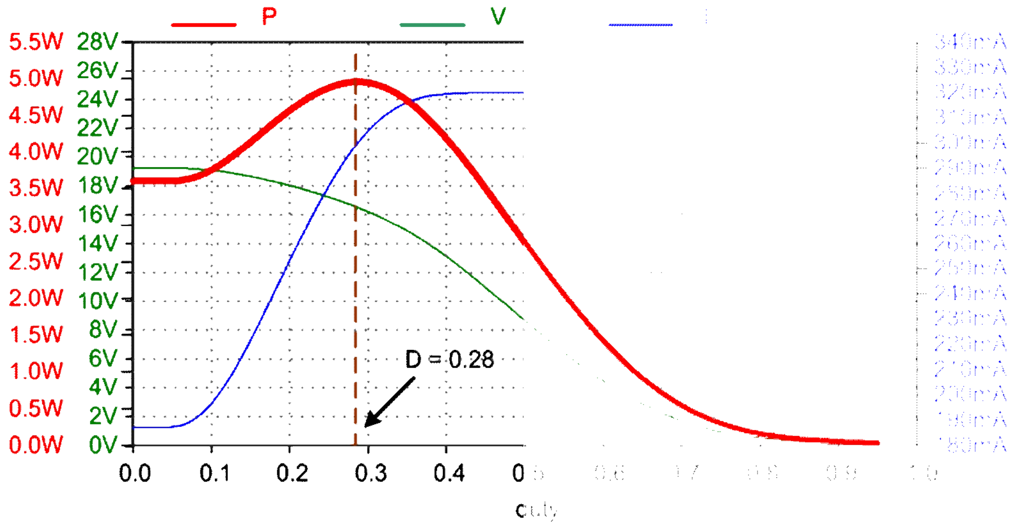

Figure 6.12. Variation of P, V and I with duty cycle

Therefore, we can say that theoretical and simulation results are consentient. At the same time we can see from simulation results given Figure 6.12 represent that for D=0.28 PV module provide maximum power.

As a result by changing the duty cycle (D), the value of R_i (the resistance seem by PV) can be matched with that of R_{opt} to obtain maximum power from PV.

6.8. Most Commonly Used DC-DC Converter Circuit Topologies

A large number of dc-dc converter circuits are known that can increase or decrease the magnitude of the dc voltage and/or invert its polarity. Most commonly used DC-DC converter topologies in the MPPT hardware is shown in Figure 6.13.

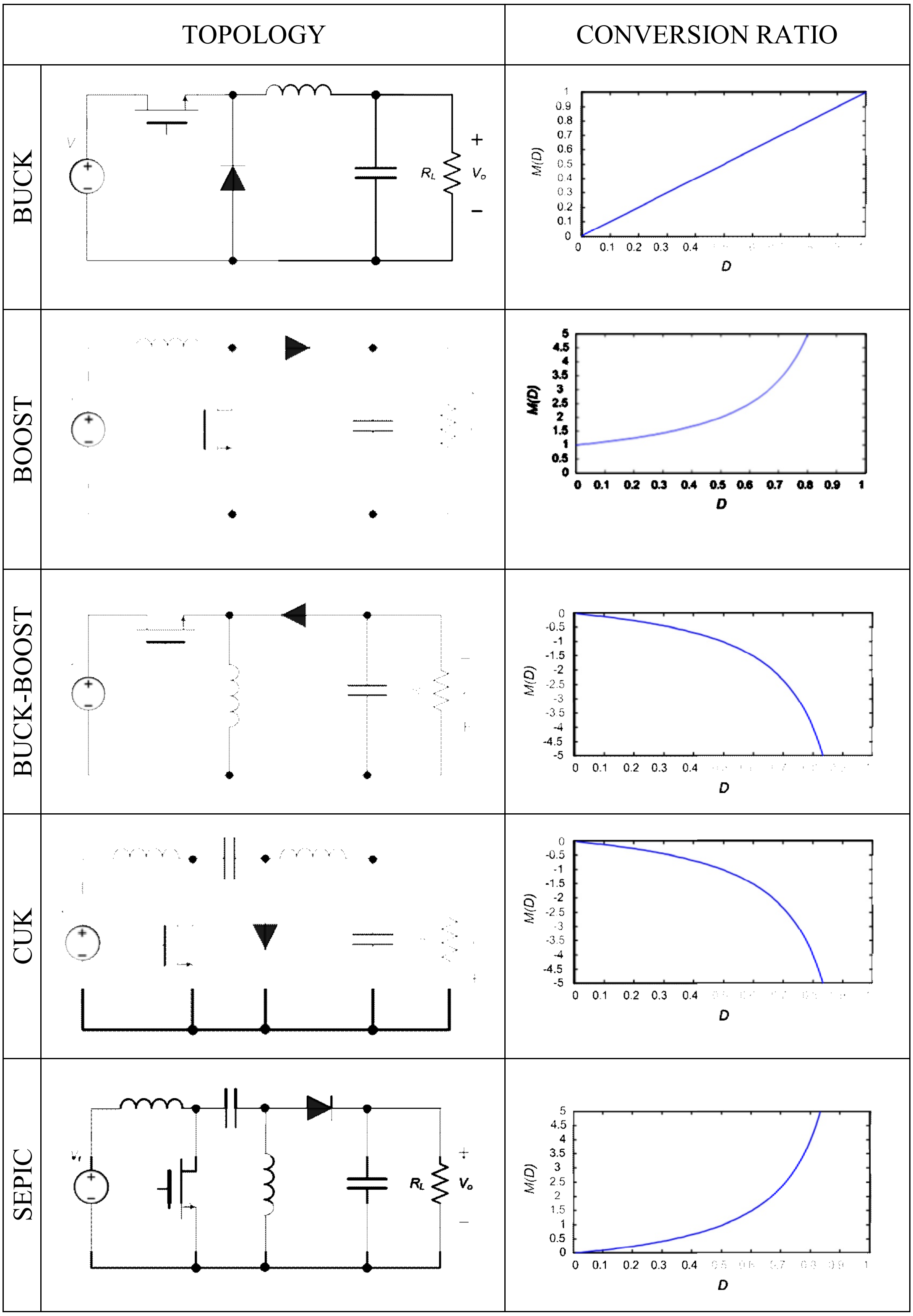

Figure 6.13. DC-DC converter topologies

6.9. SEPIC Converter

Because of that suggested in this thesis as DC-DC converter in the MPPT circuit, the Sepic converter will be explained detailed.

The buck, boost, buck-boost and Cuk converters are well known to power supply designers and information on their design is widely available. The SEPIC topology has however, not been widely used. The name SEPIC is an acronym for Single Ended Primary Inductance Converter. The circuit was first developed at AT&T Bell Laboratories in the mid 1970s. The intent of the developers was to create a new topology with properties not available in contemporary topologies. Of particular interest is the ability to buck or boost the input voltage without inverting voltage polarity. The SEPIC converter is non-inverting and can generate voltages either above or below the input. The input current is non-pulsating but the output current is pulsating.(www.intersil.com)

The boost (often called step-up) topology is the basis for the SEPIC converter. In the boost-converter V_O must be higher than V_I. In the opposite case ($V_I > V_O$) D is forward biased, and nothing prevents current flow from V_I to V_O.

The SEPIC scheme removes this limitation by inserting a capacitor (C_2) between L_1 and D as shown Figure 6.14. This capacitor obviously blocks any DC component between the input and output. Anode of D, however, must connect to a known potential. This is accomplished by connecting D to ground through a second inductor (L_2). L_2 can be separate from L_1 or wound on the same core, depending on the needs of the application.

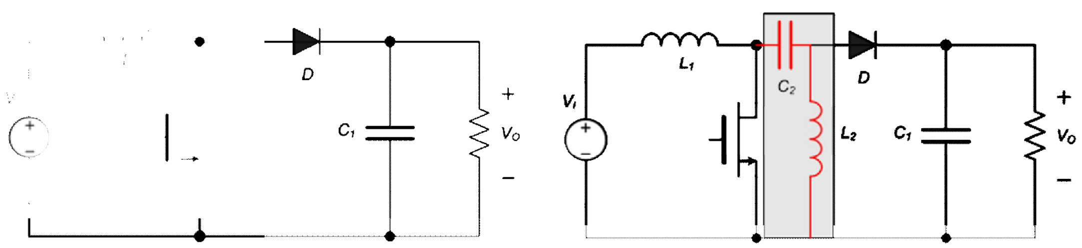

Figure 6.14. Boost and SEPIC converters

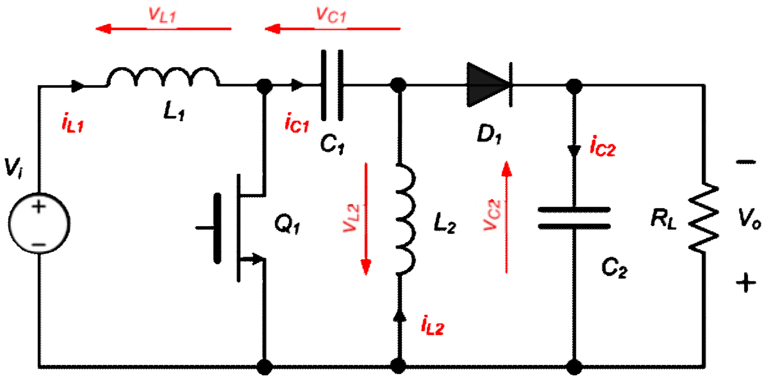

Figure 6.15. Voltages and currents in the SEPIC

The SEPIC converter circuit is shown in Figure 6.15. To briefly explain of operation of the circuit it is assumed that C_1 and C_2 are sufficiently large that the voltage ripple across them is small. By tracing the DC path from V_i through C_1, L_1, L_2 and back to V_i we see that $V_{C1} = V_i$. By inspection it can be seen that $V_{C2} = V_O$. When Q_1 is on, D_1 is off and when Q_1 is off, D_1 is on. This means there are two circuit states during each switching cycle. The two states are shown in Figure 6.16 and Figure 6.17.

As shown in Figure 6.16 when Q_1 is on, L_1 is directly across V_i and I_{L1} is increasing. Energy is being stored in L_1. C_1 is connected across L_2 and I_{L2} is increasing. The energy in C_1 is being transferred to L_2. I_O is being maintained by C_2.

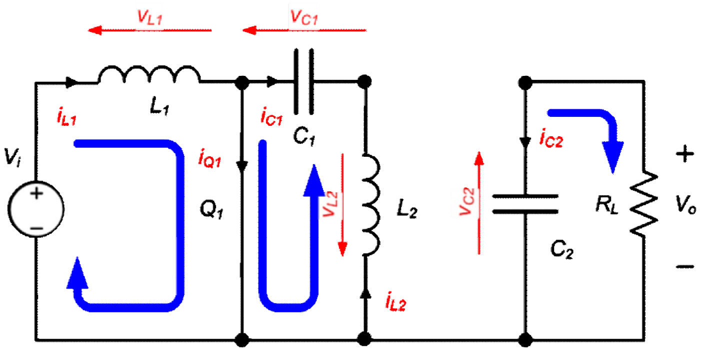

Figure 6.16. Switch on state of the SEPIC

When Q_1 is opened as shown in Figure 6.17, the energy in L_1 is discharged into C_1 and C_2. The energy in L_2 is discharged into C_2. For CCM operation some energy remains in L_1 and L_2 (I_{L1} and $I_{L2} \neq 0$). At the end of the switching sequence Q_1 is again closed and the cycle repeated.

It can be found that conversion ratio *M(D)* as ;

$$M(D) = \frac{D}{1-D} \tag{6.19}$$

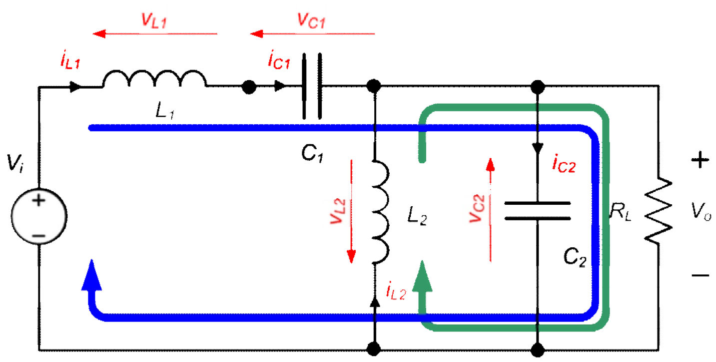

Figure 6.17. Switch off state of the SEPIC

6.10. Determination of Operation Range of the MPPT

As the curve which represents the resistive load is a straight line as shown in Figure 6.18, its inclination angle can be expressed by Equation (6.20):

$$\theta = \arctan\left(\frac{1}{R_{in}}\right) \tag{6.20}$$

If R_{in} is input resistance of the DC-DC converter seen by PV module, it can be written from Equation (6.16)

$$R_{in} = \frac{R_L}{(M(D))^2}$$

Substituting this equation into Equation (6.20)

$$\theta = \arctan\left(\frac{[M(D)]^2}{R_L}\right) \qquad (6.21)$$

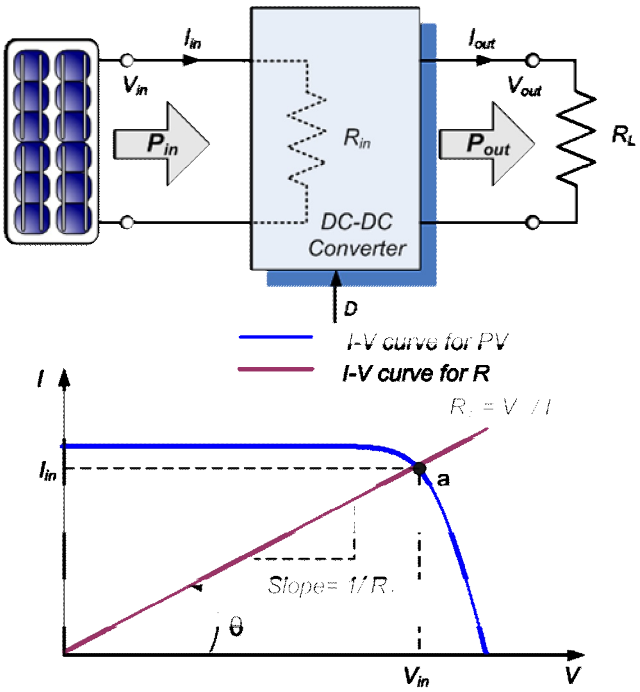

Figure 6.18. DC-DC converter as load of the PV and I-V curves

Remember that *M(D)* is conversion ratio of the DC-DC converter and it is function of the Duty cycle (D). It is clear that

$$\theta = \mathrm{F}(D, R_L) \qquad (6.22)$$

Theoretically, the duty cycle *D* is defined by a lower and an upper limits (0 < D < 1), therefore, *M(D)* will also be limited. Limits of the *M(D)* are given in Table 6.1.

Table 6.1. Interval of the conversion ratio

Converter Topology	***M(D)***	***M(D)@D*=0**	***M(D)@D*=1**
Buck	D	0	1
Boost	$1/(1-D)$	1	∞
Buck-Boost,Cuk	$-D/(1-D)$	0	-∞
SEPIC	$D/(1-D)$	0	∞

Since the angle θ is function of the *D and* R_L , θ has a interval defined by *D and* R_L , in accordance with Equation (6.1). This interval that is dependent to converter topology is shown in Table 6.2.

Table 6.2. Interval of the θ

Converter Topology	$\boldsymbol{\theta(D,R_L)}$	**Interval of the** $\boldsymbol{\theta(D,R_L)}$
Buck	$\arctan\left[D^2/R_L\right]$	$0<\theta<\arctan\left[1/R_L\right]$
Boost	$\arctan\left[1/(1-D)^2 R_L\right]$	$\arctan\left[1/R_L\right]0<\theta<90^\circ$
Buck-Boost, Cuk,SEPIC	$\arctan\left[D^2/(1-D)^2 R_L\right]$	$0<\theta<90^\circ$

Table 6.2 results are illustrated in the Figure 6.19. Interval of the θ is indicated as MPP capture zone. Capture zone means operating range of the DC-DC converter used in MPPT system. Figure 6.19 shows that buck and boost converter have limited and complementary behavior.

When a buck or boost converter is used in the MPPT system, the system will modify operating point, trying to move from A or from B to MPP. However, this will not be possible if operating point is not in the capture zone because of that the system will not reach the MPP.

As mentioned before DC-DC converter input resistance (also load resistance of the PV) is dependent on duty cycle and R_L. Variation range of the R_{in} is given in Table 6.3.

Table 6.3. Variation range of the R_{in}

Converter Topology	R_{in}	**Interval of the R_{in}**
Buck	R_L/D^2	$R_L < R_{in} < \infty$
Boost	$(1-D)^2 R_L$	$0 < R_{in} < R_L$
Buck-Boost, Cuk,SEPIC	$(1-D)^2 R_L/D^2$	$0 < R_{in} < \infty$

As can be seen from Table 6.3 and Figure 6.19 unlike Buck and Boost converters, Buck-Boost, Cuk and SEPIC converters can sweep all of operation zone.

As the MPP is always requested, and this point can be found in any position on I-V curve, depending on temperature and radiation levels, the natural DC-DC converters to be applied as MPPT are Buck-Boost, Cuk or SEPIC (Coelho, Concer, & Martins, 2009).

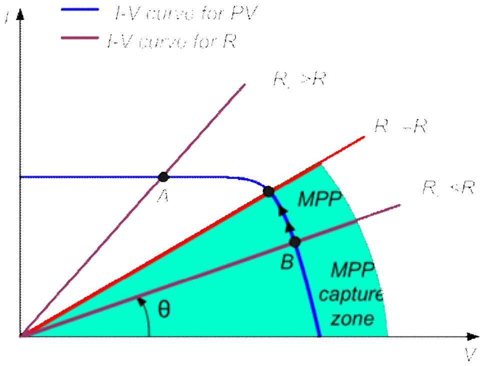

Buck converter

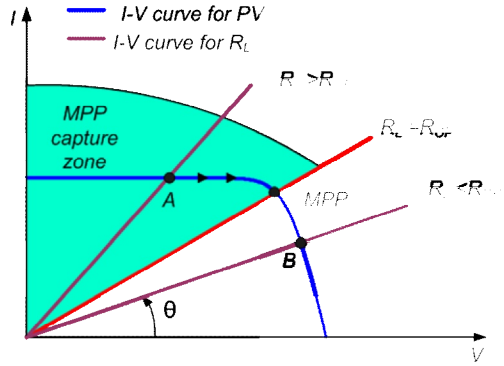

Boost converter

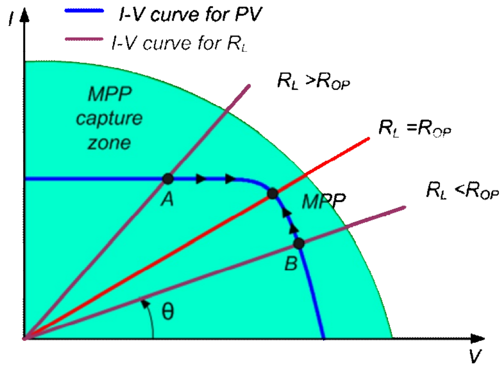

Buck-Boost, Cuk and SEPIC converter

Figure 6.19. Operation range of the DC-DC converter in MPPT

6.11. MPPT Techniques

Tracking the maximum power point (MPP) of a photovoltaic (PV) array is usually a necessity for efficiency as mentioned before. Therefore, MPPT is essential part of a PV system. As such, many MPP tracking (MPPT) methods have been developed and implemented. They can be categorized as follows.

- Load-matching methods: The current, voltage, or impedance of the load is adjusted such that the PV system operates as closely as possible near the MPP under different environmental and load conditions.
- Computational methods: The nonlinear V –I characteristics of solar panel is modeled using mathematical equations or numerical approximations. The model must be valid under different insolation, temperature, and degradation (aging) conditions. Based on the modeled V –I characteristics, the corresponding MPPs are computed for different load conditions as a function of cell open-circuit voltages or cell short-circuit currents.
- Perturbation and Observation (P&O) methods: Measured cell characteristics (current, voltage, and power) are employed along with an online search algorithm to compute the corresponding MPP, independent of insolation, temperature, or degradation levels. Problems with this approach are oscillation of operating point around the MPP, undesirable measurement errors (especially for current), which strongly affect tracker accuracy.
- Intelligent methods: Prediction of the nonlinear V –I and/or P–I characteristics under variable environmental conditions are performed based on intelligent online (e.g., fuzzy, neural network) or offline (e.g., lookup tables) algorithms. The nonlinear and time varying nature of solar cells and their dependency on radiation and temperature levels as well as degradation effects make it difficult to compute and store all possible system conditions.

Perturb and Observe Some MPPT techniques that is most commonly known and used will be explained briefly in this chapter.

6.11.1. Perturb and Observe Algorithm

The perturb & observe (P&O) algorithm, also known as the hill climbing method, is very popular and the most commonly used in practice because of its simplicity in algorithm and the ease of implementation. The most basic form of the P&O algorithm operates as follows.

Perturb and Observe (P&O) algorithms operate by periodically perturbing (i.e. incrementing or decrementing) the array terminal voltage or current and comparing the PV output power with that of the previous perturbation cycle.

Figure 7.1(a) shows output power curve of the PV module as a function of voltage (P-V curve), at the constant irradiance and the constant module temperature, assuming the PV module is operating at a point which is away from the MPP. In this algorithm the operating voltage of the PV module is perturbed by a small increment, and the resulting change of power, ΔP, is observed. It can be seen that incrementing (or decrementing) the voltage increases (or decreases) the power when operating on the left of the MPP and decreases (or increases) the power when on the right of the MPP. If the ΔP is positive, then it is supposed that it has moved the operating point closer to the MPP. Thus, further voltage perturbations in the same direction should move the operating point toward the MPP. If the ΔP is negative, the operating point has moved away from the MPP, and the direction of perturbation should be reversed to move back toward the MPP. This algorithm is summarized in Table 6.4 and Figure 6.21.

There are some limitations that reduce its MPPT efficiency. First, it cannot determine when it has actually reached the MPP. Instead, it oscillates the operating point around the MPP after each cycle and slightly reduces PV efficiency under the constant irradiance condition (Hohm & Ropp, 2002).

Second, it has been shown that it can exhibit erratic behavior in cases of rapidly changing atmospheric conditions as a result of moving clouds. The cause of this problem can be explained using Figure 7.1(b).

Starting from an operating point A, if atmospheric conditions stay approximately constant, a perturbation ΔV in the PV voltage V will bring the operating point to B and the perturbation will be reversed due to a decrease in power. However, if the irradiance increases and shifts the power curve from *P1* to *P2* within one sampling period, the operating point will move from A to C. This represents an increase in power and the perturbation is kept the same. Consequently, the operating point diverges from the MPP and will keep diverging if the irradiance steadily increases (Esram & Chapman, 2007).

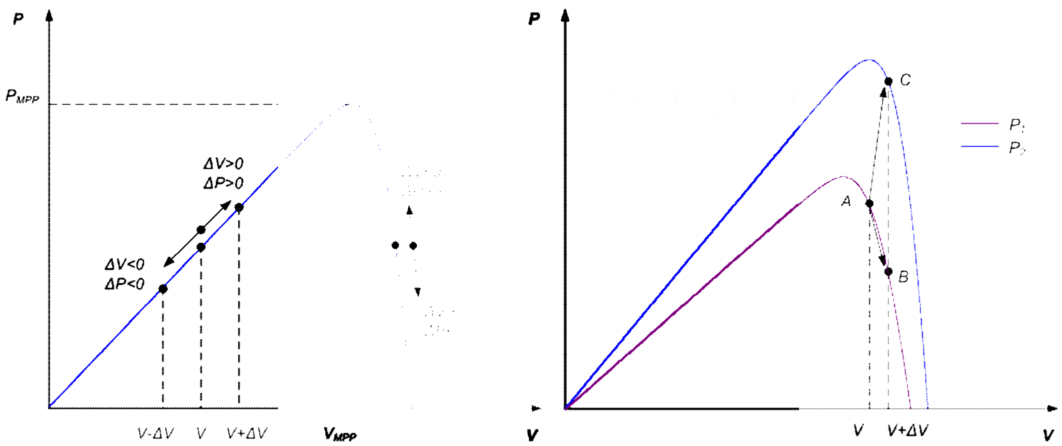

(a) (b)

Figure 6.20. P-V curve and variation of P with V

This situation can occur on partly cloudy days, and MPP tracking is most difficult because of the frequent movement of the MPP.

Table 6.4. Direction of perturbation and power

Perturbation	Change in power	Next Perturbation
+	+	+
+	–	–
–	+	–
–	–	+

There are many different P&O methods available in the literature. It can be used fuzzy logic control to optimize the magnitude of the next perturbation. In some literature proposes a two-stage algorithm can be used that offers faster tracking in the first stage and finer tracking in the second stage.

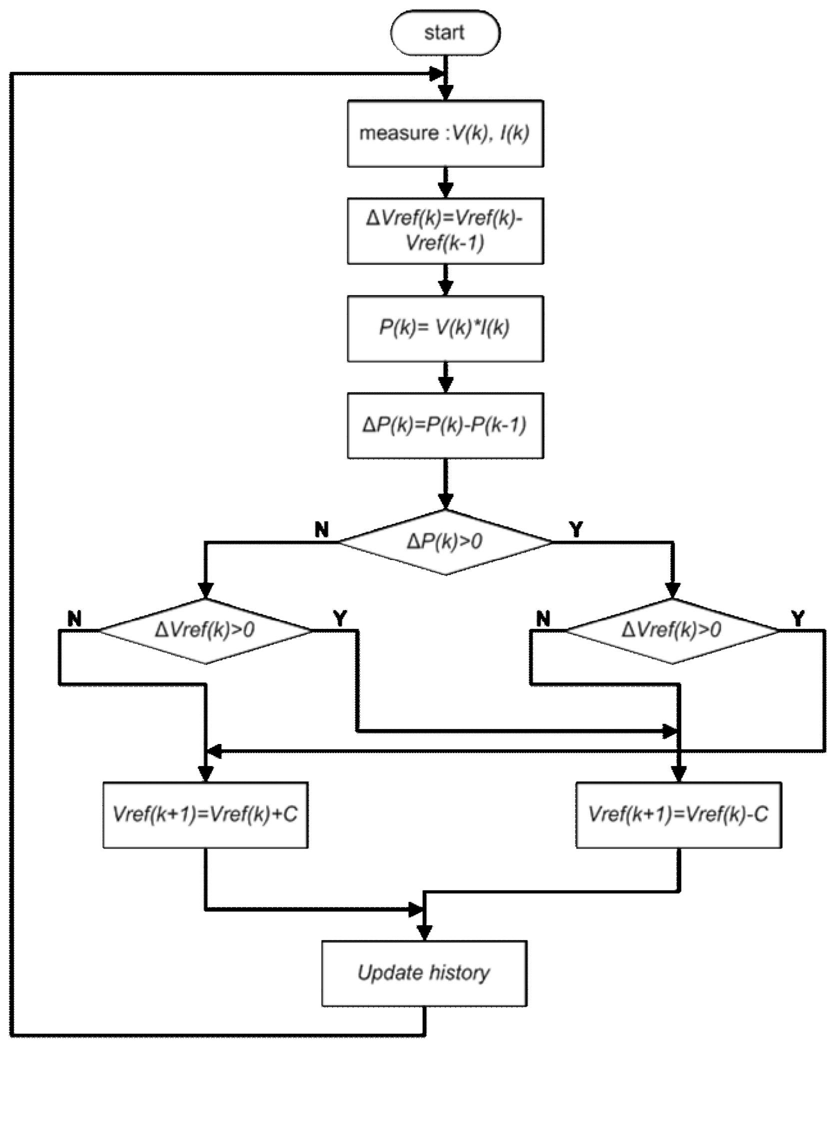

Figure 6.21. Perturb and Observe algorithm

The advent of digital controller made implementation of algorithm easy, as a result many variations of the P&O algorithm were proposed to claim improvements. The problem of oscillations around the MPP can be solved by the simplest way of making a bypass loop which skips the perturbation when the ΔP is very small which occurs near the MPP. The tradeoffs are a steady state error and a high risk of not detecting a small power change. Another way is the addition of a waiting function that causes a momentary cessation of perturbations if the direction of the perturbation is reversed several times in a row, indicating that the MPP has been reached. It works well under the constant irradiation but makes the MPPT slower to respond to changing atmospheric conditions. A more complex one uses a variable step size of perturbation, using the slope of PV power as a variable.

6.11.2. Another MPPT Techniques

As mentioned before, many MPPT techniques have been proposed in literature. Some of these are given below.

- Incremental conductance
- Fractional short circuit current
- Ripple correlation control
- Current sweep
- DC link capacitor droop control
- Load current or load voltage maximization
- dP/dV or dP/dI Feedback Control
- Fuzzy Logic Control
- Neural Network Control

6.11.3. Comparison of the MPPT Techniques

Many MPPT techniques have been proposed in the literature. These techniques vary in complexity, sensors required, convergence speed, cost, range of effectiveness, implementation hardware, popularity, and in other respects. Table shows comparison of the most known MPPT techniques (Esram & Chapman, 2007).

Table 6.5. Comparison of the MPPT Techniques

MPPT tecnique	PV array Depen-dent?	True MPPT?	Analog or Digital?	Periodic tuning	Convergence speed	Implementation complexitiy	Sensed parameters
P&O	No	Yes	Both	No	Varies	Low	V,I
IncCond	No	Yes	Digital	No	Varies	Medium	V,I
Fractional V_{OC}	Yes	No	Both	Yes	Medium	Low	V
Fractional I_{SC}	Yes	No	Both	Yes	Medium	Medium	I
Fuzzy Control	Yes	Yes	Digital	Yes	Fast	High	Varies
Neural Network	Yes	Yes	Digital	Yes	Fast	High	Varies
RCC	No	Yes	Analog	No	Fast	Low	V,I
Current Sweep	Yes	Yes	Digital	Yes	Slow	High	V,I
DC Link Cap.	No	No	Both	No	Medium	Low	V
Load I or V Max.	No	No	Analog	No	Fast	Low	V,I
dP/dV Feedback	No	Yes	Digital	No	Fast	Medium	V,I

6.12. Control of the MPPT

The MPPT algorithm tells a MPPT controller how to move the operating voltage. Then, it is a MPPT controller's task to bring the voltage to a desired level and maintain it. There are several methods often used for MPPT.

6.12.1. PI Control

As shown in Figure 6.22, the MPPT takes measurement of PV voltage and current, and then tracking algorithm (P&O, incCond, or variations of two) calculates the reference voltage (V_{ref}) where the PV operating voltage should move next. The task of MPPT algorithm is to set V_{ref} only, and it is repeated periodically with a slower rate (typically 1-10 samples per second). Then, there is another control loop that the proportional and integral (PI) controller regulates the input voltage of converter. Its task is to minimize error between V_{ref} and the measured voltage by adjusting the duty cycle. The PI loop operates with a much faster rate and provides fast response and overall system stability (Kottas, Boutalis, & Karlis, 2006). The PI controller itself can be implemented with analog components, but it is often done with DSP-based controller because the DSP can handle other tasks such as MPP tracking thus reducing parts count (Oi, 2005).

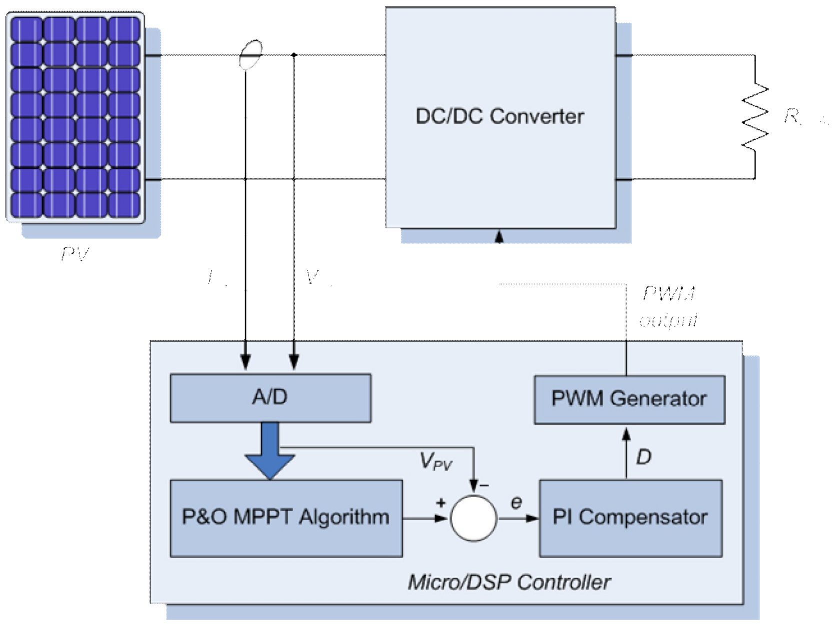

Figure 6.22. MPPT with PI controller

6.12.2. Direct Control

As shown in Figure 6.23, this control method is simpler and uses only one control loop, and it performs the adjustment of duty cycle within the MPP tracking algorithm. The way how to adjust the duty cycle is totally based on the theory of load matching explained before. The impedance seen by PV is the input impedance of converter. Using the example of the SEPIC converter in Section 6.9.2, the relationship to the load is:

$$R_{in} = \frac{(1-D)^2}{D^2} R_{load} \tag{6.23}$$

where D is the duty cycle of the SEPIC converter. Increasing D will decrease the input impedance (R_{in}), thus the PV operating voltage moves to the left. Similarly, decreasing D will increase R_{in}, thus the operating voltage moves to the right. The tracking algorithm (P&O) makes the decision how to move the operating voltage. The time response of the power stage and PV source is relatively slow (10-50*msec* depending on the type of load) (Hohm & Ropp, 2002). The MPPT algorithm changes the duty cycle, then the next sampling of PV voltage and current should be taken after the system reaches the periodic steady state to avoid measuring the transient behavior. The typical sampling rate is 10-100 samples per second. The sampling rate of PI controller is much faster, thus it provides robustness against sudden changes of load. The system response is, however, slow in general. The direct control method can operate stably for applications such as battery equipped systems and water pumping systems. Since sampling rates are slow, it is possible to implement with inexpensive microcontrollers (Kottas, Boutalis, & Karlis, 2006).

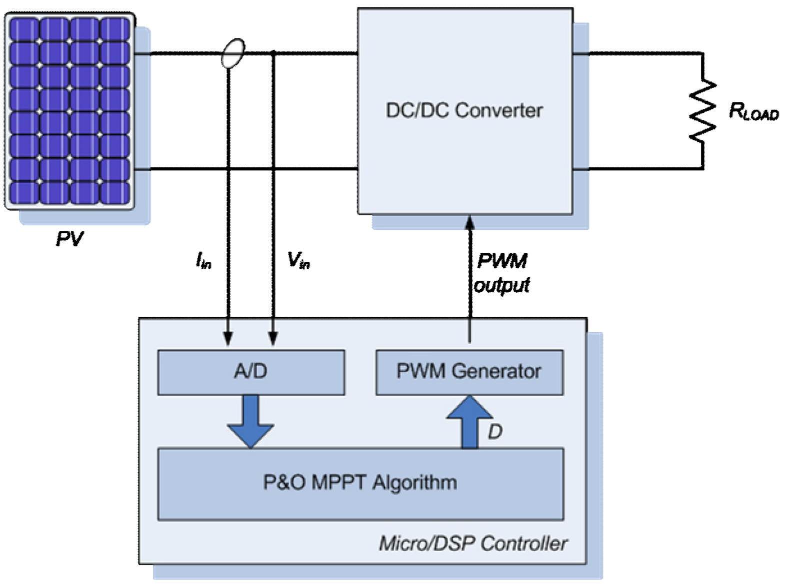

Figure 6.23. MPPT with direct control

7. DESIGN AND SIMULATION

7.1. System Overview

Previous chapters give a basic overview of the MPTT system. This chapter describes the hardware used to implement the system. And also simulation results of the MPPT control algorithm and some hardware simulations are given in this chapter.

MPPT system architecture is shown in Figure 7.1. Perturb and Observation algorithm with direct control which is explained before is proposed in this thesis as MPPT control algorithm.

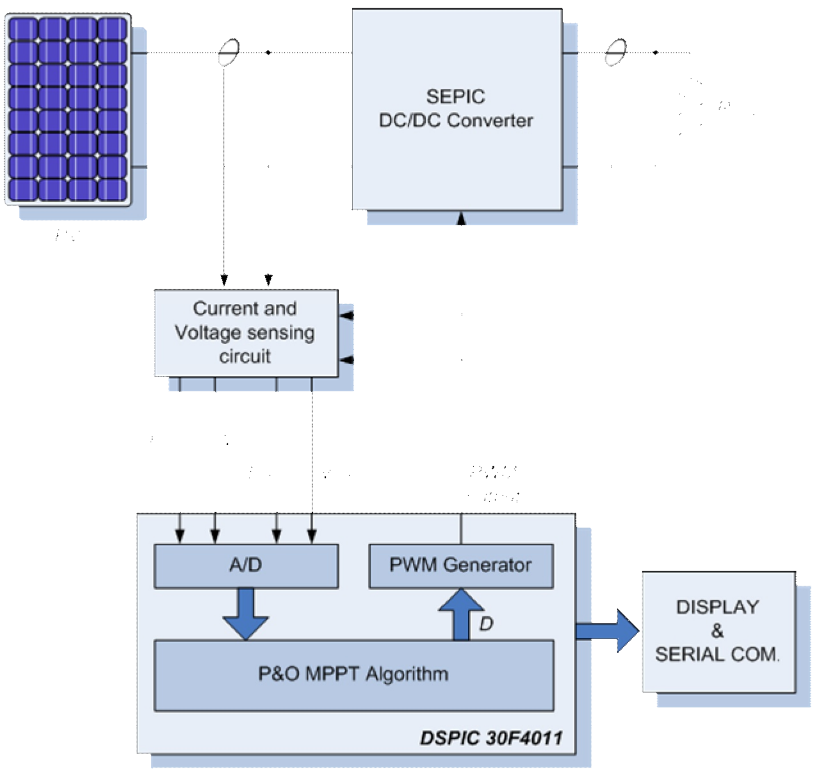

Figure 7.1. MPPT system with DSPIC controller

SEPIC converter was selected as DC-DC converter. The controller for the system is based on a high performance Microchip 16 bit DSPIC 30F4011 digital signal controller.

7.2. PV Module Selection

STP005S monocrystal PV module is selected and modeled as explained before. This module is produced by Suntech. The key specifications of PV module taken from the datasheet are given in Table 5.1.

7.3. Controller Selection

Low cost 16 bit Digital Signal Controller DSPIC30F4011 is selected as MPPT system controller. This controller has 30MIPS operating speed, 10 bit ADC (1000 ksps), 16 bit motor control PWM and DSP engine.

7.4. SEPIC Converter Design

To design a SEPIC converter for MPPT system, it must be considered variation of the maximum power points with irradiance and temperature.

Maximum power points of STP005 PV module at different irradiance and temperature levels are shown in Figure. It can be seen that the locus of the maximum power point varies a certain interval depending on irradiance and temperature level.

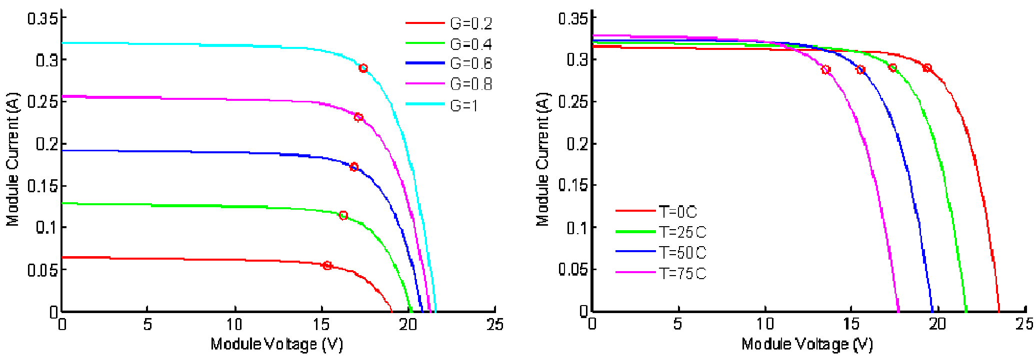

Figure 7.2. Variation of the MPP with irradiance and temperature

The maximum power transfer occurs when the input impedance of converter matches with the optimal impedance of PV module, as described in the Equation (7.1) below and explained before.

$$R_{optimum} = R_{MPP} = \frac{V_{MPP}}{I_{MPP}} \tag{7.1}$$

PV module data obtained from the MATLAB simulation model at different irradiance and temperatures levels are tabulated in the Table 7.1.

Table 7.1. R_{MPP} at different temperature and irradiance levels

Temperature (°C)	Irradiance (kW/m^2)	P_{MPP} (W)	V_{MPP} (V)	I_{MPP} (A)	R_{MPP} (Ω)
25	1	5,05	17,41	0,29	60,03
	0,8	3,96	17,16	0,23	74,61
	0,6	2,89	16,85	0,17	99,12
	0,4	1,84	16,29	0,11	148,09
	0,2	0,84	15,31	0,05	**306,20**
50	1	4,40	15,45	0,28	55,18
	0,8	3,50	15,20	0,23	66,09
	0,6	2,55	14,86	0,17	87,41
	0,4	1,62	14,34	0,11	130,36
	0,2	0,73	13,38	0,05	267,60
75	1	3,89	13,54	0,28	**48,36**
	0,8	3,04	13,20	0,22	60,00
	0,6	2,21	12,90	0,17	75,88
	0,4	1,40	12,45	0,11	113,18
	0,2	0,62	12,00	0,05	240,00

It is obvious that R_{MPP} varies between 48 Ω and 306 Ω . The Equation (6.16) for the SEPIC converter is solved for duty cycle (*D*).

$$D = \frac{1}{1 + \sqrt{\frac{Rin}{R_L}}} \tag{7.2}$$

From the equation (6.15), the output voltage of converter is:

$$V_o = \frac{D}{1-D} V_{in} \tag{7.3}$$

Remember that V_{in} is output voltage of the PV. From Equation (6.9) output current of the converter is:

$$I_o = \frac{1-D}{D} I_{in} \tag{7.4}$$

Limits of parameters of the converter (D, V_o, I_o) can be calculated as shown in the Table 7.2. , for R_L=100 Ω resistive load using Equations (7.2)-(7.4).

Table 7.2. Limits of MPPT

Temp. (°C)	Irrad. (kW/m²)	PV				MPPT		
		P_{MPP} (W)	V_{MPP} (V)	I_{MPP} (A)	R_{MPP} (Ω)	D	Vo (V)	Io (A)
25	1	5.05	17.41	0.29	60.03	0.56	22.15	**0.22**
25	0,2	0,84	15,31	0,05	**306,20**	**0,37**	8.9	0,085
75	1	3,89	13,54	0,28	**48,36**	**0,69**	**30.1**	0,125
75	0.2	0.62	12	0.05	240	0.39	**7.6**	**0,07**

It can be seen that, D_{min} is 0.37 and D_{max} is 0.69 for 100 Ω load resistance. Converter must be designed taking account of these two limits and other parameters given in the Table 7.3.

Table 7.3. Key parameters of the converter

Input Voltage (V_{in})	12−18 V
Input Current (I_{in})	0.05−0.32 A
Output Voltage (V_{out})	7−23 V
Output Current (I_{out})	0.08−0.23 A
Maximum Output Power (P_{max})	5 W
Duty Cycle (D)	0.3−0.7
Switching Frequency (f)	80 kHz

7.4.1. Inductor Selection

One of the first steps in designing any PWM switching regulator is to decide how much inductor ripple current, ΔI_L, to allow. Too much ripple increases EMI, while too little may result in unstable PWM operation. A rule of thumb is to use 20 to 40% of the input current for classic PWM design. Current ripple is important for accuracy of the current measuring. Therefore, it must be defined as low as possible. The inductor sizes are decided such that the change in inductor currents is no more than 10% of the average inductor current.

The worst current ripple will occur under the maximum power condition at 25° C and 1kW/m^2 irradiance level. Under this condition, the average current (I_{L1}) of the input inductor (L_1) is 0.29 A, and the current ripple is;

$$\Delta IL1 = 0.1 \cdot IL1 = 0.1 \cdot 0.29 = 0.029\text{A} \tag{7.5}$$

The following equation gives the change in inductor current.

$$\Delta I_{L1} = \frac{V_{in} D T_S}{L_1} \quad , \quad \Delta I_{L2} = \frac{V_{in} D T_S}{L_2} \tag{7.6}$$

It can be found L_1 and L_2 solving Equation (7.6);

$$L_1 = L_2 = L = \frac{V_{in} D}{\Delta I_L \cdot f_S} \qquad (7.7)$$

Using this equation;

$$L = \frac{17.41 \cdot 0.56}{0.029 \cdot 80 \text{x} 10^3} = 4.2 \text{ mH} \qquad (7.8)$$

Standard 4.7 mH inductor is selected for L_1 and L_2.

7.4.2. SEPIC Coupling Capacitor Selection

The selection of SEPIC capacitor, C_S, depends on the RMS current ad ripple voltage. RMS is given by:

$$I_{CS(RMS)} = I_{in} \sqrt{\frac{1-D}{D}} \qquad (7.9)$$

Maximum current will occur under the maximum power condition at 25° C and 1kW/m^2 irradiance level. At this condition $I_{CS(RMS)}$ is found ;

$$I_{CS(RMS)} = 029 \cdot \sqrt{\frac{1-0.56}{0.56}} = 0.25\text{A} \qquad (7.10)$$

The design criterion for capacitors is that the ripple voltage across coupling capacitor should be less than 5%. Peak to Peak ripple voltage on C_S is given(assuming no ESR);

$$\Delta V_{CS} = \frac{I_O D}{C_S f_S} \qquad (7.11)$$

Solving Equation (7.11) it is found;

$$C_S \geq \frac{I_O D}{\Delta V_{CS} f_S} \tag{7.12}$$

Maximum voltage ripple will occur under the maximum power condition at 25° C and 1kW/m^2 irradiance level. So, it is found ΔC_S is found;

$$\Delta V_{CS} = 17.41 \cdot 0.05 = 0.87 \text{ V} \tag{7.13}$$

and SEPIC capacitor Cs is found as;

$$C_S \geq \frac{0.22 \cdot 0.56}{0.87 \cdot 80\text{x}10^3} = 1.7 \ \mu\text{F} \tag{7.14}$$

Standard 2.2 μf capacitor is selected as SEPIC capacitor.

7.4.3. Output Capacitor Selection

In a SEPIC converter, when the power switch is turned on, the inductor is charging and the output current is supplied by the output capacitor. As a result, the output capacitor sees large ripple currents. The RMS current in the output capacitor is:

$$I_{Cout(RMS)} = I_O \sqrt{\frac{D}{1-D}} \tag{7.15}$$

Maximum current will occur under the maximum power condition at 25 °C and 1kW/m^2 irradiance level. At this condition $I_{Cout(RMS)}$ is found ;

$$I_{Cout(RMS)} = 0.22 \cdot \sqrt{\frac{0.56}{1-0.56}} = 0.24 \text{ A} \tag{7.16}$$

Minimum C_o is given by;

$$C_O \geq \frac{I_O D}{\Delta V_{CO} f_S} \tag{7.17}$$

For maximum ripple condition and assuming the peak-to-peak ripple is 2% of the output voltage,

$$C_O \geq \frac{0.22 \cdot 0.56}{22.1 \cdot 0.02 \cdot 0.5 \cdot 80\text{x}10^3} = 7 \ \mu\text{f} \tag{7.18}$$

Standard 10 μf capacitor is selected for output capacitor.

7.4.4. Diode Selection

The rated reverse voltage of the diode must be higher than $V_{in}+V_{out}$ and the average diode current is equal to the maximum output current. Schottky diode should be selected because it has a low forward voltage and very good reverse recovery time. Maximum $V_{in}+V_{out}$ is 17.4 V+22 V=30.4 V . Adding the 30% of safety factor gives the voltage rating of 40V.

The average forward current (I_F) of diode is 0.22 A (maximum output current). Adding the 30% of safety factor gives the current rating of 0.28A. MBR 150 (50V/1A) Schottky diode is selected.

7.4.5. Power MOSFET Selection

MOSFET peak current is:

$$\begin{aligned} I_{Q(peak)} &= I_{L1(peak)} + I_{L2(peak)} \\ &= 0.29\left(1+0.05/2\right) + 0.22\left(1+0.05/2\right) = 0.52 \text{ A} \end{aligned} \tag{7.19}$$

And RMS current is;

$$I_{Q(RMS)} = \sqrt{\frac{(V_{out} + V_{in}) \cdot V_{out}}{(V_{in})^2}} = \sqrt{\frac{(22.1 + 17.4) \cdot 22.1}{(17.4)^2}} \tag{7.20}$$
$$= 0.37 \text{ A}$$

The rated drain voltage for the MOSFET must be higher than $V_{in}+V_{out}$. IRFD110 power MOSFET (1A/100V) is selected as switch. (www.national.com).

7.4.6. Spice Simulation of the SEPIC Converter

To validate component values of the SEPIC converter designed in previous sections LTSpice is used. LTSpice simulation circuit is shown in Figure 7.3. Figure 7.4(a) shows input inductor ($L1$) current ripple and Figure 7.4(b) shows output voltage ripple at V_{in}=17.41 V , D=0.56 . Simulation results show that criterions of design about current and voltage ripples and transfer ratio of the converter are ensured.

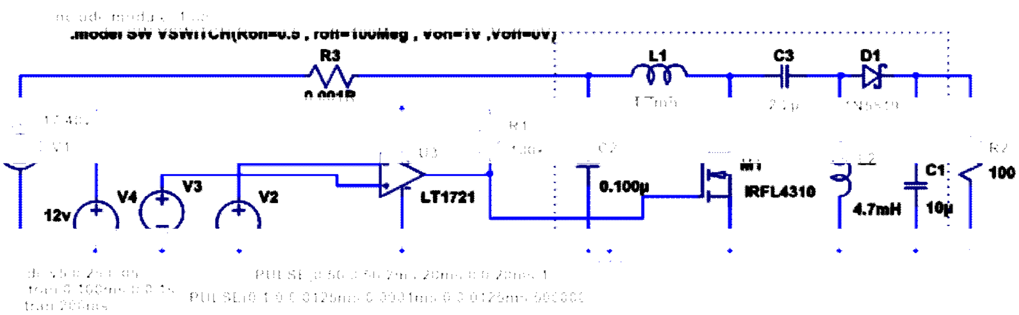

Figure 7.3. Spice simulation circuit of the SEPIC

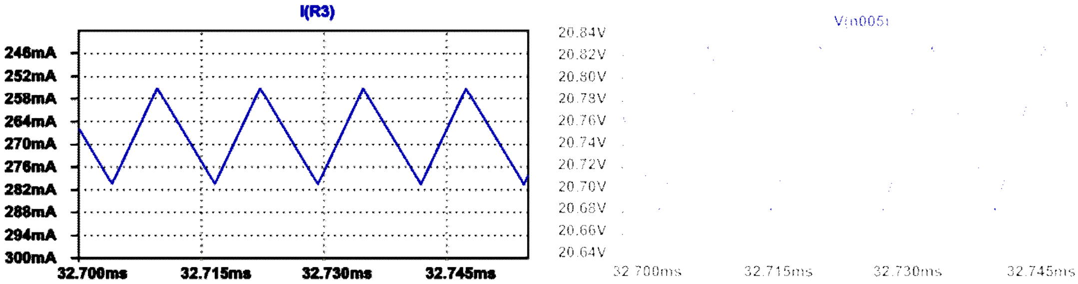

ΔIL_1 =25 mA p-p ΔV =140 mV p-p

(a) L_1 current ripple (b) Output voltage ripple

Figure 7.4. L_1 current and output voltage ripples

7.4.7. Current and Voltage Sensing Circuits

Current and voltage sensing circuit are important components of the MPPT system. Current and voltage sensing circuit implemented using instrumentation amplifier and op-amp are shown in Figure 7.5. INA122 instrumentation amplifier and OPA347 op-amp are used in this circuit. Considering maximum sensing current is 320 mA shunt resistances R_1 and R_5 are selected 330mΩ. If full-scale value of the output of current sensing circuit is defined as 5 V, it can be defined R_4 and R_5 according this.

Maximum voltage on the shunt at 330 mA is $(330\text{ m}\Omega)\cdot(330\text{ mA})=108\text{ mV}$. Therefore, gain of the amplifier is found as $5\text{V} / 0.108\text{V} = 46.2$. INA122 gain is given as $5+200\text{k}/R_G$. R_G (R_4–R_8) is found as 4.8 kΩ. Standard 4.7 kΩ is selected for R_4 and R_8.

Input current circuit is simulated using TINA 7 simulation software obtained by Texas Instrument (www.ti.com). Figure 7.6 shows simulation circuit and simulation result.

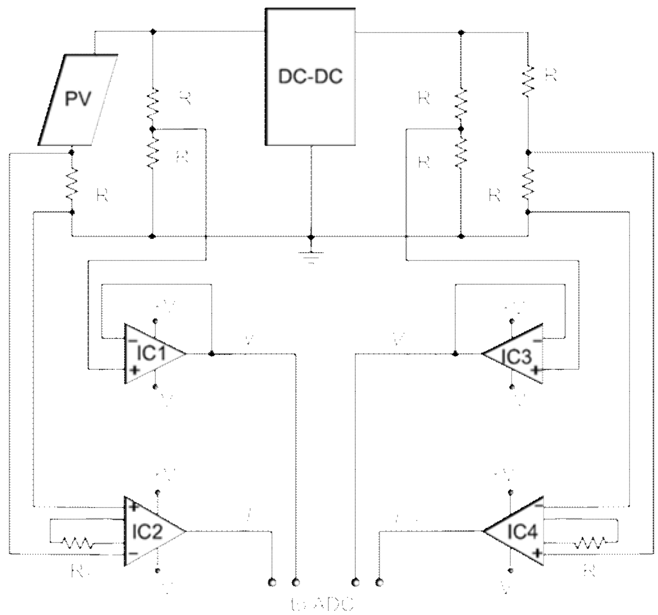

Figure 7.5. Current and voltage sensing circuits

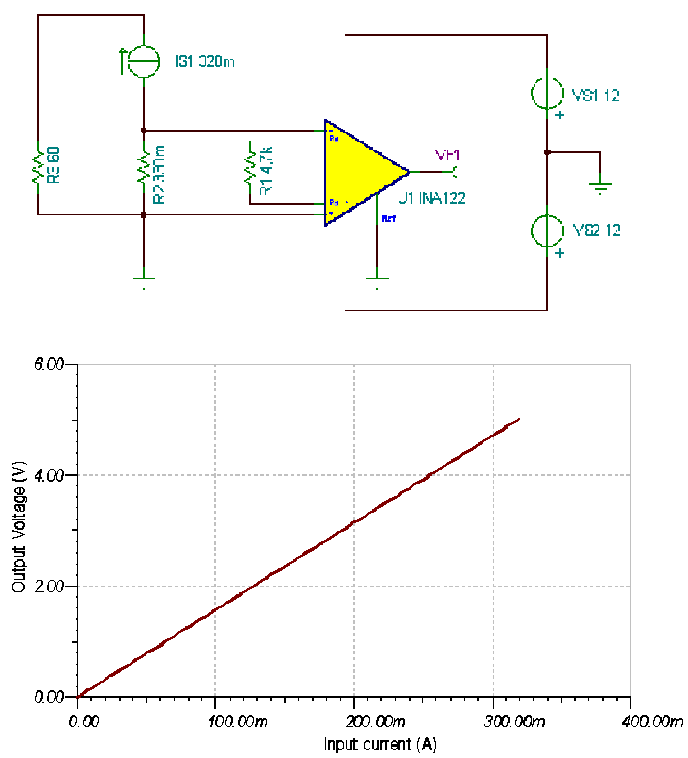

Figure 7.6. Simulation circuit of the Input current sensing circuit and result

7.4.8. Circuit Schematic of the System

Schematic diagram of the designed MPPT system is shown in Figure 7.7.

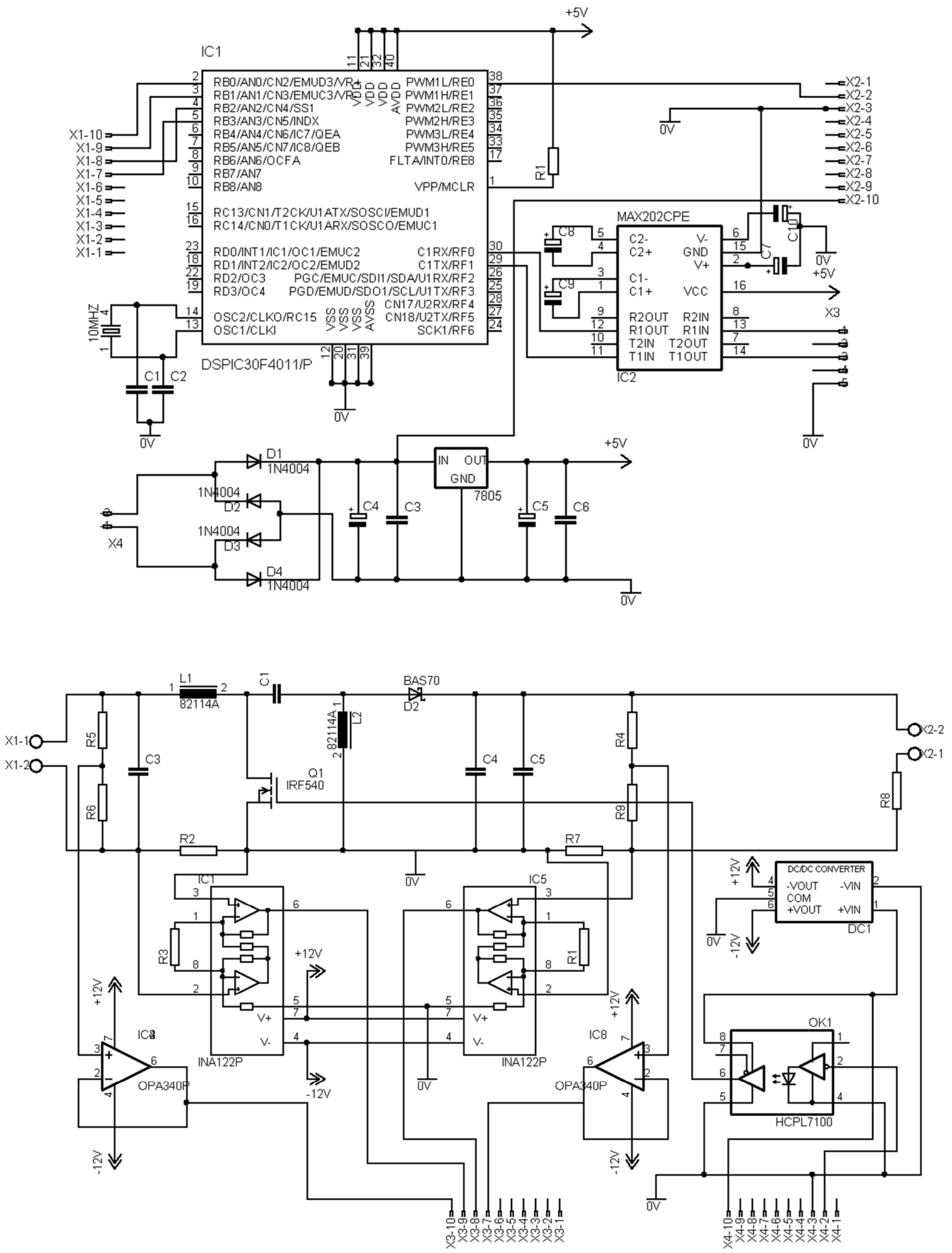

Figure 7.7. Circuit Schematic of the MPPT system

7.5. MPPT Simulation with MATLAB

MPPT with a resistive load is implemented in MATLAB simulation and verified. The simulated system consists of the Suntech STP005S PV model, the ideal SEPIC converter, the MPPT control, and the resistive load (100Ω). The MATLAB function that models the PV module is the following:

$$I_{PV} = STP005\left(V_{PV}, G, T\right) \tag{7.21}$$

The function, STP005, calculates the module current (I_{PV}) for the given module voltage (V_{PV}), irradiance (G in kW/m^2), and module temperature (T in °C). The operating point of PV module is located by its relationship to the load resistance (R) as explained in Section 6.2.

$$R_{operating} = \frac{V_{PV}}{I_{PV}} \tag{7.22}$$

The irradiance (G) and the module temperature (T) for the function STP005 are known variables, thus it is possible to say that I_{PV} is the function of V_{PV} hence

$$I_{PV} = f\left(V_{PV}\right) \tag{7.23}$$

Substituting Equating (8.23) into the Equation (8.22) gives:

$$V_{PV} - R_{operating} \cdot f\left(V_{PV}\right) = 0 \tag{7.24}$$

Knowing the value of $R_{operating}$ enables to solve this equation for the operating voltage (V_{PV}).

MATLAB uses *fzero* function to do so. Placing V_{PV}, back to the Equation (7.21) gives the operating current I_{PV}.

Each sampling of voltage and current is done at a periodic steady state condition of the converter. Therefore, the steady state analysis discussed in Section 6.9 provides sufficient modeling of the SEPIC converter. The following equations describe the input/output relationship of voltage and current, and they are used in the MATLAB simulation.

$$V_o = \frac{D}{1-D} V_i \ , \ I_o = \frac{1-D}{D} I_i \tag{7.25}$$

where D is the duty cycle of the SEPIC converter.

The following flowchart, shown in Figure 7.7, explains the simulation of the MPPT system. MPPT algorithm can also be simulated directly without resistive load as shown in Figure 7.7(b) using MATLAB (Oi, 2005).

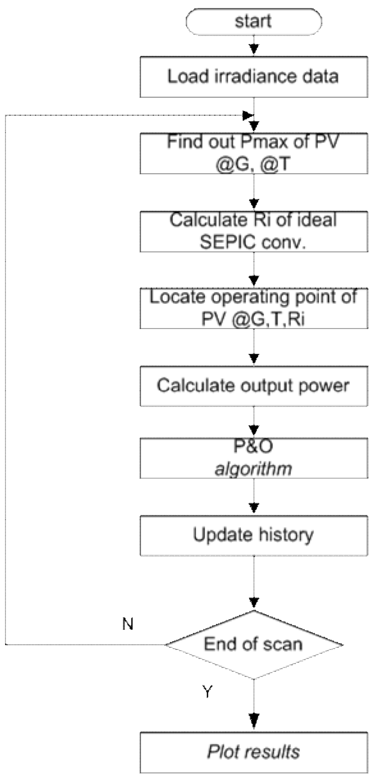

(a)

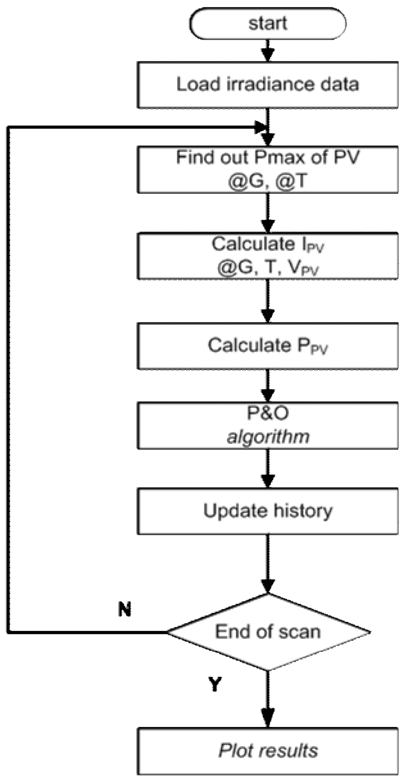

(b)

Figure 7.8. Flowchart of the MPPT simulation with/without load

7.5.1. Direct V_{ref} Control under Constant Irradiance

P&O algorithm is verified to locate the MPP correctly under constant irradiance. Sampling time is 1 second and ΔV_{ref} is 1V for this simulation. Results are shown in Figure 7.9 and Figure 7.10. Figure 7.10 shows variation of the module voltage.

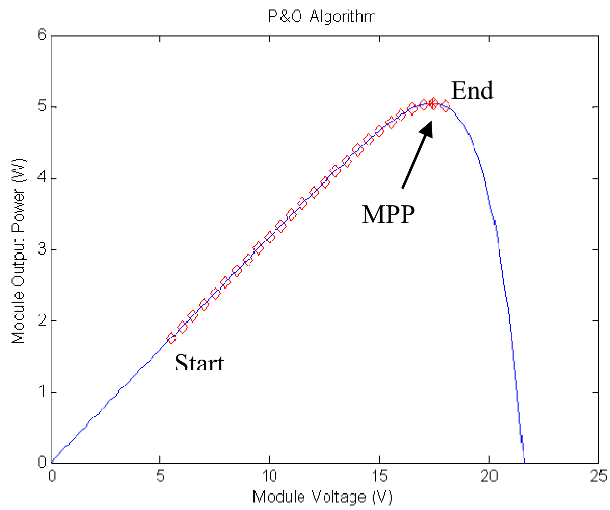

Figure 7.9. Tracking way of the P&O under constant irradiance (G=1000 W/m2)

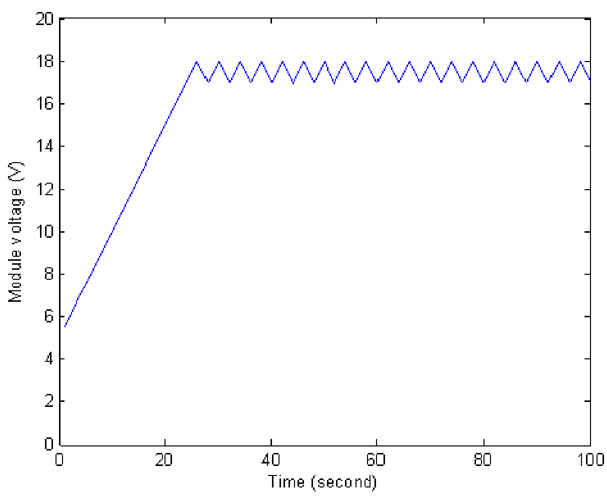

Figure 7.10. Variation of the module voltage

Note that V_{MPP} of the STP005 is 17.4 V. It can be seen that module voltage oscillates around V_{MPP} as a result of P&O algorithm. This result is a drawback for P&O algorithm.

7.5.2. Direct V_{ref} Control Under Linearly Varying Irradiance

This simulation is performed under the linearly increasing/decreasing irradiance varying 0-1000W/m² with a moderate rate of 0.55W/m² per sample. Results are shown in Figure 7.11 and Figure 7.12.

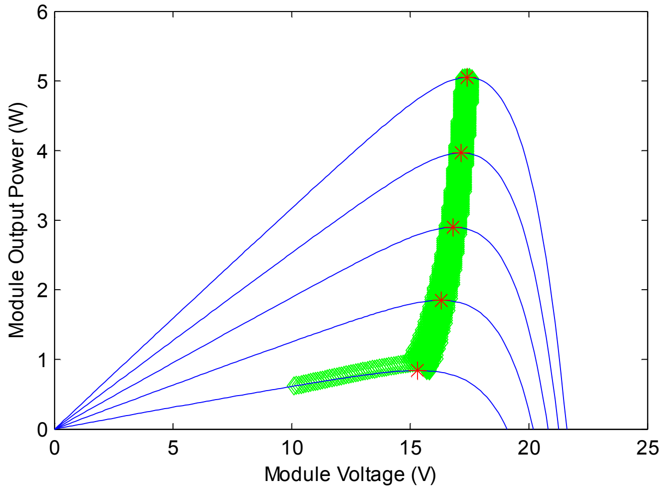

Figure 7.11. Simulation without Load and Under Linearly Varying Irradiance

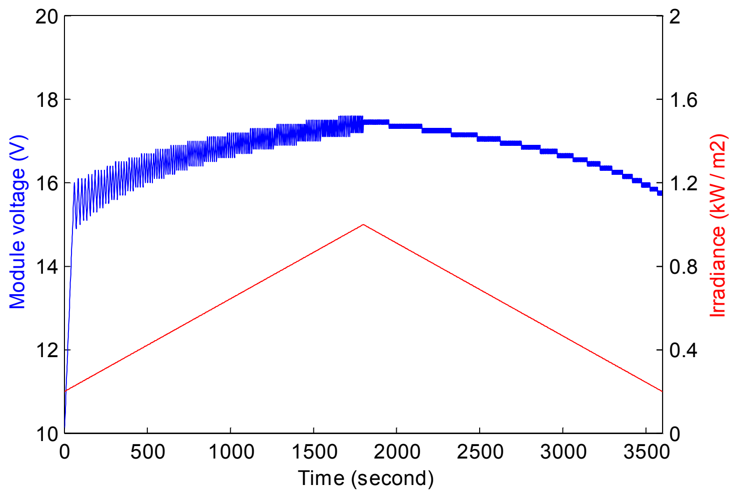

Figure 7.12. Simulation without Load and Under Linearly Varying Irradiance

Green marks indicate instantaneous PV power, red marks on the P-V curves indicate locus of the MPP. Sampling time is 1 second and ΔV_{ref} is 0.1 V for this simulation.

7.5.3. Simulation of Step Response of the Direct *Vref* Control

This simulation is performed under the stepping increasing irradiance from 200 W/m² to1000 W/m² to simulate fast changing atmospheric conditions. Results are shown in Figure 7.13 and Figure 7.14. Sampling time and ΔV_{ref} is defined as 1 second and 0.75 V to find out erratic tracking case.

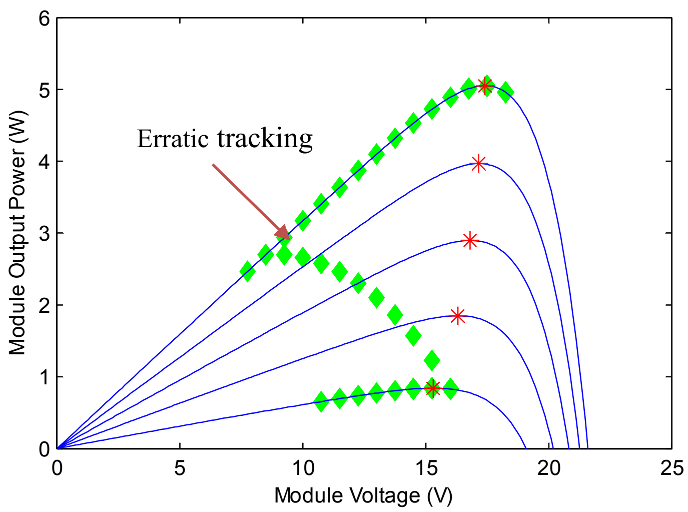

Figure 7.13. Erratic tracking case

Another important drawback of the P&O algorithm is erratic tracking and this case appears under fast changing irradiance as can be seen clearly in Figure 7.13.

Figure 7.14 shows variation of the module voltage versus irradiance. Erratic variation of the module voltage caused by fast irradiance variation can be seen in Figure 7.14.

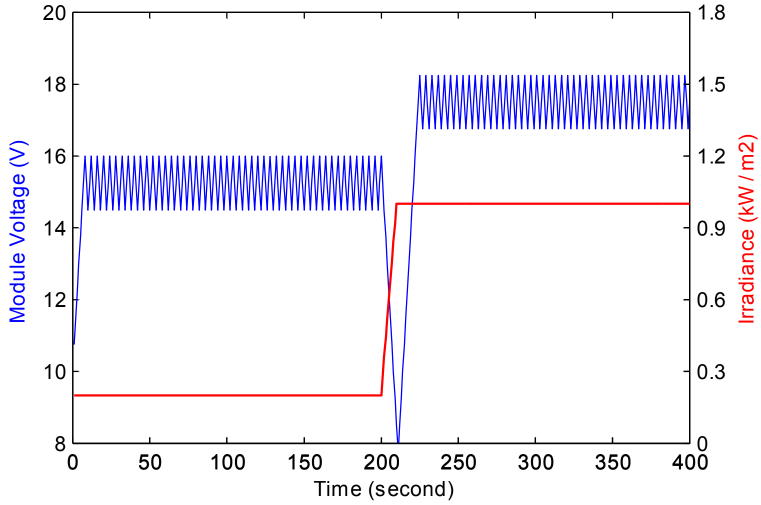

Figure 7.14. Erratic variation in the module voltage

7.6. Duty Control with Load and DC-DC Converter

Differently from simulations in previous sections, simulations in this section are performed with 100 Ω load resistance and ideal SEPIC DC-DC converter. In this simulation method, duty cycle is controlled instead of V_{ref} as control output as explained before.

7.6.1. Duty Control with Load and Under Linearly Varying Irradiance

Firstly, to check whether simulation processes is correct, simulation is performed under the linearly increasing from 100 to 1000W/m2 with a moderate rate of 0.30 W/m^2 per sample. Figure 7.15 shows operating point of the PV indicated green marks on the P-V (power-voltage) and I-V (current-voltage) curves. Figures show that the trace of operating point is staying close to the MPPs during the simulation.

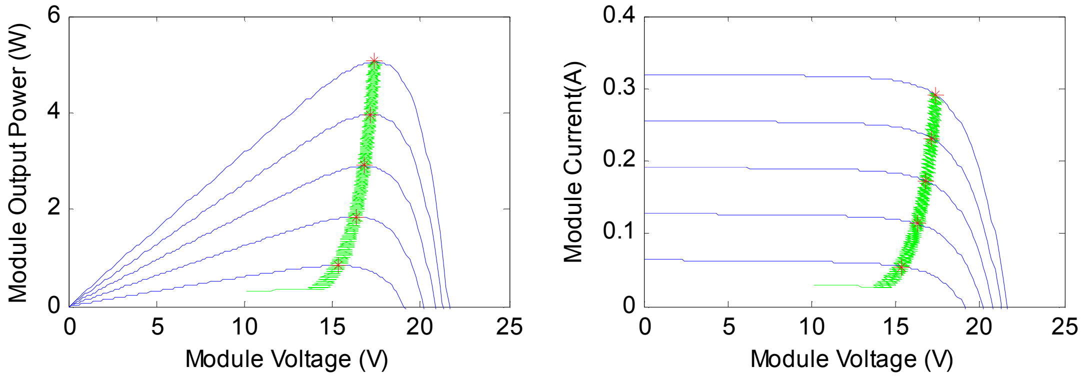

Figure 7.15. Operating points of the PV on the P-V and I-V curves

Figure 7.16 shows duty cycle of the DC-DC converter and irradiance versus time. Figure 7.17 shows input resistance of the DC-DC converter (R_{in}) seen by PV and irradiance versus time. It is clear that both of them are very consistent with MPTT theory.

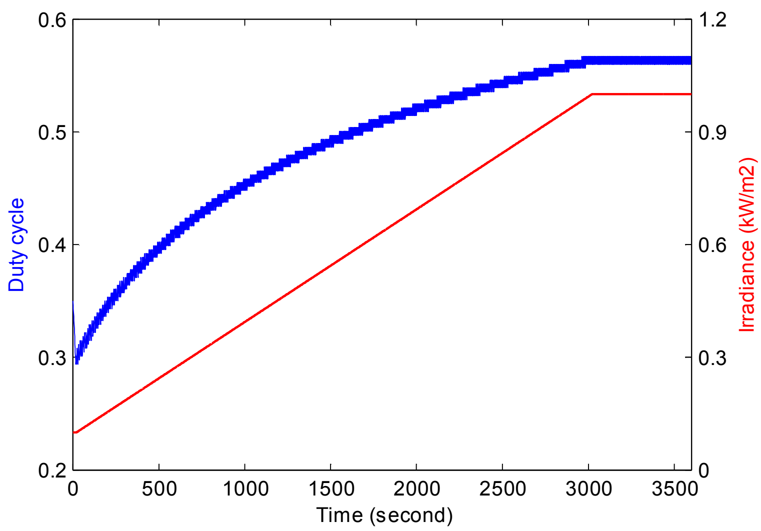

Figure 7.16. Duty cycle (D) and irradiance versus time

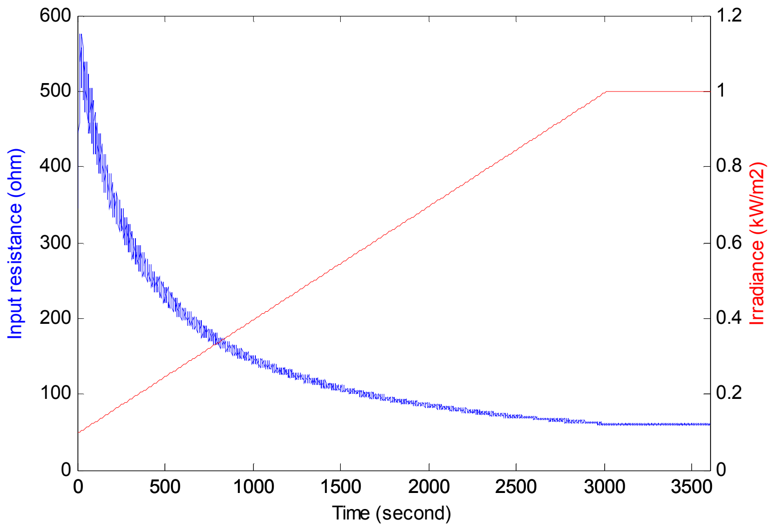

Figure 7.17. R_{in} and irradiance versus time

7.6.2. Duty Control Simulation with Real Irradiance Data

These simulations in this section are performed using real irradiance data provided by Castaner,L. and Silvestre,S. (2002). Set of data is the measurements of a cloudy day in April in Barcelona, Spain. The data contain the irradiance measurements taken every two minutes for 12 hours. Irradiance values between two data points are estimated by the cubic interpolation in MATLAB functions. Therefore, data set is reproduced using original data set in order that contain more samples. Reproduced data set contain 43200 samples for 12 hours. So, there is an irradiance data for every second in new data set. Irradiance versus time plot is given in Figure 7.18 that is produced by MATLAB using new data set.

Figure 7.19 shows operating points of the PV marked with green markers on P-V curves. Also Figure 7.20 shows operating points of PV on I-V curve. Red markers on the both of figure indicate maximum power points. Figure 7.19 and Figure 7.20 show that the trace of operating point stays close to the MPPs throughout the simulation.

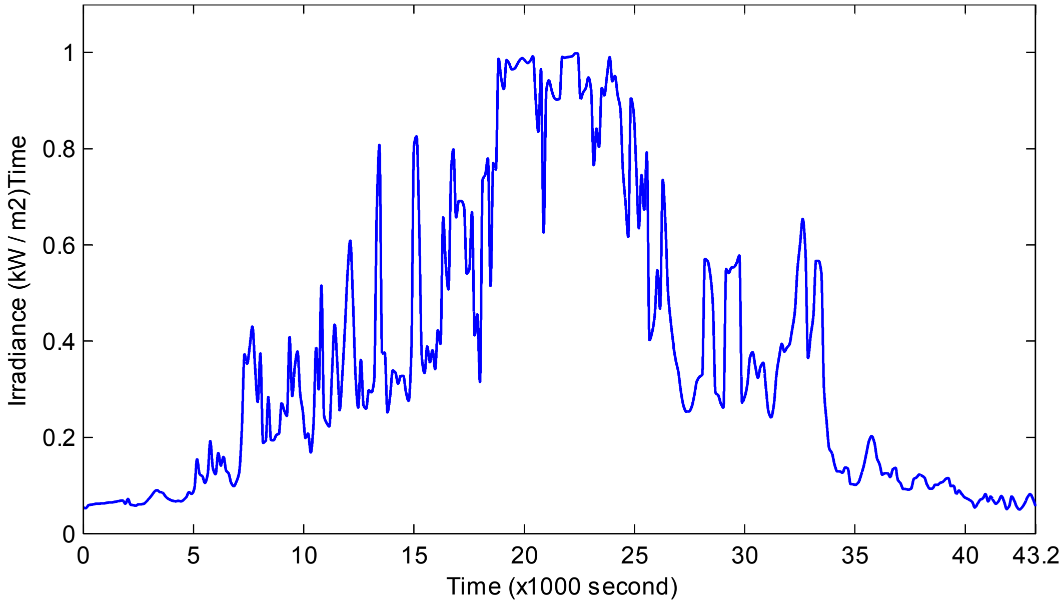

Figure 7.18. Real irradiance data (Castaner & Silvestre, 2002)

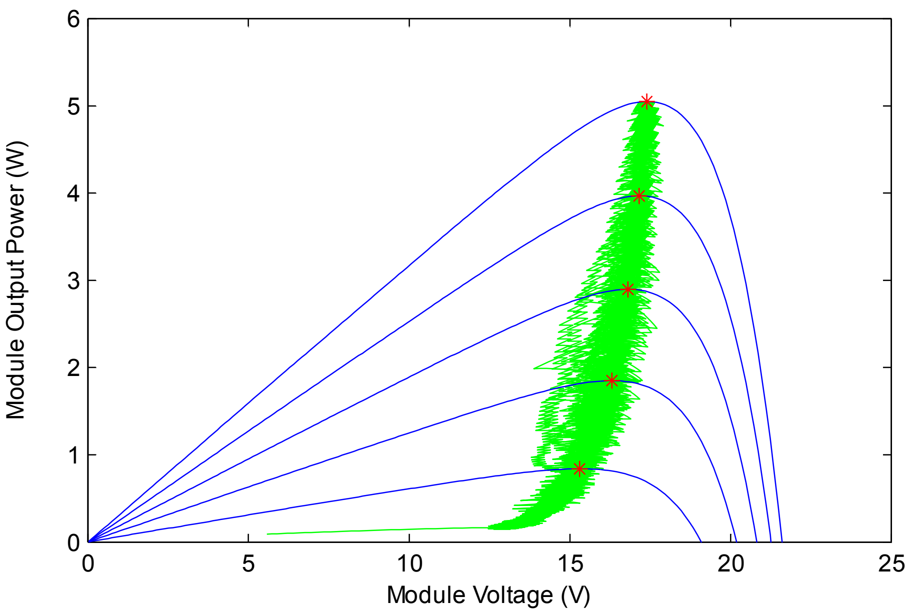

Figure 7.19. Operating points of PV marked on the P-V curves

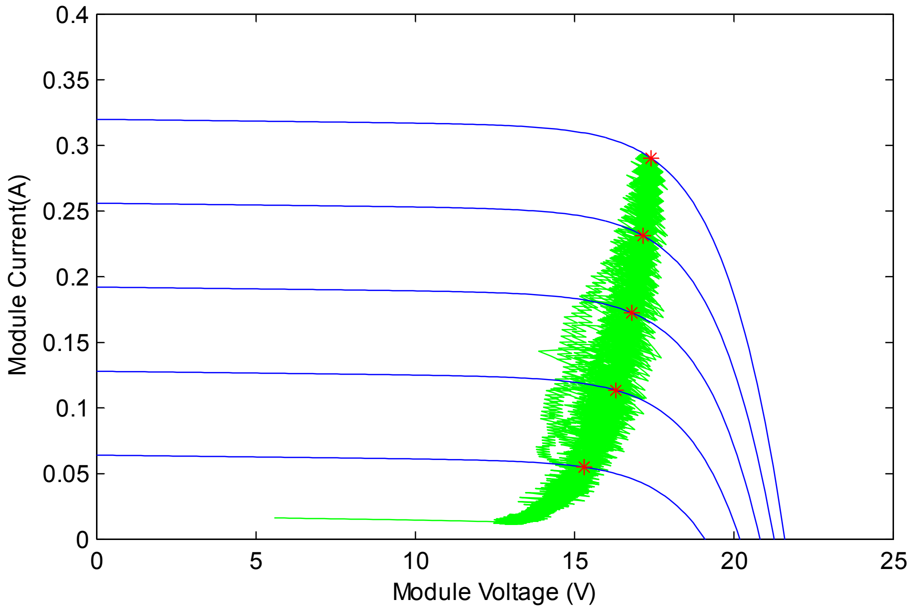

Figure 7.20. Operating points of PV marked on the I-V curves

Variation of the Duty cycle of DC-DC converter and DC-DC converter input resistance R_{in} seen by PV versus time are shown in Figure 7.21 and Figure 7.22 respectively.

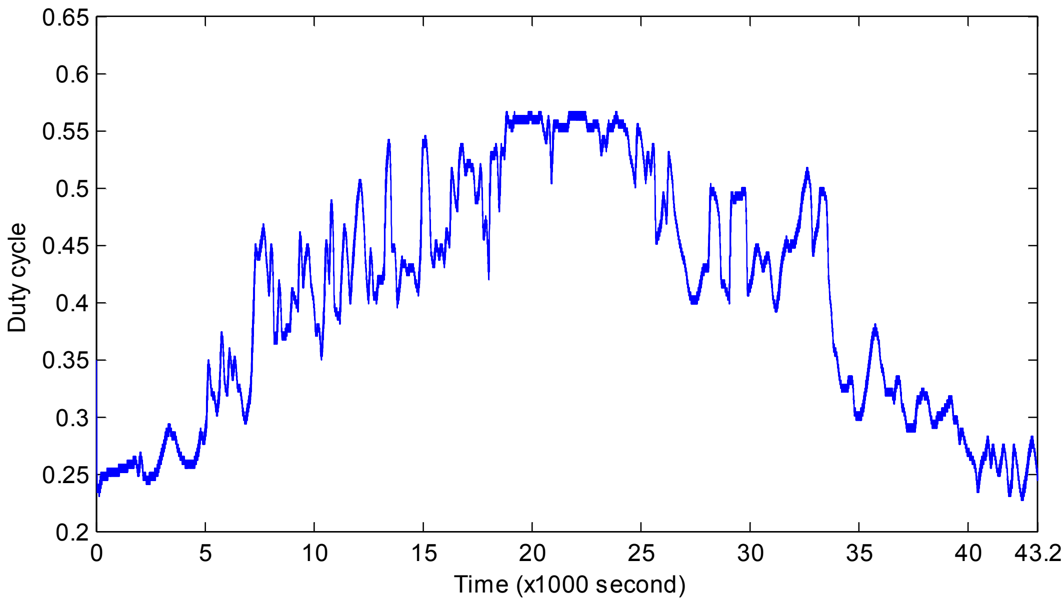

Figure 7.21. Variation of the duty cycle versus time

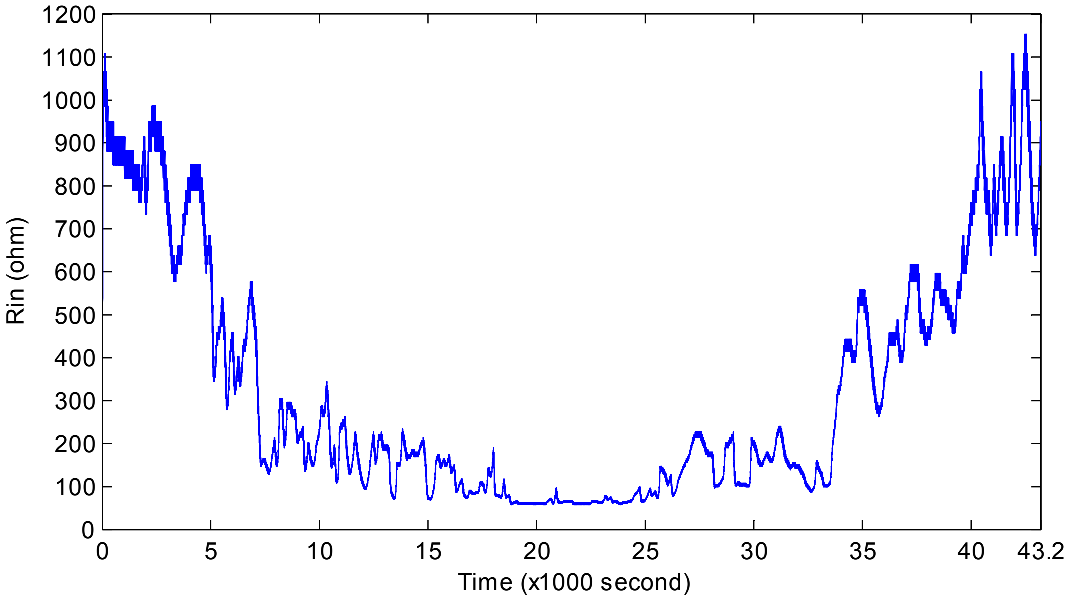

Figure 7.22. Variation of the R_{in} cycle versus time

Figure 7.23 shows time versus theoretical maximum module power and actual module power under given in Figure 7.18 real irradiance. Figure 7.23 shows that there is almost no difference between theoretical and actual module power. Figure 7.24 is obtained using zoom on section between 20050-20450 second.

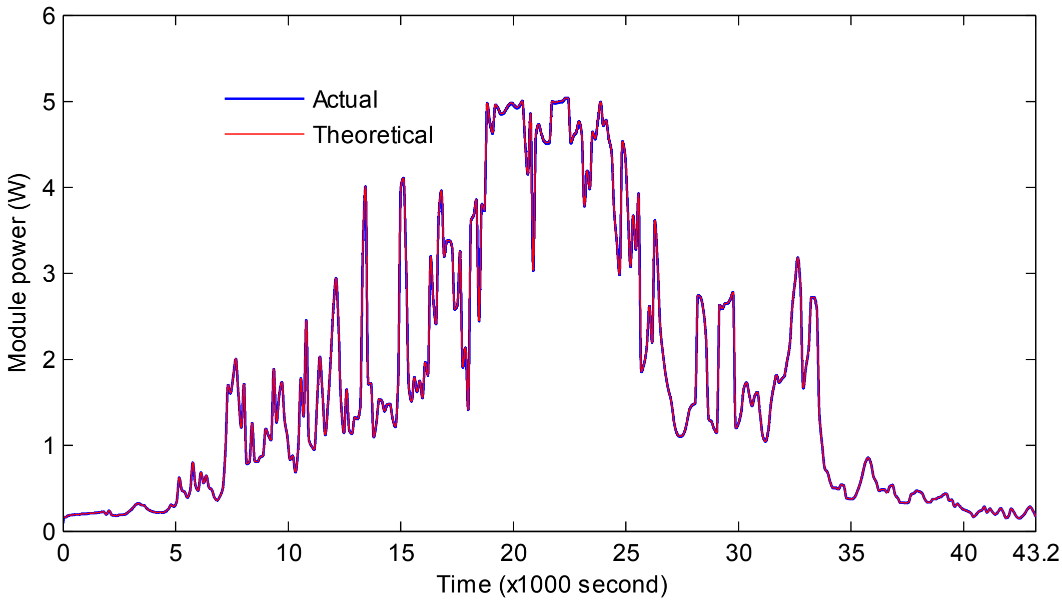

Figure 7.23. Theoretical and actual module power versus time

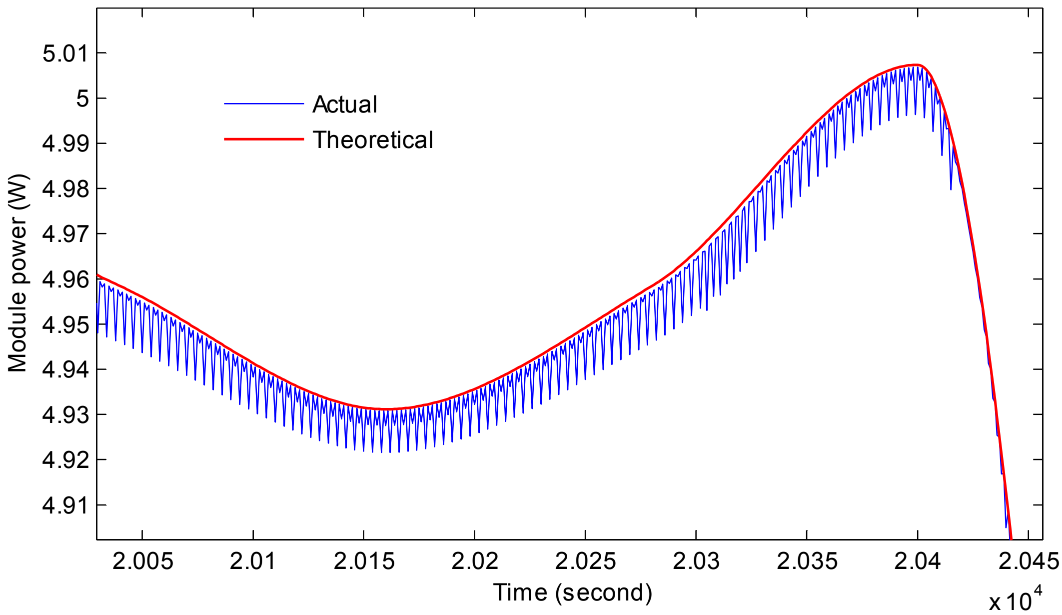

Figure 7.24. A zooming section from Figure 8.22

Figure 7.25 shows difference between theoretical and actual power versus time. It is clear that differences are very little except differences. This result is approved by energy assessment.

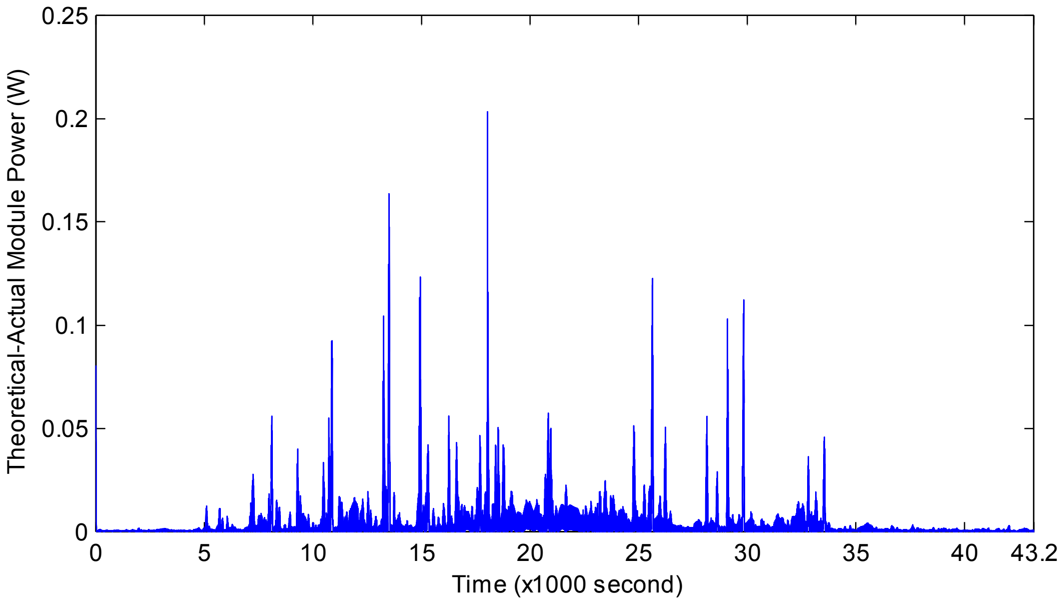

Figure 7.25. Difference between theoretical and actual module power

7.6.3. Simulation of the Direct Connected PV Module and Load

This simulation is performed with direct connected PV and resistive load without MPPT system. Figure 7.26 shows P-V and I-V curves. It is obvious that these curves are indicated pure resistive load.

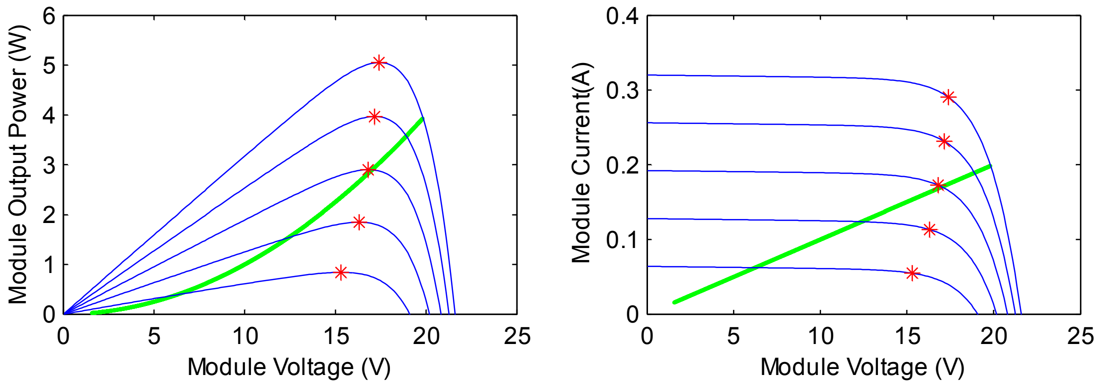

Figure 7.26 P-V and I-V curves of the direct connected PV

8. RESULTS AND CONCLUSION

8.1. Simulation Results

The PV MPPT system simulated in the previous section is compared with the direct-coupled PV system without MPPT. The irradiance data used here are the measurements of a cloudy day in April in Barcelona, Spain, introduced in Section 7.6.2. The total electric energy produced during a 12 hour period is calculated with MATLAB and tabulated in Table 8.1.Theoretical energy production of the PV under mentioned irradiance is calculated using Equation (8.1) with MATLAB.

$$E = \left(\sum_{0}^{43200} P\max \right) / 3600 \text{ Wh} \quad (8.1)$$

Theoretical maximum total energy produced during 12 hour period Obtained by this way is 20.70 Wh. It is remembered that P_{MPP} of the module is 5 W.

Table 8.1. Energy assessment of MPPT system

Load resistance (Ω)	Without MPPT		With MPPT	
	Energy (Wh)	Efficiency	Energy (Wh)	Efficiency
45	11.80	0.57	20.66	0.99
100	16.37	0.79	20.66	0.99
145	15.22	0.73	20.66	0.99

It is difficult to adjust duty cycle from 0 to 1 because some limitations (over input current, over output voltage, coil and capacitor size). Because of that duty cycle of the DC-DC converter must be limited.

If duty cycle is limited as $0.35 \leq D \leq 0.70$, efficiency is happened as given in Table 8.2.

Table 8.2. Energy assessment of MPPT system with limited duty cycle

Load resistance (Ω)	Without MPPT		With MPPT	
	Energy (Wh)	Efficiency	Energy (Wh)	Efficiency
45	11.80	0.57	19.50	0.94
100	16.37	0.79	20.38	0.98
145	15.22	0.73	20.57	0.99

8.2. Experimental Results

8.2.1. Efficiency of the SEPIC

Efficiency values of the SEPIC DC-DC converter at different operating conditions are given in Table 8.3.

Table 8.3.Efficiency of the SEPIC

Input			Output			Duty	Efficiency %
V_i (V)	I_i (mA)	P_i (W)	V_o (V)	I_o (mA)	P_o (W)		
12	119	1.428	11.69	113	1,320	50	91
17	307	5.219	21.61	214	4,624	56	88
17	49	0.833	8.55	87	0.743	35	90

8.2.2. SEPIC Waveforms

The waveforms of the SEPIC DC-DC converter which is working at Vi=17 V and D=0.35 obtained from hardware using oscilloscope are shown in Figure 8.1.

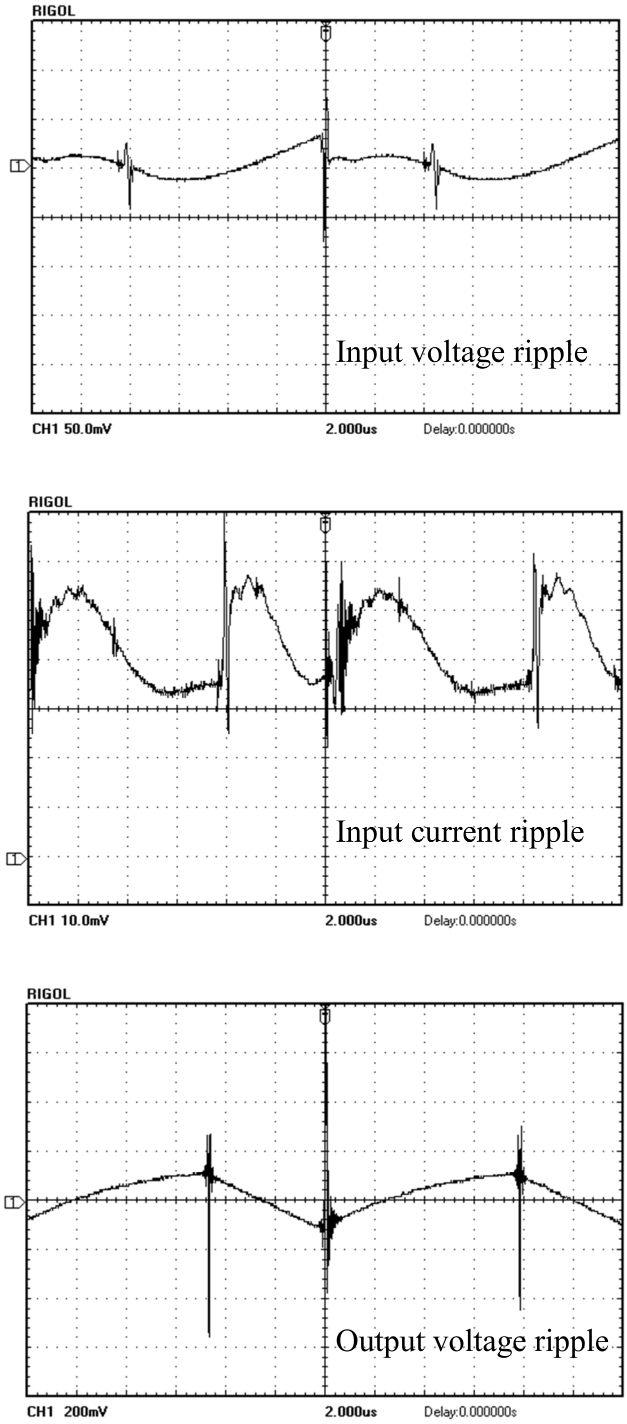

Figure 8.1. Waveforms of the SEPIC

8.2.3. MPPT System Results

Input voltage and current values produced by DSPIC ADC at every sampling are sent to PC via serial port. Followed figures are obtained using these data. Irradiance is 0.2 kW/m^2, temperature is 25 °C , sampling time of the ADC is 500 ms and duty increment/decrement step is 0.2 .

Figure 8.2 shows variation of the DC-DC converter input resistance with duty cycle. Variation of the module voltage with time is given in Figure 8.3. Figure shows that MPPT algorithm finds out MPP at the end of 30 samples. It can be seen that there is an oscillating around MPP.

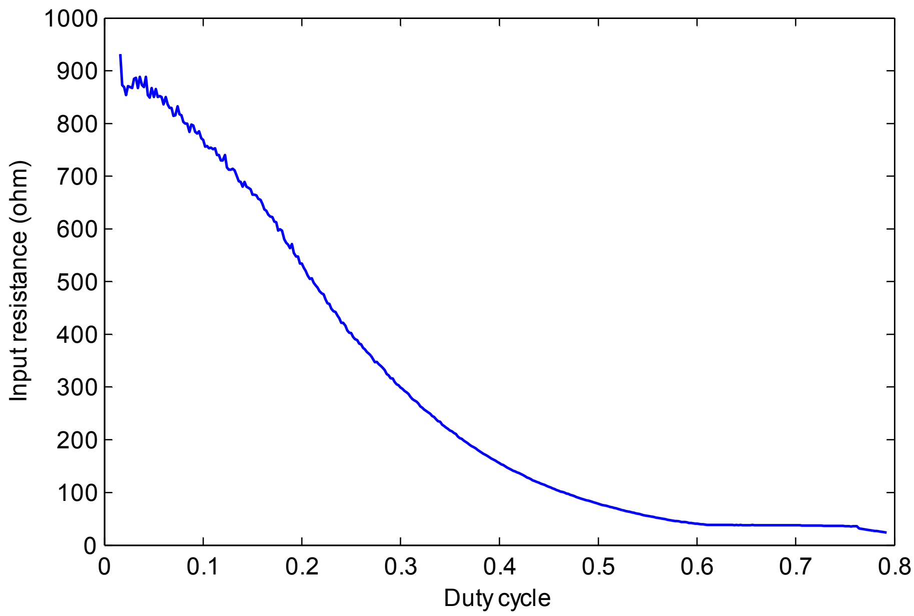

Figure 8.2. Variation of the input resistance

Module Power-Voltage curve is given in Figure 8.4.This figure shows instantaneous module power at every sampling while searching MPP. From Table 7.2 at 0.2 kW/m^2 irradiance level V_{MPP} is 15.31 V and P_{MPP} is 0.84 W. At the MPP, measured values with digital multimeter are given in Table 8.4.

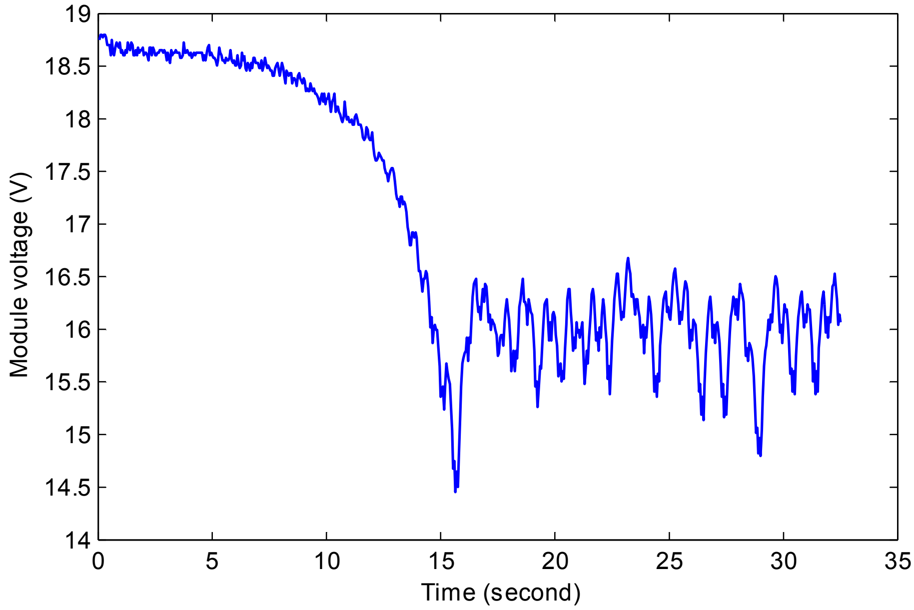

Figure 8.3. Module voltage versus time

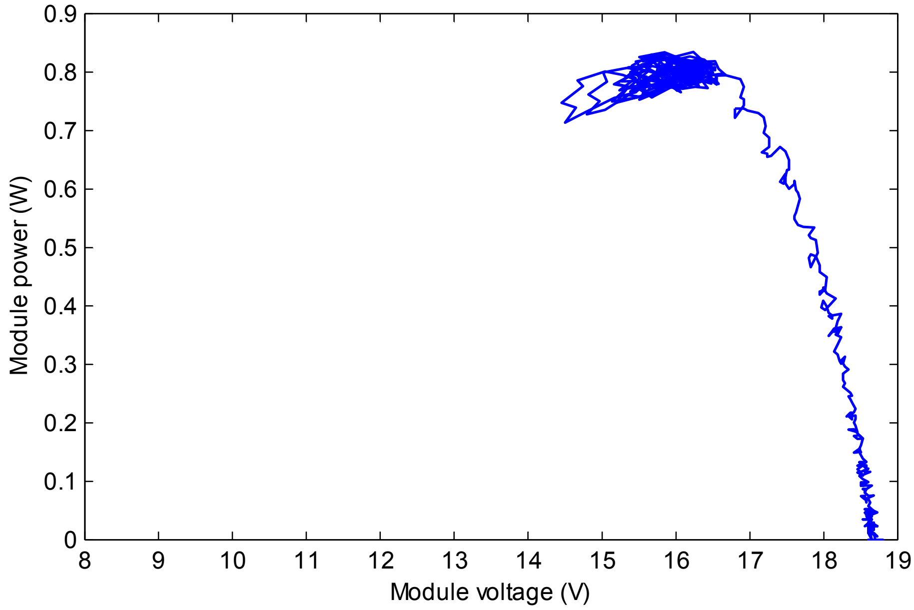

Figure 8.4. Operating points of the module

Table 8.4.Measured values at MPP

V_{in} (V)	I_{in} (mA)	P_{in} (W)	V_{out} (V)	I_{out} (V)	P_{out} (W)	Duty	Efficiency
15.6	47	0.733	8.2	81	**0.664**	33.6	0.905

Without MPPT system, measured values are given in Table 8.5. Load powers at with/without MPPT system conditions are shown in table 8.6.

Table 8.5. Load power without MPPT

V_{LOAD} (V)	I_{LOAD} (mA)	P_{LOAD} (W)
6.37	63	**0.401**

Table 8.6. Increase in load power

Without MPPT	With MPPT	Increase in Power (%)
P_{LOAD} (W)	P_{LOAD} (W)	
0.401	0.664	65

8.3. Conclusion

This study presents a simple but efficient photovoltaic system. It models each component and simulates the system using MATLAB. Comparison result shows that the PV model using the equivalent circuit in moderate complexity provides good matching with the real PV module.

Simulations perform tests for the MPPT with Direct V_{ref} Control and MPPT with Duty Control using unreal and real irradiance data. Ideal SEPIC DC-DC converter is used in this simulation.

The results show that the PV system without MPPT has poor efficiency because of mismatching between the PV module and load. At the same time simulation result s show that the direct connected PV system efficiency depends on load resistance. On the other hand, it shows that the system with MPPT can utilize more than 99% of PV capacity. Assuming a DC-DC converter has efficiency more than 90%, the system can increase the overall efficiency by more than 32% compared to the system without MPPT.

In order to develop a simple low-cost system, this thesis adopts the direct control method which employs the P&O algorithm. This control method offers another benefit of allowing steady-state analysis of the DC-DC converter, as opposed to the more complex state-space averaging method, because it performs sampling of voltage and current at the periodic steady state.

It performs simulations of the whole system and verifies functionality and benefits of MPPT. Simulations also make comparisons with the system without MPPT in terms of total energy produced by PV a day. The results validate that MPPT can significantly increase the efficiency of energy production from PV and the performance of the PV.

Implemented low cost MPPT system can be used in the commercial PV lighting and battery charging systems.

Future studies into maximum power point tracking could include the use of a different DC/DC converter and also some different MPPT algorithm could be implemented.

REFERENCES

ALTAS, I., SHARAF, A. ,2007. A photovoltaic array simulation model for Matlab-Simulink GUI environment., IEEE (pp. 341-345).

ARCHER,MARY D., HILL, ROBERT., 2001. Clean Electricity From Photovoltaics. Imperial College Press.

CASTANER, L., SILVESTRE, S., 2002. Modelling Photovoltaic Systems using PSPice. John Wiley and Sons.

COELHO, R., CONCER, F., MARTINS, D., 2009. A study of the basic DC-DC converters applied in maximum power point tracking. IEEE, (pp. 673-678).

DOLARA, A., FARANDA, R., LEVA, S., 2009. Energy Comparison of Seven MPPT Techniques for PV Systems .

ERICKSON, R. W., MAKSIMOVIC, D., 2004. Fundamentals of Power Electronics. Kluwer Academic Publishers.

ESRAM, T., CHAPMAN, P., 2007 . Comparison of photovoltaic array maximum power point tracking techniques . IEEE Transactions on Energy Conversion , 22 (2), 439-449.

FARANDA, R., LEVA, S. , 2008. Energy comparison of MPPT techniques for PV Systems . WSEAS Transactions On Power Systems , 3 (6), 446-455.

FARANDA, R., LEVA, S., MAUGERI, V., 2008. MPPT techniques for PV Systems: energetic and cost comparison. IEEE, (pp. 1-6).

GILBERT, M., 1998. Renewable and Efficient Electric Power Systems.Wiley Online Library.

GOETZBERGER, A., HOFFMANN, V., 2005. Photovoltaic Solar Energy Generation. Springer.

GOW, J., MANNING, C., 1999. Development of a photovoltaic array model for use in power-electronics simulation studies. IEE Proceedings-Electric Power Applications , 146, 193.

HOHM, D. P., ROPP, M. E., 2002. Comparative Study of Maximum Power Point Tracking. Progress in Photovoltaics: Research and Applications , 47-62.

HUA, C., SHEN, C., 2002. Comparative study of peak power tracking techniques for solar storage system. IEEE, 2, pp. 679-685.

HUA, C., LIN, J., SHEN, C.,2002. Implementation of a DSP-controlled photovoltaic system with peak power tracking . Industrial Electronics, IEEE Transactions on , 45 (1), 99-107.

HUSSEIN, K., MUTA, I., HOSHINO, T., OSAKADA, M., 1995. Maximum photovoltaic power tracking: an algorithm for rapidly changing atmospheric conditions . IEE Proceedings-Generation, Transmission and Distribution , 142 (1),59-64.

KOTTAS, T., BOUTALIS, Y., KARLIS, A., 2006. New maximum power point tracker for PV arrays using fuzzy controller in close cooperation with fuzzy cognitive networks. Energy Conversion, IEEE Transactions on , 21 (3), 793-803.

KOUTROULIS, E., KALAITZAKIS, K., VOULGARIS, N., 2002. Development of a microcontroller-based, photovoltaic maximum power point tracking control system. Power Electronics, IEEE Transactions on , 16 (1), 46-54.

LUQUE, A., HEGEDUS, S., 2003. Handbook of Photovoltaic Scienece and Engineering. Wiley Online Library.

LYNN, P. A., 2010 . Electricity From Sunlight. John Wiley.

MESSENGER, R. A., VENTRE, J.,2004. Photovoltaic Systems Engineering. CRC Press LLC.

MUNEER, T., 2004. Solar Radiation and Daylight Models. Butterworth-Heinemann

NEAMEN, D. A.,1996. Electronic Circuit Analysis and Design. McGraw-Hill.

NEMA, R., NEMA, S., AGNIHOTRI, G.,2009. Computer Simulation Based Study of Photovoltaic Cells/Modules and their Experimental Verification. International Journal of Recent Trends in Engineering , 1 (3), 151-156.

OI, A. ,2005. Design and Simulation of Photovoltaic Water Pumping System. California Polytechnic State University.

SERA, D., TEODORESCU, R., RODRIGUEZ, P., 2007. PV panel model based on datasheet values., (pp. 2392-2396).

SHAHAT, A. E., 2005. PV Cell Module Modeling & ANN Simulation for Smart Grid Application.

SHEKOOFA, O., TAHERBANEH, M., 2007.Modelling of Silicon Solar Panel by MATLAB/Simulink and Evaluating the Importance of Its Parameters in a Space Application., Recent Advances in Space Technologies, 2007. RAST'07. 3rd International Conference (pp. 719-724).

SUN, X., WU, W., LI, X., ZHAO, Q., 2002.A research on photovoltaic energy controlling system with maximum power point tracking. IEEE, 2, pp. 822-826.

TSAI, H., TU, C., SU, Y. ,2008. Development of Generalized Photovoltaic Model Using MATLAB/SIMULINK., (pp. 22-24).

WALKER, G. ,2001. Evaluating MPPT converter topologies using a MATLAB PV model. Journal of Electrical \& Electronics Engineering, Australia , 21 (1), 49-55.

WENHAM, S. R., GREEN, M. A.,2007. Applied Photovoltaics. Earthscan Publications.

www.intersil.com (2010)

www.mathworks.com (2010)

www.national.com. (2010)

YANG, E. S.,1978. Fundamentals of Semiconductor Devices. McGraw-Hill Book Company.

CURRICULUM VITAE

Bülent BÜYÜKGÜZEL was born in Silifke, Turkey in 1963. He received B.Sc. degree in Electronic Engineering Department from Uludağ University, Bursa in 1985. He worked in Turkish Telekom for many years. He is working in Çukurova University as an engineer.